Doctoral Thesis

# Stimuli-responsive cancer therapy based on porous materials

Kibeom Kim

Department of Chemistry

Graduate School of UNIST

2019

# Stimuli-responsive cancer therapy based on porous materials

Kibeom Kim

Department of Chemistry

Graduate School of UNIST

# Stimuli-responsive cancer therapy based on porous materials

A thesis/dissertation
submitted to the Graduate School of UNIST
in partial fulfillment of the
requirements for the degree of
Doctor of Philosophy

Kibeom Kim

06/20/2019 of submission
Approved by

_____

Advisor
Ja-Hyoung Ryu

# Stimuli-responsive cancer therapy based on porous materials

Kibeom Kim

This certifies that the thesis/dissertation of Kibeom Kim is approved.

6/20/2019 of submission

signature

_____

Advisor: Prof. Ja-Hyoung Ryu

signature

_____

Prof. Tae-Hyuk Kwon: Thesis Committee Member

signature

_____

Prof. Chaekyu Kim: Thesis Committee Member

signature

_____

Prof. Myoung-Hwan Park: Thesis Committee Member

signature

_____

Prof. Youngdo Jeong: Thesis Committee Member

# Abstract

Surgical treatment, radiation therapy, and chemotherapy drugs are used to treat cancer. However, this treatment often kills normal cells and causes side effects. In addition, most cancer drugs are hydrophobic and therefore pose a number of problems to apply to the body. To solve this problem, nanomedicinehas been used for cancer treatment. This nanomedicine selectively accumulates to the cancer cells through passive and active targeting.

Organic nanomedicine, involving micelle, liposomes, and proteins, has low stability in the body. Inorganic nanomedicine, on the other hand, has high stability, but a low loading capacity because it is limited to the direct modification method. To overcome this challenge, research has been conducted into porous materials in drug delivery. Porous material has high body-stability and drug-loading capacity. In addition, a variety of functional molecules are modified to the outer and inner surfaces, and the multifunctionality of porous materials facilitates stimulated drug release.

In this dissertation, various stimuli-responsive porous materials were described for cancer therapy.

A membrane composed of a Dendrimer (Den) and a gold nanorod (GNR) has pores through which the drug can be released. In addition, GNR shows the effect of surface plasmon resonance (SPR) even after membrane synthesis, and it generates heat by NIR irradiation and increases the local temperature that promotes drug release. This controlled release of the drug sustains the drug concentration within the therapeutic window, thereby reducing side effects and enhancing benefits.

Unlike bare GNR, GNR capped with mesoporous silica (GNR@MS) has pores that facilitate drug loading, thereby increasing the chemotherapy effect of nanoparticles. However, the weak interaction between the drug and the MS surface causes the loaded drug to be released from the nanoparticle during the delivery process. In order to prevent premature release, a glutathione (GSH)-responsive polymer (PEG-PDS) is coated on GNR@MS surfaces to block the pores. Polymer coated GNR@MS (GNR@MS@PDS) increases the local temperature in response to NIR irradiation, which induces drug-release by expanding PEG-PDS. Furthermore, the PEG-PDS polymer is degraded by GSH, opening the pore of GN @MS and releasing the drug at the cancer cells. This dual-stimulus system can control the time and space of drug release in the body.

NanoMOF with high surface and porosity is attracting much attention as a drug-delivery system. In particular, PCN-224 has high stability in aqua state, and the porphyrin derivative organic linker constituting of PCN is used as a PDT agent. That facilitates the photodynamic therapy under light irradiation without any additional processes. These properties enable combined chemo & PDT to enhance cancer treatment effectiveness. In addition, MOF can be easily modified by hyaluronic acid, while HA can control the drug release in response to HAdase as well as interact with the CD44

receptor to selectively target cancer.

The unsaturated metal clusters of nanoMOF can form a coordination bond with the Lewis base, and the nanoMOF can easily be post-functionalized using this character. Various systems use this phenomenon to convert the cancer-targeting ligand to MOF. However, proteins and biochemicals, which have Lewis bases, are present in the body and compete with modified ligands to interact with MOF and induce ligand detachment. To overcome these problems, Folic acid-modified polyacrylic acid (PAA) was coated to the MOF surface. The polyvalent coordination between PAA and MOF increases the binding force of the ligand and the stability of the drug-delivery system in the body.

Stimulus-responsive systems based on porous materials can effectively treat cancer with advantages like drug-concentration control, dual-stimulus response, combined therapy and increased biostability.

# Contents

# List of Figure

Apicture of a bare AAO membrane (left) and a GNR-Den composite membrane (right)

**Figure 2-4.** (a) The temperature traces with and without a GNR-Den film on AAO measured by using an infrared camera at a NIR power of 0, 0.18, 0.36, and 0.54 W $cm^{-2}$. (b) The temperature response from the device by NIR irradiation with a power of 0.54 W $cm^{-2.}$

**Figure 2-5.** (a) The Dox release profiles for accumulated amounts from the device at NIR powers of 0, 0.18, 0.36, and 0.54 W $cm^{-2}$. (b) The Dox release rate profile is based on temperature controlled by a NIR power.

**Figure 2-6.** (a) Schematic illustration of the fluidic system experimental set-up with the GNR-Den composite membrane, (b) Dox release profile in the absence (OFF) and presence (ON) of the NIR light (850 nm, 0.54 W $cm^{-2}$, 5 min collection interval), and (c) in vitro cytotoxicity of aliquots collected at 80 (NoLight1) and 160 min (NoLight2) with no irradiation and at 40 (NIR1) and 120 min (NIR2) with NIR irradiation after 48 h and 72 h incubation.

**Figure 2-3.** Molecular structures and their pulsatile release profiles from a mixture of calcein and Rh-6G from the TMA-GNR-Den membrane contained fluidic device (850 nm, 0.54 W $cm^{-2}$, 2.5 min collection interval).

**Figure 2-8.** (a) The Dox release percent profile for accumulated amounts from the device at a NIR power of 0.54 W/$cm^2$. After 9 hours NIR irradiation at a NIR power of 0.54 W/$cm^2$, the release amount was significantly decreased with almost 50% Dox release from the total payload (180 μg) and reached a plateau during next 18 hours even in the presence of NIR. (b) The Dox release percent profile for accumulated release amounts from the device in the absence of NIR for a long time period.

**Figure 2-9.** The temperature response from the fluidic device used for the experiment in Figure 5b by NIR irradiation (10 min) with a power of 0.54 W/$cm^2$. It shows a little hysteresis in light response. The media in the drug reservoir have been slowly heated with light and rapidly cooled without light, because the continuous water flow under the membrane in the fluidic device could be acted like a cooling system. We observed the fast increase in 10 sec up to 40 °C, but the slow increase to 50 °C after next 10 min because the media in the drug reservoir have been heated together by the localized heat from GNRs in the presence of light. With no heat source in the absence of light, the continuous supply of fresh PBS rapidly cooled the media in drug reservoir, showing fast decease in drug release rate.

# List of tables

# Nomenclature

| | |
|---|---|
| EPR | Enhanced permeability and retention |
| GNP | Gold nanoparticles |
| Den | Dendrimers |
| GNR | Gold nanorod |
| CTAB | Cetyltrimethylammonium bromide |
| MS | Mesoporous silica |
| SPR | Surface plasmon resonance |
| Dox | Doxorubicin |
| NIR | Near infrared |
| MOF | Metal organic framework |
| Photodynamic therapy | PDT |
| Photosensitizer | PS |
| TCPP | Tetra(4-carboxyphenyl)porphine |
| DTC | Dithiocarbamate |
| AAO | Anodized aluminum oxide |
| SEM | Scanning electron microscopy |
| UV-Vis | Ultraviolet-visible |
| PDMS | Polydimethyl siloxane |
| Rh-6G | Rhodamine 6G |
| TMA | Trimethyl ammonium |
| GSH | Glutathione |
| PTT | Photo thermal therapy |
| DTT | Dithiolthreitol |
| PDS | PEG-PDS |
| PI | Propidium iodide |
| HA | Hyaluronic acid |
| PXRD | Powder X-ray diffraction |
| BET | Brunauer-Emmett-Teller |
| RES | Reticuloendothelial system |
| DFT | Density functional theory |
| MD | Molecular dynamics |
| PAA | Poly acrylicacid |
| FBS | Fetal bovine serum albumin |

# Chapter 1. Introduction

## 1.1 Overview

Cancer is one of the world's most dangerous diseases, with 10 million new people suffering from cancer each year.[1] However, recent studies and understanding of cancer have become more intense, and the number of deaths by cancer has been decreasing due to the increased diagnostic and treatment sophistication.[2] Surgical intervention,[3-5] radiation,[6-8] and chemotherapeutic drug method[9-11] are popular therapeutic methods for cancer treatment. These often kill normal cells and induce side effects.[12] In addition, most cancer drugs are hydrophobic, which pose many problems for physiological application[12-13]. To overcome these problems, nanomedicine has recently been studied to improve the stability of hydrophobic drugs through the combination of drugs and nanoparticles.[14-15] Several nanomedicines, USFDA-approved drugs, have been used for treatment (Figure 1-1).[16]

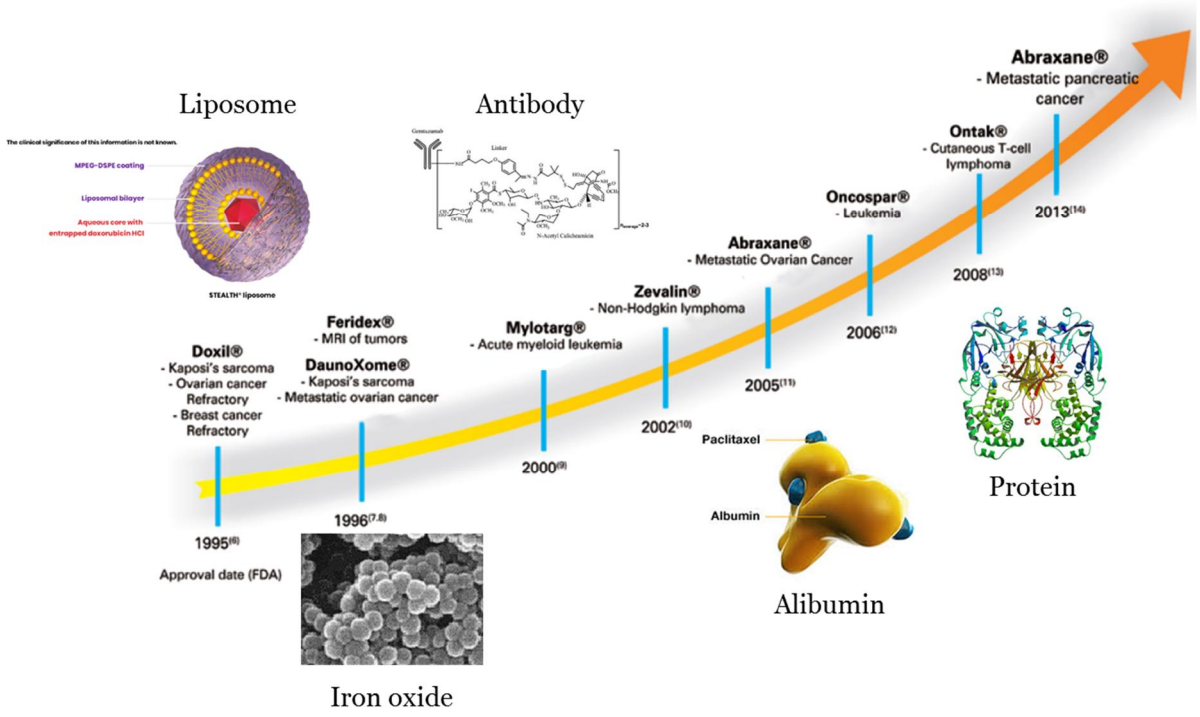


**Figure 1-1.** Timeline with some examples of nanoparticles approved by Food and Drug Administration.) Doxil® is the liposomal doxorubicin formulation; Feridex® includes superparamagnetic iron nanoparticles associated with dextran, DaunoXome® is the liposomal daunorubicin, Mylotarg® has gemtuzumab ozogamicin molecules bonded to monoclonal antibody, Zevalin® includes mouse monoclonal antibody IgG1 with tiuxetan chelator associated with radioactive isotope Yttrium-90, Abraxane® has paclitaxel bonded to albumin; Oncaspar® is the modified version of the L-asparaginase enzyme, and Ontak® includes the fusion protein denileukin diftitox. Reproduced with permission.[16] Copyright 2016, Scientific Electronic Library Online.

Nanomedicine not only improves drug stability but also selectively transfers the drug to cancer cells.[17] Nanomedicine can deliver drugs to cancer cells by passive targeting, which accumulates selectively in cancer cells according to their size, and active targeting, which targets cancer by reacting with substances present on cancer cells and nanoparticles (Figure 1-2).[18-21] Passive targeting is a method of targeting cancer cells by the enhanced permeability and retention (EPR) effect. Unlike normal cells, cancer cells proliferate indiscriminately and promote angiogenesis. Generated blood vessels have poorly aligned defective endothelial cells with wide fenestrations, lacking a smooth muscle layer, or innervation with a wider lumen.

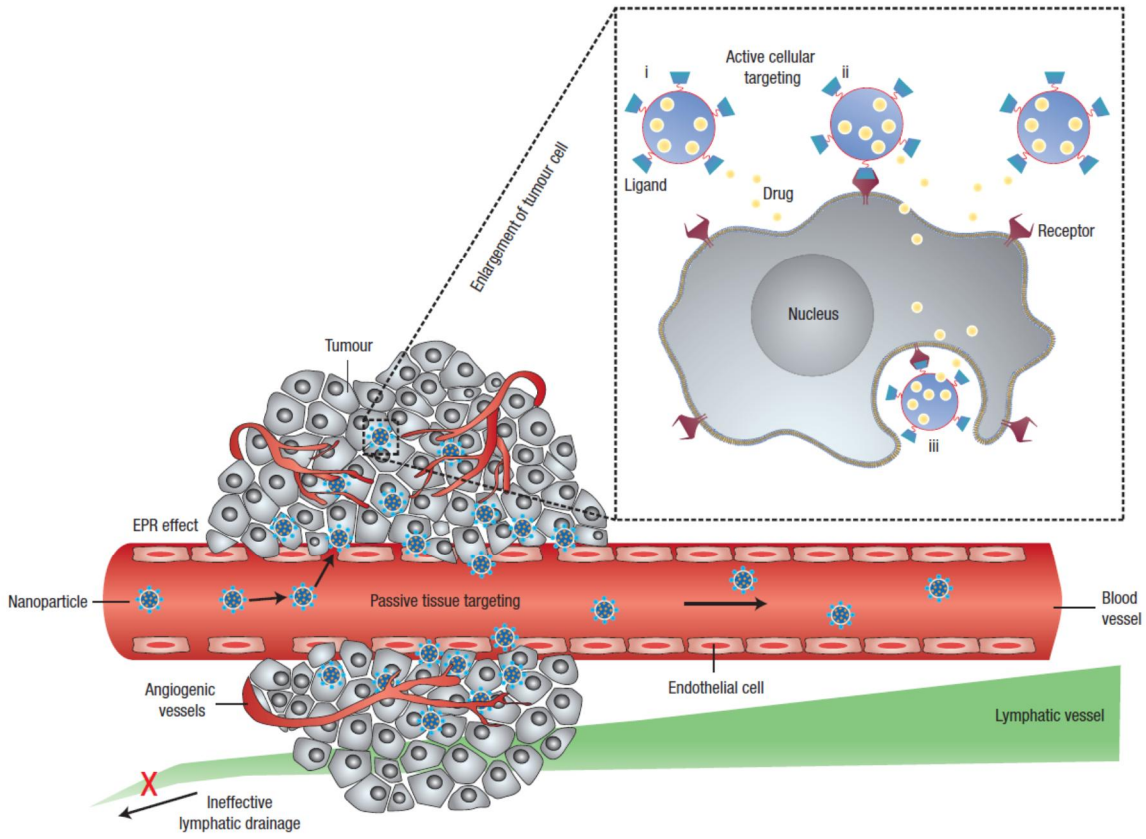


**Figure 1-2.** Schematic representation of different mechanisms by which nanomedicine can deliver drugs to tumors. Nanomedicine is shown as representative nanocarriers (circles). Passive tissue targeting is achieved by extravasation of nanomedicine through increased permeability of the tumor vasculature and ineffective lymphatic drainage (EPR effect). Active cellular targeting (inset) can be achieved by functionalizing the surface of nanomedicine with ligands that promote cell-specific recognition and binding. Nanomedicine can (i) release their contents in close proximity to the target cells; (ii) attach to the membrane of the cell and act as an extracellular sustained-release drug depot; or (iii) internalize into the cell. Reproduced with permission.[23] Copyright 2007, Nature Publishing Group.

These characters induce the higher accumulation of the nanoparticle to the cancer cell than normal cells. In particular, nanoparticles are removed by biological barriers, which remove nanoparticles greater than 100 nm from the liver and spleen, and nanoparticles of less than 10 nm from the kidney. Therefore, nanoparticles having a size of 30-100 nm increase the residence time in the body and electively accumulate in cancer cells, potentiating the effects of the cancer drug. [22-26]

Active targeting is a method of targeting a cancerous cell by interacting with an overexpressed receptor by acting on the nanoparticle surface with a ligand. Methods used for cancer targeting include monoclonal antibody, antibody fragment, aptamer, and ligand-based targeting methods.[22-26]

Although various nanomedicine is used for their ability to target cancer and increase drug stability, the low stability of micelle and liposomes in the body make them difficult to encapsulate as drugs[27-29] and inorganic nanoparticles have low drug-loading capacity because they depend on covalent bonding for drug modification.[30-31] In addition, premature release during the drug delivery process causes side effects.[32-34] To solve these problems, drug delivery systems that respond to stimuli based on porous materials have received much interest.

### 1.2 Porous material for drug delivery.

**Gold nanostructure and dendrimer porous material (Den-GNP)**

Gold nanoparticles (GNP) and organic compound dendrimers (Den) can be used to synthesize porous materials. The gold nanoparticles serve to immobilize the dendrimer, and the dendrimer provide space for the drug pathway. These porous materials (Den-GNP) are coated to glass or other materials and used for drug or protein control release.[35-37]

*Park et al.* demonstrated a system for effectively releasing drugs using Den-GNP porous materials.[36] These Den-GNP feature release profiles that can be controlled by the dendrimers generation and nanoparticle building blocks. In addition, these materials are reusable. The encapsulation and release of the drug can be repeated several times using the same porous material (Figure 1-3).

In another paper, Den-GNP was developed to control the various drug release.[35] Charge of Den-GNP was regulated by modifying the functional groups at the end of the dendrimer. These changes facilitate controlled release of the drugs and proteins with different charge characteristics (Figure 1-4b). The porosity of the Den-GNP material can be controlled by changing the dendrimer generation providing size-dependent selectivity. In addition, the surface function of Den-GNP can be easily modified to control chemo selectivity by charge and hydrophobicity of the membranes, which are adjusted after simple functionalization (Figure 1-4b). This porous material improves selectivity for analytes based on size, charge and hydrophobicity. As a result, Den-GNP materials facilitate the separated release of small molecules, chemicals and biopolymers.

.

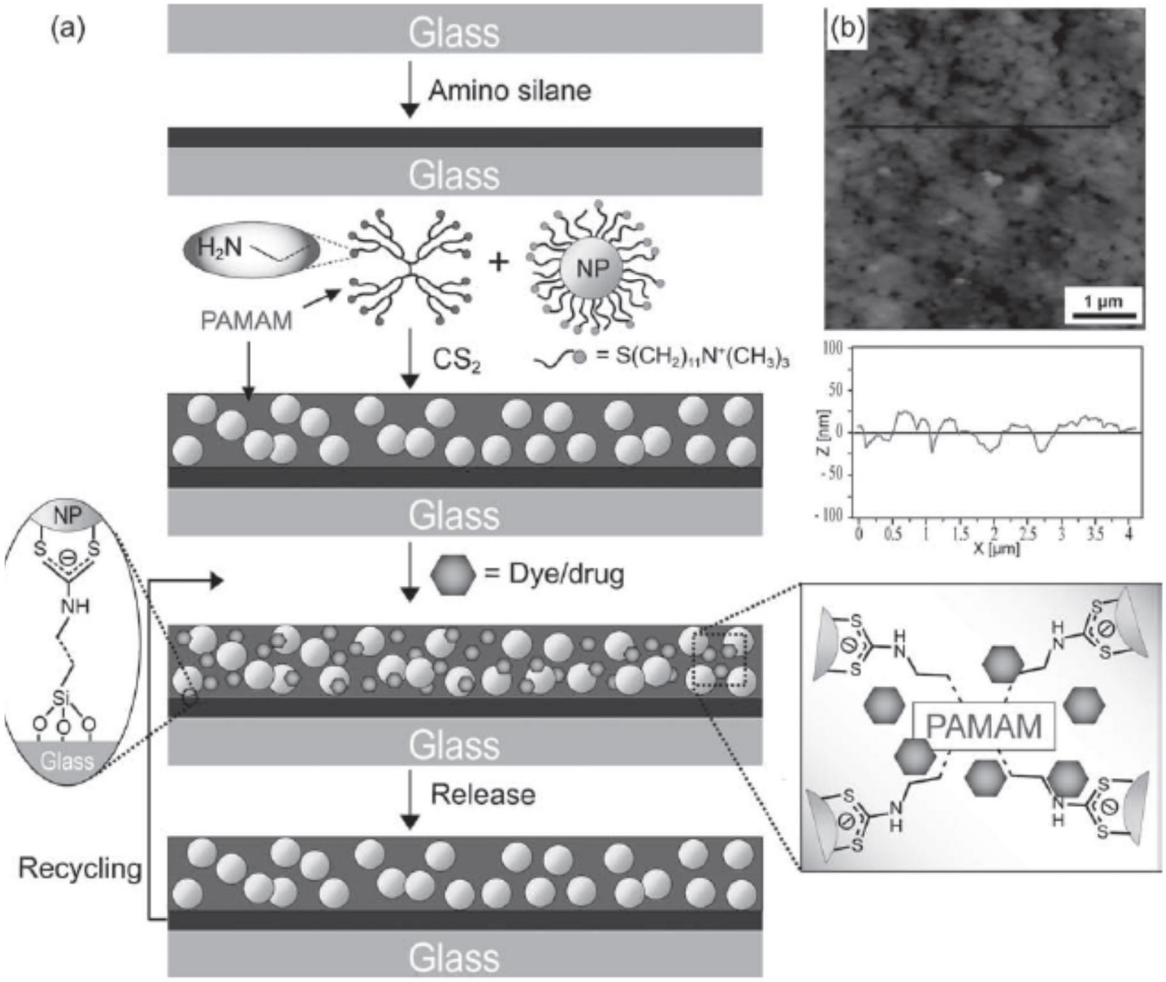


**Figure 1-3.** Schematic illustration of the formation of Den-NP porous material films and the incorporation and release of dyes or drugs and b) an AFM image of Den-GNP porous films on an amine-functionalized glass surface. The bottom graph shows the line profile image and a film thickness of ≈ 700 nm determined by profilometry. Reproduced with permission.[36] Copyright 2011, WILEY-VCH Verlag GmbH & Co. KGaA, Weinheim.

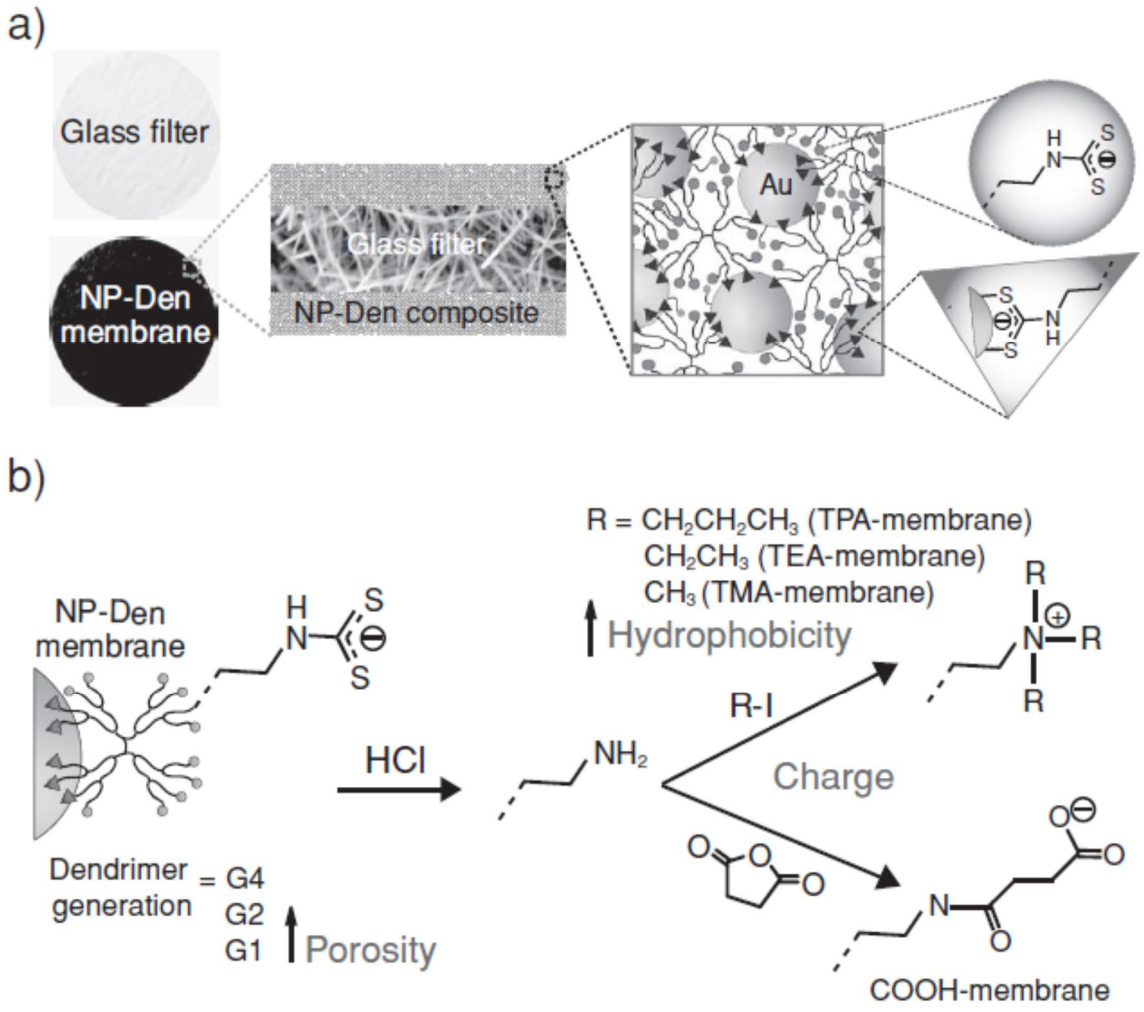


**Figure 1-4.** Schematic illustration of fabrication and post-functionalization of hybrid porous material membranes. (a) A glass filter, hybrid membrane consisting of Den-GNP composites formed. (b) Scheme for post-functionalization within a hybrid porous material membrane to obtain various functionalities. Reproduced with permission.[35] Copyright 2012, WILEY-VCH Verlag GmbH & Co. KGaA, Weinheim.

**Mesoporous silica capped gold nanorod (GNR@MS)**

Gold nanorod (GNR) is attracting much attention for the bio application of its various features, such as high biocompatibility, plasmonic properties, and easy surface functionalization. In particular, optical characteristics can be adjusted by controlling the shape of GNR. Using this inherent property, absorption of GNR can be tuned in the 700 to 1200 nm range (water window), which is most useful for in vivo imaging and treatment, and is widely studied as a photo therapy tool (figure 1-5).[38] Despite these advantages, the toxicity of the cetyltrimethylammonium bromide (CTAB) bilayer capping the GNR surface still has many problems in bio applications. In addition, bare GNR has a low loading capacity due to the direct ligand modification between drugs and GNR.[30-31] To solve these problems,

the GNR surface is coated with organic ligands, small biomolecules, and silica. Among theese, mesoporous silica (MS)-coated GNR (GNR@MS) may have the greatest potential as a drug delivery system. Mesoporous silica cavities can be used as drug reservoirs, and local heat was generated by the surface plasmon resonance (SPR) effect. These inherent properties of GNR@MS facilitate the combined chemo & photothermal therapy for effective cancer treatment.[39-40]

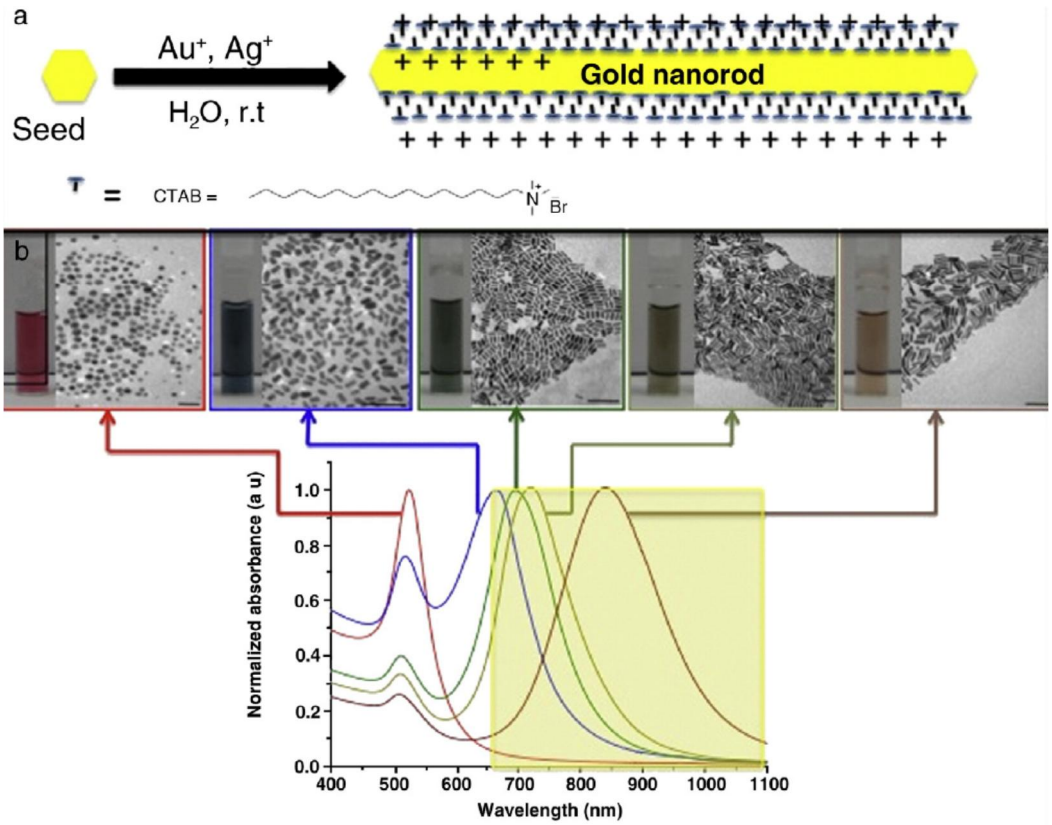


**Figure 1-5.** a: Synthesis of gold nanorods from spherical gold seeds in the presence of CTAB as a shape-directing agent in water at room temperature, showing a cartoon of the final CTAB bilayer. b: UV–Vis spectra, transmission electron micrographs, and photographs of aqueous solutions of gold nanorods of different aspect ratio (length/width). Aspect ratio increases from left to right. All scale bars=100 nm. The yellow shaded area of the spectra is the biological "water window". Reproduced with permission.[38] Copyright 2011, Elsevier B.V.

*Zhang et al*. have developed a system that enables imaging, chemotherapy, and PTT using GNR@MS (figure 1-6).[31] Dos was loaded to the GNR@MS pore by electrostatic interaction. Dox loaded to the GNR@MS show the higher cellular uptake ability than free dox. In addition, heat generated by the near infrared (NIR) irradiation not only induces drug release but also facilitates photothermal therapy. By introducing a heat-responsive gatekeeper system to the GNR@MS, the NIR can be used to turn on and off the drug release (figure 1-7).

Liu et al. have developed a system in which pores of GNR@MS were blocked by thermo-responsive material, 1-tetradecanol (TD) to control drug release.[30] This system facilitates sequential drug release by the NIR irradiation. In particular, folic acid was modified to the GNR@MS surface to endow the cancer cell-targeting ability. This cancer targeting, and controlled drug release system promotes the effects cancer therapy by minimum drug feeding.

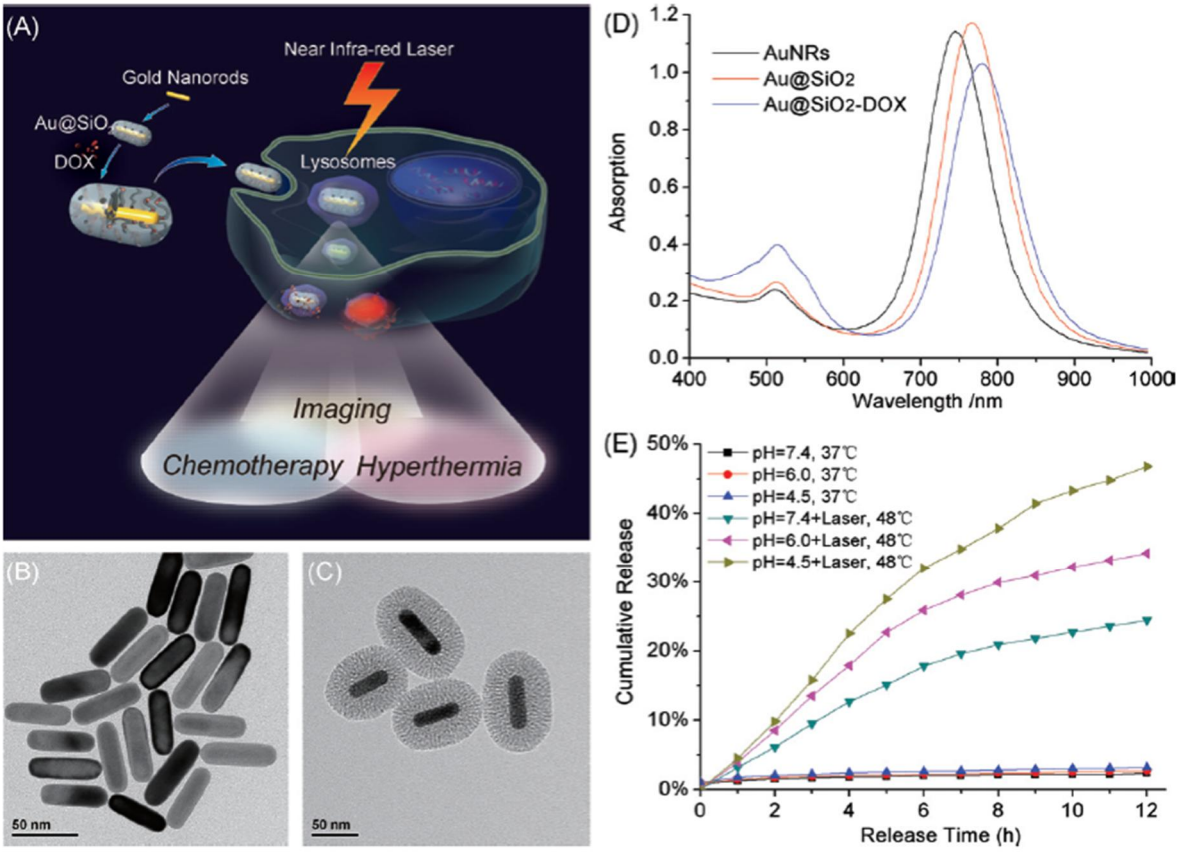


**Figure 1-6.** A) Schematic illustration of GNR@MS as a novel multifunctional theranostic platform for cancer treatment. TEM images of B) GNR and C) GNR@MS, D) extinction spectra of GNR, GNR@MS, and Dox-GNR@MS, and E) Doxorubicin (Dox) release profiles from Dox-GNR@MS with and without NIR laser irradiation at different pHs. Reproduced with permission.[31] Copyright 2012, WILEY-VCH Verlag GmbH & Co. KGaA, Weinheim.

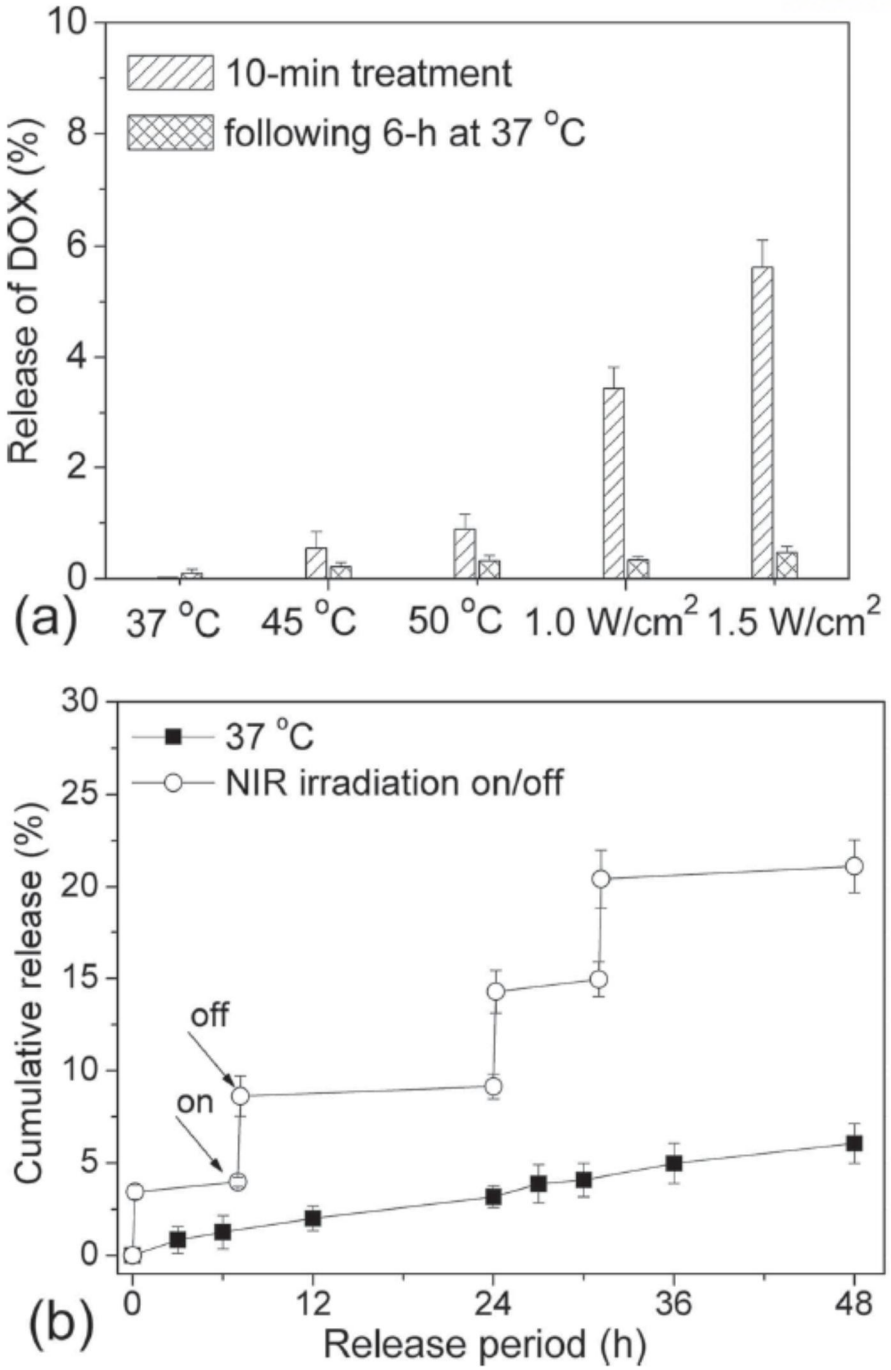


**Figure 1-7.** a) NIR-induced release profiles of DOX from the Dox-GNR@MS@TD aqueous suspension (100 mg $L^{-1}$ for Dox-GNR@MS@TD, and ≈84 mg $L^{-1}$ for GNR@MS) in RPMI-1640 medium (W/O PR) under NIR light irradiation or external heating, and b) cumulative release of DOX from the Dox-GNR@MS@TD aqueous suspension (100 μg $mL^{-1}$) under multiple NIR light irradiation on/off cycle treatment (1.0 W $cm^{-2}$, 802 nm), while cumulative release profile at 37 °C was taken for comparison. The cumulative release was presented as mean value ± standard deviation ($n$ = 3). Reproduced with permission. [30] Copyright 2015, WILEY-VCH Verlag GmbH & Co. KGaA, Weinheim.

**Metal organic framework (MOF)**

Metal organic frameworks (MOF) have been designed through a variety of synthesis strategies and have been studied in many areas, such as gas storage[41-43] and separation,[44-46] catalysis,[47-49] and sensing.[50-52] In recent years, nanosize MOF has received extensive interest as a drug-delivery and cancer-therapy system.[53]

MOFs display a number of advantages over traditional drug carriers. First, the morphology, composition, size, and chemical properties of MOF can be tailored for multifunctionalities and stimulus-responsive drug release. Second, MOF has a high loading capacity because of its large surface area and high porosity. These desirable properties render MOF a promising platform for drug delivery and clinical tumor therapy.[54] Figure 1-8 show research field of nanomedicine MOF.[55]

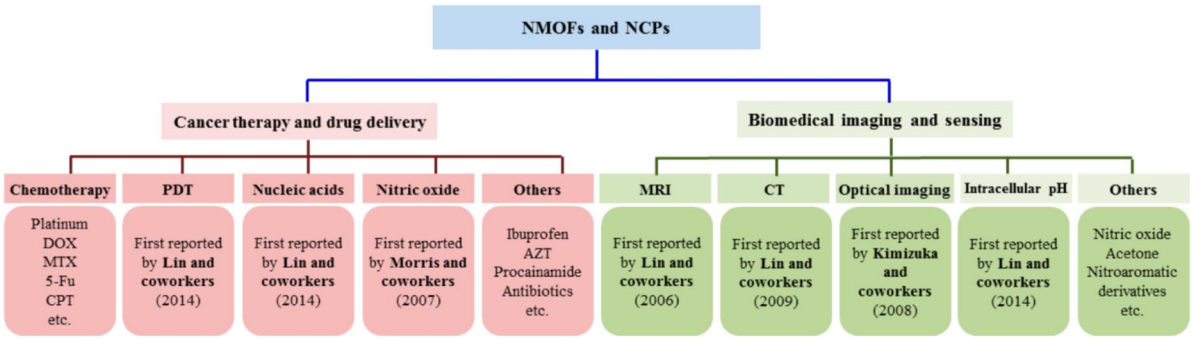


**Figure 1-8.** Key developments in the nanomedicine applications of NMOFs and NCPs. Reproduced with permission.[55] Copyright 2015, American Chemical Society.

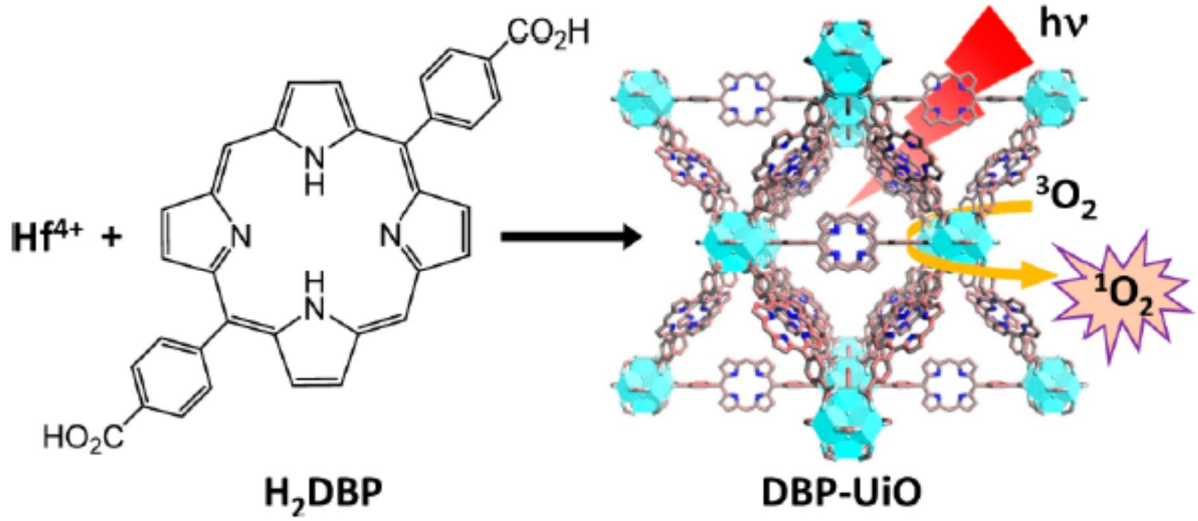


**Figure 1-9.** Synthesis of Hf–DBP NMOF and the Schematic Description of Singlet Oxygen Generation Process. Reproduced with permission.[56] Copyright 2015, American Chemical Society.

Recently, *Lu et al.* have developed a MOF system that enables photodynamic therapy using nanoscale MOF (Figure 1-9).[56] Photodynamic therapy (PDT) is a type of phototherapy that needs a photosensitizer (PS), light source and tissue oxygen to treat the cancer cells. However, most PSs are inherently hydrophobic, which induce the PS aggregation and reduce PDT efficacy. To overcome this challenge, DBP-UiO, a Hf-porphyrin nanoscale metal-organic framework, was synthesized as an effective photosensitizer for PDT. This system has several advantages. First, PS molecules are well isolated in framework structure to prevent agglomeration and self-quenching of the excited state. Second, porous nano MOF structures provide a pathway that facilitates the diffusion of singlet oxygen inside of MOF to increase a cytotoxic effect in the cancer cells.

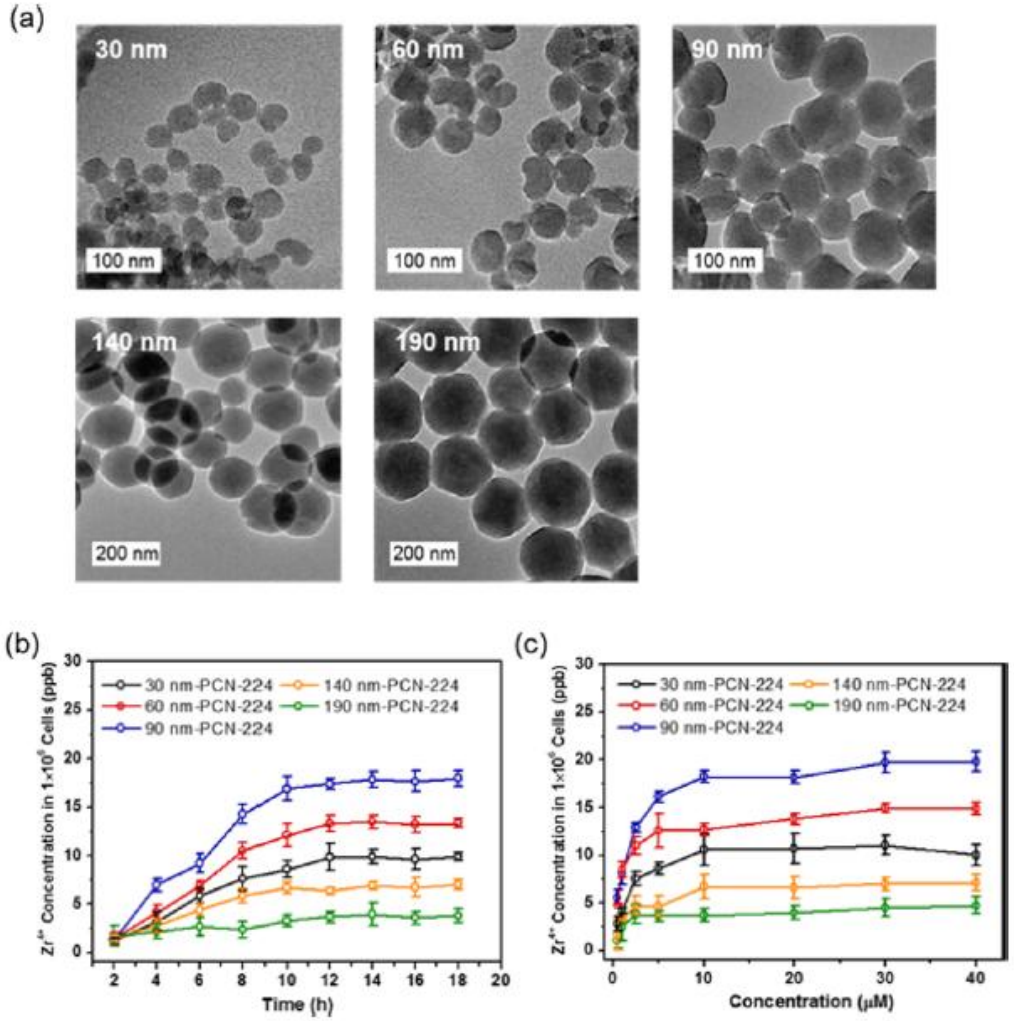


**Figure 1-10.** (a) TEM images of PCN-224 nanoparticles of 30, 60, 90, 140, and 190 nm. (b) Cellular uptake of PCN-224 samples with different sizes at various incubation time. Concentration = 20 μM. (c) Cellular uptake of different sized PCN-224 nanoparticles at various concentrations. Incubation time = 24 h. Data are based on ICP analysis of the Zr concentration internalized into HeLa cells. Data are means ± s.d. (N = 3). Reproduced with permission.[57] Copyright 2016, American Chemical Society.

*Parke et al.* have developed the PCN-224 synthesis method that controls the size of MOF (Figure 1-10). [57] The understanding of nanomaterials for targeted cancer therapy is important because it relates to cellular responses. Despite the variety of nanomaterials used in these studies, however, there was a rare platform that could control the core of nanoparticles at the molecular level. PCN-224 was synthesized through a bottom-up approach. The size of MOF nanoparticles has been precisely tuned to a wide range with designed functional motifs. In particular, the molecular properties of porphyrin linkers, regardless of size, are maintained in MOF nanoparticles. Thus, size-dependent cellular uptake and PDT allowed optimal size screening of MOF nanoparticles for PDT, whereas MOF nanoparticle formation of photosensitizers showed better PDT efficacy than free PS molecules. In addition, the $Zr_6$ cluster of MOF further enhanced PDT efficacy by enabling active targeting through post-synthesis modification.

### 1.3 Thesis summary

In this thesis, we introduce effective cancer treatment using the stimuli-responsive drug system based on porous material.

Chapter 2 describes stable porous materials composed of dendrimers and GNR. This material was coated onto the AAP membrane to facilitate controlled drug release by NIR light. GNR not only serves as a dendrimer 's anchor point but also generates heat in response to the 850 NIR laser, which belongs to the water window range. Dendrimers maintain structure and provide a pathway for drug release. The system can increase the temperature to 52 °C in response to NIR, which can rapidly increase the drug release rate. This controlled release allows for more effective cancer treatment by maintaining the drug concentration in the therapeutic window.

Chapter 3 describe the dual stimuli responsive system, which consists of mesoporous silica-coated GNR (GNR@MS) and glutathione reactive polymer (PEG-PDS). Unlike bare GNR, GNR@MS is more effective as a drug delivery system because it has pores for drug loading. However, the loaded drug causes an unexpected release during the delivery process, which causes drug side effects. To prevent this phenomenon, the pores of GNR@MS was blocked by GSH responsive PEG-PDS. The drug is stored stably in the MS cavity by the polymer, and when it reaches cancer cells it is released from the nanoparticle because PEG-PDS, which blocks the pore, is degraded by GSH and the pore is opened. NIR irradiation also causes the polymer expansion by heat and to induce drug release. This dual responsive system can regulate the timing and space of drug release, enabling more effective cancer treatment. NIR irradiation causes the polymer expansion inducing the drug release. This dual responsive system can regulate the timing and space of drug release, enabling more effective cancer treatment.

Chapter 4 describes the hyaluronic-capped PCN-224 MOF system, which can load doxorubicin (Dox) for combined therapy. PCN-224 MOF has a higher stability in aqua than other MOFs. The

organic linker of PCN (TCPP) is a porphyrinic compound that is widely used as a photosensitizer for PDT. Therefore, it is possible to treat chemotherapy by Doxorubicin delivery and PDT by light irradiation. HA, that is degraded by HAdase not only controls the drug release but also interacts with the overexpressed CD44 receptor on the cancer cell to selectively target the cancer cells. These systems facilitate combined therapy and selectively targeted cancer cells to reduce drug side effects and improve cancer therapeutic efficacy.

Chapter 5 describes the polyvalent coordination bonds of MOF with polymers, which have the carboxylic acid to develop a stable nanomedicine in the body for enhanced cancer treatment effectiveness. NanoMOF, which has a high surface, porosity, and easily controllable structure, has received much attention in the drug delivery systems. In particular, the unsaturated metal clusters present on the surface of MOF can easily form the coordination bond with other compounds for post modification. Various nanoMOF drug delivery systems utilize this feature to modify the cancer-targeting ligand or DNA on the surface of MOF, but a variety of proteins and biocompounds that have a Lewis base, and these materials induce the detachment of compounds that modified MOF surface. Therefore, in order to prevent above detachment and to increase cancer therapeutic effects, we researched stable systems in the body by using a polyvalent coordination bond of MOF with polymer.

Portions of the thesis have been published

Chapter 2: Kim, K.; Jo, M.C.; Jeong, S.; Palanikumar, L.; Rotello, V. M.; Ryu, J.-H.; Park, M.-H. "Externally controlled drug release using a gold nanorod contained composite membrane" *Nanoscale,* **2016,** *8,* 11949-11955.

**1.4 Reference**

1. Stewart, B.; Kleihues, P., IARC, World Cancer Report. *IARC. Lyon* **2003**.

2. Society, A. C., *Breast cancer facts & figures*. American Cancer Society: 2007.

3. Ballard-Barbash, R.; Potosky, A. L.; Harlan, L. C.; Nayfield, S. G.; Kessler, L. G., Factors associated with surgical and radiation therapy for early stage breast cancer in older women. *JNCI: Journal of the National Cancer Institute* **1996,** *88* (11), 716-726.

4. Laurie, J. A.; Moertel, C.; Fleming, T.; Wieand, H.; Leigh, J.; Rubin, J.; McCormack, G.; Gerstner, J.; Krook, J.; Malliard, J., Surgical adjuvant therapy of large-bowel carcinoma: an evaluation of levamisole and the combination of levamisole and fluorouracil. The North Central Cancer Treatment Group and the Mayo Clinic. *Journal of Clinical Oncology* **1989,** *7* (10), 1447-1456.

5. Singletary, S. E., Surgical margins in patients with early-stage breast cancer treated with breast conservation therapy. *The American journal of surgery* **2002,** *184* (5), 383-393.

6. Chithrani, D. B.; Jelveh, S.; Jalali, F.; van Prooijen, M.; Allen, C.; Bristow, R. G.; Hill, R. P.; Jaffray, D. A., Gold nanoparticles as radiation sensitizers in cancer therapy. *Radiation research* **2010,** *173* (6), 719-728.

7. D'amico, A. V.; Whittington, R.; Malkowicz, S. B.; Schultz, D.; Blank, K.; Broderick, G. A.; Tomaszewski, J. E.; Renshaw, A. A.; Kaplan, I.; Beard, C. J., Biochemical outcome after radical prostatectomy, external beam radiation therapy, or interstitial radiation therapy for clinically localized prostate cancer. *Jama* **1998,** *280* (11), 969-974.

8. Milenic, D. E.; Brady, E. D.; Brechbiel, M. W., Antibody-targeted radiation cancer therapy. *Nature Reviews Drug Discovery* **2004,** *3* (6), 488.

9. DeVita, V. T.; Chu, E., A history of cancer chemotherapy. *Cancer research* **2008,** *68* (21), 8643-8653.

10. Frei III, E.; Canellos, G. P., Dose: a critical factor in cancer chemotherapy. *The American journal of medicine* **1980,** *69* (4), 585-594.

11. Matsumura, Y.; Maeda, H., A new concept for macromolecular therapeutics in cancer chemotherapy: mechanism of tumoritropic accumulation of proteins and the antitumor agent smancs. *Cancer research* **1986,** *46* (12 Part 1), 6387-6392.

12. Allen, T. M.; Cullis, P. R., Drug delivery systems: entering the mainstream. *Science* **2004,** *303* (5665), 1818-1822.

13. Chowdhary, R. K.; Shariff, I.; Dolphin, D., Drug release characteristics of lipid based benzoporphyrin derivative. *J Pharm Pharm Sci* **2003,** *6* (1), 13-9.

14. Doane, T. L.; Burda, C., The unique role of nanoparticles in nanomedicine: imaging, drug delivery and therapy. *Chemical Society Reviews* **2012,** *41* (7), 2885-2911.

15. Ranganathan, R.; Madanmohan, S.; Kesavan, A.; Baskar, G.; Krishnamoorthy, Y. R.; Santosham, R.; Ponraju, D.; Rayala, S. K.; Venkatraman, G., Nanomedicine: towards development of patient-

friendly drug-delivery systems for oncological applications. *International journal of nanomedicine* **2012,** *7*, 1043.

16. Vieira, D. B.; Gamarra, L. F., Advances in the use of nanocarriers for cancer diagnosis and treatment. *Einstein (São Paulo)* **2016,** *14* (1), 99-103.

17. Liu, Y.; Miyoshi, H.; Nakamura, M., Nanomedicine for drug delivery and imaging: a promising avenue for cancer therapy and diagnosis using targeted functional nanoparticles. *Int J Cancer* **2007,** *120* (12), 2527-37.

18. Bertrand, N.; Wu, J.; Xu, X.; Kamaly, N.; Farokhzad, O. C., Cancer nanotechnology: the impact of passive and active targeting in the era of modern cancer biology. *Adv Drug Deliv Rev* **2014,** *66*, 2-25.

19. Danhier, F.; Feron, O.; Preat, V., To exploit the tumor microenvironment: Passive and active tumor targeting of nanocarriers for anti-cancer drug delivery. *J Control Release* **2010,** *148* (2), 135-46.

20. Kelso, G. F.; Porteous, C. M.; Coulter, C. V.; Hughes, G.; Porteous, W. K.; Ledgerwood, E. C.; Smith, R. A.; Murphy, M. P., Selective targeting of a redox-active ubiquinone to mitochondria within cells: antioxidant and antiapoptotic properties. *J Biol Chem* **2001,** *276* (7), 4588-96.

21. Ye, J.; Wang, Q.; Zhou, X.; Zhang, N., Injectable actarit-loaded solid lipid nanoparticles as passive targeting therapeutic agents for rheumatoid arthritis. *Int J Pharm* **2008,** *352* (1-2), 273-9.

22. Brannon-Peppas, L.; Blanchette, J. O., Nanoparticle and targeted systems for cancer therapy. *Advanced Drug Delivery Reviews* **2012,** *64*, 206-212.

23. Peer, D.; Karp, J. M.; Hong, S.; Farokhzad, O. C.; Margalit, R.; Langer, R. Nanocarriers as an emerging platform for cancer therapy. *Nature nanotechnology*, **2007** *2* (12), 751-760.

24. Sykes, E. A.; Chen, J.; Zheng, G.; Chan, W. C., Investigating the impact of nanoparticle size on active and passive tumor targeting efficiency. *ACS Nano* **2014,** *8* (6), 5696-706.

25. Singh, R.; Lillard, J. W., Jr., Nanoparticle-based targeted drug delivery. *Exp Mol Pathol* **2009,** *86* (3), 215-23.

26. Torchilin, V. P., Recent advances with liposomes as pharmaceutical carriers. *Nat Rev Drug Discov* **2005,** *4* (2), 145-60.

27. Palanikumar, L.; Choi, E. S.; Oh, J. Y.; Park, S. A.; Choi, H.; Kim, K.; Kim, C.; Ryu, J. H., Importance of Encapsulation Stability of Nanocarriers with High Drug Loading Capacity for Increasing in Vivo Therapeutic Efficacy. *Biomacromolecules* **2018,** *19* (7), 3030-3039.

28. Palanikumar, L.; Kim, H. Y.; Oh, J. Y.; Thomas, A. P.; Choi, E. S.; Jeena, M. T.; Joo, S. H.; Ryu, J. H., Noncovalent Surface Locking of Mesoporous Silica Nanoparticles for Exceptionally High Hydrophobic Drug Loading and Enhanced Colloidal Stability. *Biomacromolecules* **2015,** *16* (9), 2701-14.

29. Chacko, R. T.; Ventura, J.; Zhuang, J.; Thayumanavan, S., Polymer nanogels: a versatile nanoscopic drug delivery platform. *Adv Drug Deliv Rev* **2012,** *64* (9), 836-51.

30. Liu, J.; Detrembleur, C.; De Pauw-Gillet, M. C.; Mornet, S.; Jerome, C.; Duguet, E., Gold nanorods coated with mesoporous silica shell as drug delivery system for remote near infrared light-activated release and potential phototherapy. *Small* **2015,** *11* (19), 2323-32.

31. Zhang, Z.; Wang, L.; Wang, J.; Jiang, X.; Li, X.; Hu, Z.; Ji, Y.; Wu, X.; Chen, C., Mesoporous silica-coated gold nanorods as a light-mediated multifunctional theranostic platform for cancer treatment. *Adv Mater* **2012,** *24* (11), 1418-23.

32. Zhang, Q.; Wang, X.; Li, P.-Z.; Nguyen, K. T.; Wang, X.-J.; Luo, Z.; Zhang, H.; Tan, N. S.; Zhao, Y., Biocompatible, Uniform, and Redispersible Mesoporous Silica Nanoparticles for Cancer-Targeted Drug Delivery In Vivo. *Advanced Functional Materials* **2014,** *24* (17), 2450-2461.

33. Kim, H.; Kim, S.; Park, C.; Lee, H.; Park, H. J.; Kim, C., Glutathione-induced intracellular release of guests from mesoporous silica nanocontainers with cyclodextrin gatekeepers. *Adv Mater* **2010,** *22* (38), 4280-3.

34. Mura, S.; Nicolas, J.; Couvreur, P., Stimuli-responsive nanocarriers for drug delivery. *Nat Mater* **2013,** *12* (11), 991-1003.

35. Park, M. H.; Subramani, C.; Rana, S.; Rotello, V. M., Chemoselective nanoporous membranes via chemically directed assembly of nanoparticles and dendrimers. *Adv Mater* **2012,** *24* (43), 5862-6.

36. Park, M. H.; Agasti, S. S.; Creran, B.; Kim, C.; Rotello, V. M., Controlled and sustained release of drugs from dendrimer-nanoparticle composite films. *Adv Mater* **2011,** *23* (25), 2839-42, 2843.

37. Li, Z.; Huang, P.; Zhang, X.; Lin, J.; Yang, S.; Liu, B.; Gao, F.; Xi, P.; Ren, Q.; Cui, D., RGD-conjugated dendrimer-modified gold nanorods for in vivo tumor targeting and photothermal therapy. *Mol Pharm* **2010,** *7* (1), 94-104.

38. Alkilany, A. M.; Thompson, L. B.; Boulos, S. P.; Sisco, P. N.; Murphy, C. J., Gold nanorods: their potential for photothermal therapeutics and drug delivery, tempered by the complexity of their biological interactions. *Adv Drug Deliv Rev* **2012,** *64* (2), 190-9.

39. Liu, W.; Zhu, Z.; Deng, K.; Li, Z.; Zhou, Y.; Qiu, H.; Gao, Y.; Che, S.; Tang, Z., Gold nanorod@chiral mesoporous silica core-shell nanoparticles with unique optical properties. *J Am Chem Soc* **2013,** *135* (26), 9659-64.

40. Shen, S.; Tang, H.; Zhang, X.; Ren, J.; Pang, Z.; Wang, D.; Gao, H.; Qian, Y.; Jiang, X.; Yang, W., Targeting mesoporous silica-encapsulated gold nanorods for chemo-photothermal therapy with near-infrared radiation. *Biomaterials* **2013,** *34* (12), 3150-8.

41. He, Y.; Zhou, W.; Qian, G.; Chen, B., Methane storage in metal−organic frameworks. *Chemical Society Reviews* **2014,** *43* (16), 5657-5678.

42. Ma, S.; Zhou, H.-C., Gas storage in porous metal−organic frameworks for clean energy applications. *Chemical Communications* **2010,** *46* (1), 44-53.

43. Mason, J. A.; Veenstra, M.; Long, J. R., Evaluating metal−organic frameworks for natural gas storage. *Chemical Science* **2014,** *5* (1), 32-51.

44. Chen, B.; Liang, C.; Yang, J.; Contreras, D. S.; Clancy, Y. L.; Lobkovsky, E. B.; Yaghi, O. M.; Dai, S., A Microporous Metal−Organic Framework for Gas-Chromatographic Separation of Alkanes. *Angewandte Chemie International Edition* **2006,** *45* (9), 1390-1393.

45. Li, J.-R.; Kuppler, R. J.; Zhou, H.-C., Selective gas adsorption and separation in metal−organic frameworks. *Chemical Society Reviews* **2009,** *38* (5), 1477-1504.

46. Li, J.-R.; Sculley, J.; Zhou, H.-C., Metal−organic frameworks for separations. *Chemical reviews* **2011,** *112* (2), 869-932.

47. Lee, J.; Farha, O. K.; Roberts, J.; Scheidt, K. A.; Nguyen, S. T.; Hupp, J. T., Metal−organic framework materials as catalysts. *Chemical Society Reviews* **2009,** *38* (5), 1450-1459.

48. Rogge, S. M.; Bavykina, A.; Hajek, J.; Garcia, H.; Olivos-Suarez, A. I.; Sepúlveda-Escribano, A.; Vimont, A.; Clet, G.; Bazin, P.; Kapteijn, F., Metal−organic and covalent organic frameworks as single-site catalysts. *Chemical Society Reviews* **2017,** *46* (11), 3134-3184.

49. Zhu, L.; Liu, X.-Q.; Jiang, H.-L.; Sun, L.-B., Metal−organic frameworks for heterogeneous basic catalysis. *Chemical reviews* **2017,** *117* (12), 8129-8176.

50. Chen, B.; Wang, L.; Xiao, Y.; Fronczek, F. R.; Xue, M.; Cui, Y.; Qian, G., A luminescent metal−organic framework with Lewis basic pyridyl sites for the sensing of metal ions. *Angewandte Chemie International Edition* **2009,** *48* (3), 500-503.

51. Hu, Z.; Deibert, B. J.; Li, J., Luminescent metal−organic frameworks for chemical sensing and explosive detection. *Chemical Society Reviews* **2014,** *43* (16), 5815-5840.

52. Kreno, L. E.; Leong, K.; Farha, O. K.; Allendorf, M.; Van Duyne, R. P.; Hupp, J. T., Metal−organic framework materials as chemical sensors. *Chemical reviews* **2011,** *112* (2), 1105-1125.

53. Horcajada, P.; Chalati, T.; Serre, C.; Gillet, B.; Sebrie, C.; Baati, T.; Eubank, J. F.; Heurtaux, D.; Clayette, P.; Kreuz, C.; Chang, J. S.; Hwang, Y. K.; Marsaud, V.; Bories, P. N.; Cynober, L.; Gil, S.; Ferey, G.; Couvreur, P.; Gref, R., Porous metal-organic-framework nanoscale carriers as a potential platform for drug delivery and imaging. *Nat Mater* **2010,** *9* (2), 172-8.

54. Wu, M. X.; Yang, Y. W., Metal-Organic Framework (MOF)-Based Drug/Cargo Delivery and Cancer Therapy. *Adv Mater* **2017,** *29* (23).

55. He, C.; Liu, D.; Lin, W., Nanomedicine Applications of Hybrid Nanomaterials Built from Metal-Ligand Coordination Bonds: Nanoscale Metal-Organic Frameworks and Nanoscale Coordination Polymers. *Chem Rev* **2015,** *115* (19), 11079-108.

56. Lu, K.; He, C.; Lin, W., Nanoscale metal-organic framework for highly effective photodynamic therapy of resistant head and neck cancer. *J Am Chem Soc* **2014,** *136* (48), 16712-5.

57. Park, J.; Jiang, Q.; Feng, D.; Mao, L.; Zhou, H. C., Size-Controlled Synthesis of Porphyrinic Metal-Organic Framework and Functionalization for Targeted Photodynamic Therapy. *J Am Chem Soc* **2016,** *138* (10), 3518-25.

# Chapter 2. Externally controlled drug release using a gold nanorod contained composite membrane.

## 2.1 Abstract

Versatile drug delivery devices using nanoporous membranes consisting of gold nanorods and dendrimers have been demonstrated to provide light-triggered on-demand pulsatile release from a reservoir containing highly enriched therapeutics for a real patient's needs. The drug release rate is directly correlated with the temperature increase and irradiated energy of a near-IR laser in both static and fluidic devices. This biocompatible platform for on-demand control was further confirmed by in vitro experiments. Interestingly, different responses to stimuli were obtained from each drug in the absence and presence of NIR light, indicating the versatile potential of our on-demand drug delivery system in less-invasive therapies requiring multi-drug delivery strategies. The enhanced delivery system will improve therapeutic efficacy and reduce side effects through regulation of plasma drug profiles.

## 2.2 Introduction

Biomaterials with stimuli-responsive properties, also known as smart materials, have the unique ability to alter their chemical or physical properties for applications in optoelectronics, sensors and actuator devices, surface coating, storage, and drug delivery applications.[1-3] The responsiveness of these biomaterials can be changed or tuned in a reproducible and predictable manner through chemical, biological, and physical stimuli. These responses can be generated by a number of stimuli relating to the properties of scaffolds for example solvent dissolution, pH, ionic strength, and temperature, and response to external fields for example near-infrared, visible light, ultrasound, or electric and magnetic fields, and molecular functions for example receptor recognition and enzymemediated reactions.[4-11] The Stimuli-responsive biomaterials are critical in the province of drug delivery because of the difficulty in sustaining an effective therapeutic range of the drugs over a defined period of time to avoid overdosing or underdosing.[12-15] Additionally, many drugs require frequent and continuous administration over long periods.[16-18] Finally, the ability of drug delivery systems to be manipulated externally and programmed spatially and temporally within the desired therapeutic window provides an important tool to satisfy the needs of a patient.[19-22] However, only a few studies have been applied in commercial clinical settings because delivering pulsatile or variably programmed drug release patterns in an easy manner has not been well studied yet.[23]

A light-activated drug delivery system provides several benefits such as ease of control, locally selective exposure, and harmlessness to body tissues.[24-26] Near-infrared (NIR) light, in the range from 650 and 900 nm, provides a particularly useful avenue because hemoglobin and water strongly absorb infrared light (>900 nm) and visible (<650 nm), respectively, leaving the NIR as a window.[27-29]

Plasmonic materials are particularly promising for these applications: NIR light can penetrate body tissues at a depth of 10 cm over with no significant damage, inducing localized heat at a NIR wavelength corresponding to the plasmonic resonance of the contained nanoparticles, called the photothermal effect.[30-36]

Recently, we reported a dendrimer-nanoparticle composite film formed via dithiocarbamate (DTC) crosslinking of small gold nanoparticles in the presence of carbon disulfide ($CS_2$).[37,38] This biocompatible, highly flexible composite film is capable of delivering various molecules such as biologics and drugs, enabling the controlled release of therapeutics and the design of devices capable of sustained release. We report here the use of a nanoporous membrane consisting of gold-nanorods (GNRs) and dendrimers that enables on-demand pulsatile release from a reservoir containing highly enriched therapeutics. These light-responsive GNR-dendrimer (GNR-Den) composites generate localized heat around the GNRs in the membrane when stimulated with NIR light. The increasing heat of the membrane increases the diffusion coefficient, accelerating the release rate of drugs and ultimately enabling high-resolution control of drug release based on the patient's state (Figure 2-1).

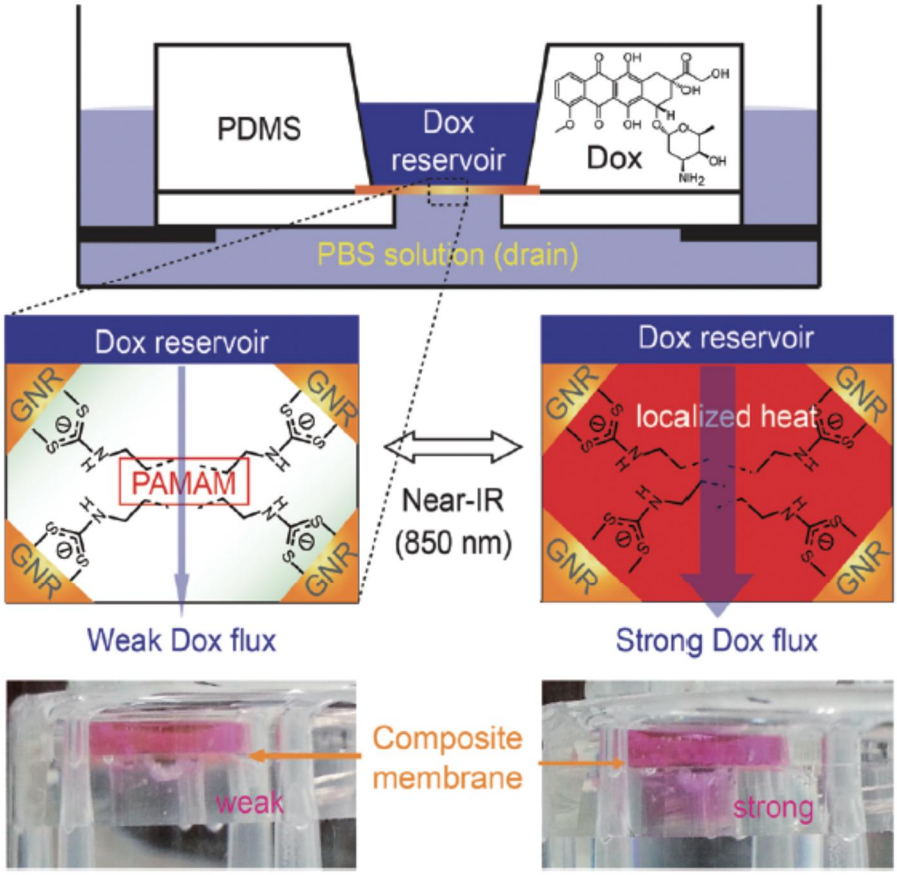


**Figure 2-4.** A schematic illustration for light triggered Dox release using the device with the GNR–Den composite membrane and the bottom pictures indicate each color change in the absence and presence of NIR light in the drain passage of the device.

**2.3 Results and discussion**

The GNR–Den films were formed via chemical reaction by DTC crosslinking between dendrimers and GNRs (60 nm length and 15 nm width) capped with cetyltrimethylammonium bromide (CTAB). The films were coated on the both sides of amine-functionalized anodized aluminum oxide (AAO) membrane having hexagonally packed cylindrical nano-channels with uniform pore sizes with a diameter of 20 nm.[40] The image of scanning electron microscopy (SEM) and picture of membranes indicate the successful formation of a smooth composite film with a thickness of ~0.7 μm on an AAO membrane (Figure 2-2 & Figure 2-3b). The GNR-Den film was fabricated on a slide glass substrate and characterized by ultraviolet-visible (UV-Vis) spectroscopy to determine the optical properties. As shown in Figure 2-2b, the black line indicates the typical longitudinal plasmonic band of the original CTAB-GNRs, while a strong red shift (the red line) is seen in the dry state after film formation due to the decrease in the interparticle spacing between GNRs.[41] In an aqueous solution, the composite film containing highly permeable dendrimers can be extended because of solvent swelling, causing an increase in distance between the chemically assembled GNRs and concomitant with blue shift in the UV-Vis spectrum (the blue line) (Figure. 2-3a).

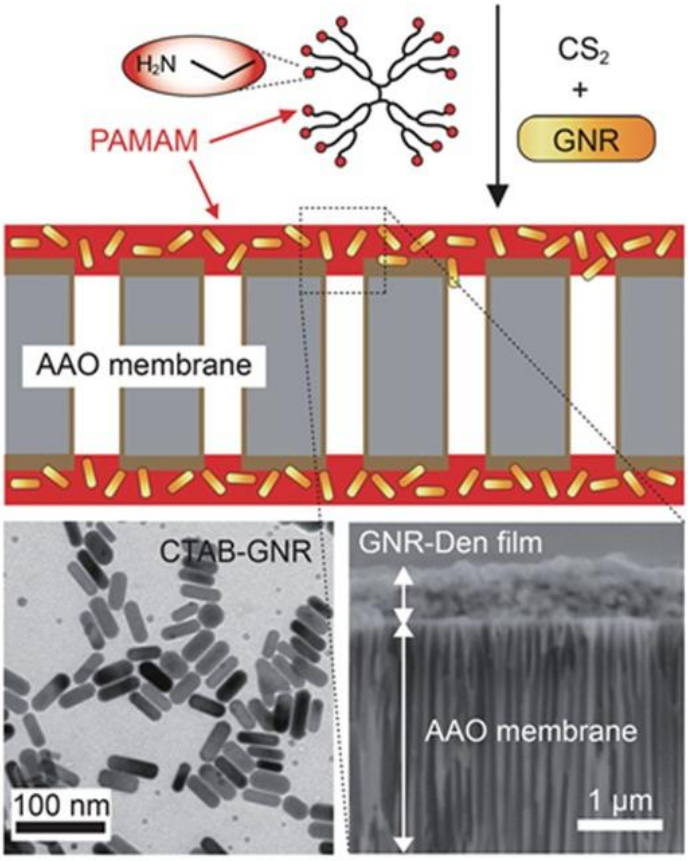


**Figure 2-5.** Schematic illustration for the formation of a GNR-Den composite membrane, a TEM image used in the membrane fabrication, and a SEM image of the composite membrane onto AAO.

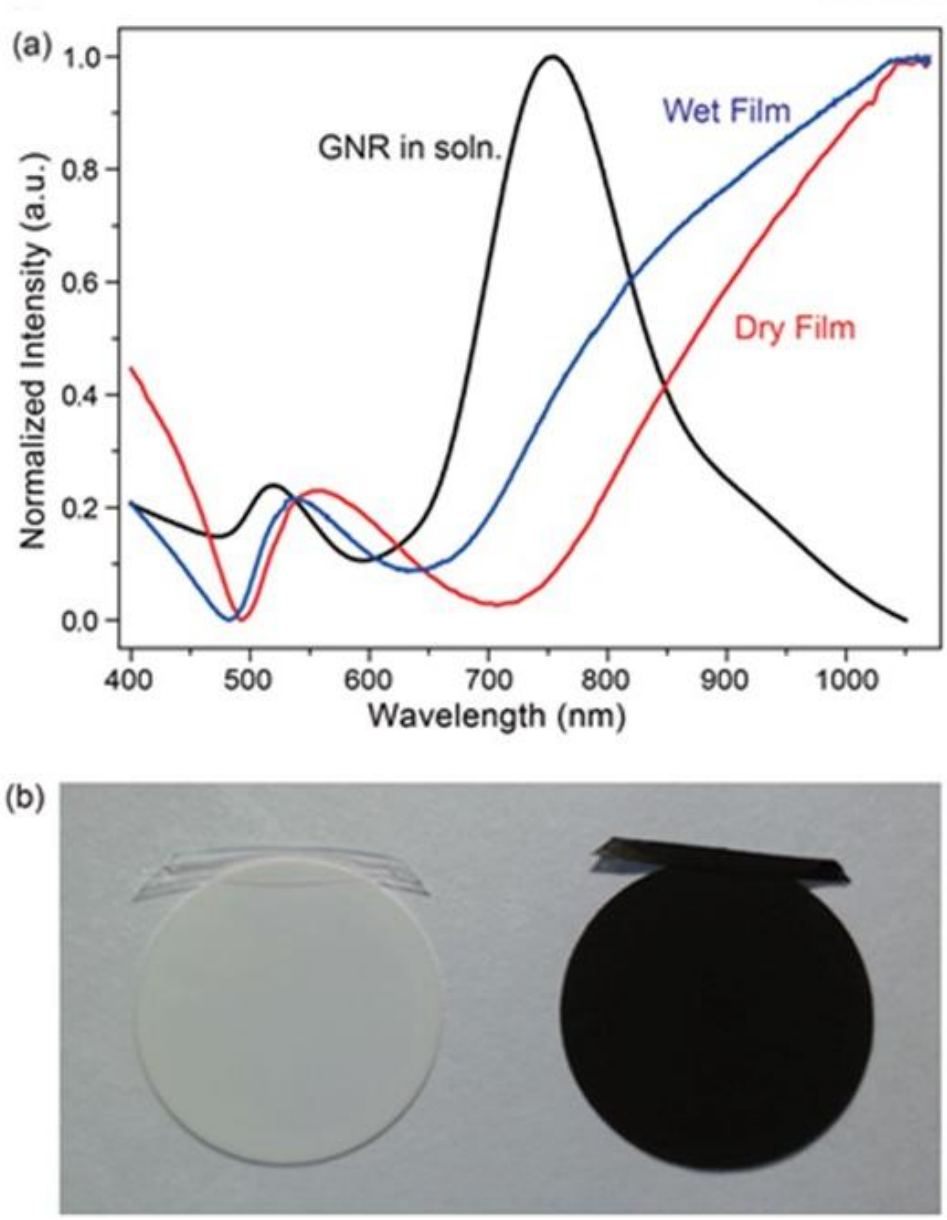


**Figure 2-6.** (a) UV-Vis spectra of a GNR solution (black), dry film (red), and wet film (blue). (b) Apicture of a bare AAO membrane (left) and a GNR-Den composite membrane (right)

The fabricated GNR-Den-AAO membrane was fitted between polydimethyl siloxane(PDMS) replicas to form a programmable passage for drug supplies from a reservoir (Figure 2-1). Diffusion is the process of the kinetic energy by which molecules and particles randomly blend together, leading to a phenomenon where they move from an area of high concentration to an area of low concentration. The rate of diffusion is affected by several factors including temperature, density of the diffusing substance, medium of diffusion, and concentration gradient. Among them, temperature is a key factor for diffusion that can be explicated using the Stokes-Einstein-Sutherland equation.

$$D = uk_BT = \frac{k_BT}{6\pi\eta R} \qquad (1)$$

where D is the diffusion constant, μ is the mobility of particles, $k_B$ is Boltzmann's constant, and T is the absolute temperature. For diffusion of spherical particles through a liquid, η is the dynamic viscosity and R is the radius of the spherical particle. In addition, as the temperature increases, the average kinetic energy of molecules increases, and the increased kinetic energy causes increased velocities, providing a greater chance of collisions between molecules and resulting in an increased rate of diffusion. Therefore, the delivery mechanism with our device based on diffusion should be strongly related to temperature, both due to basic diffusion parameters and changes in the thermoresponsive membrane.[42]

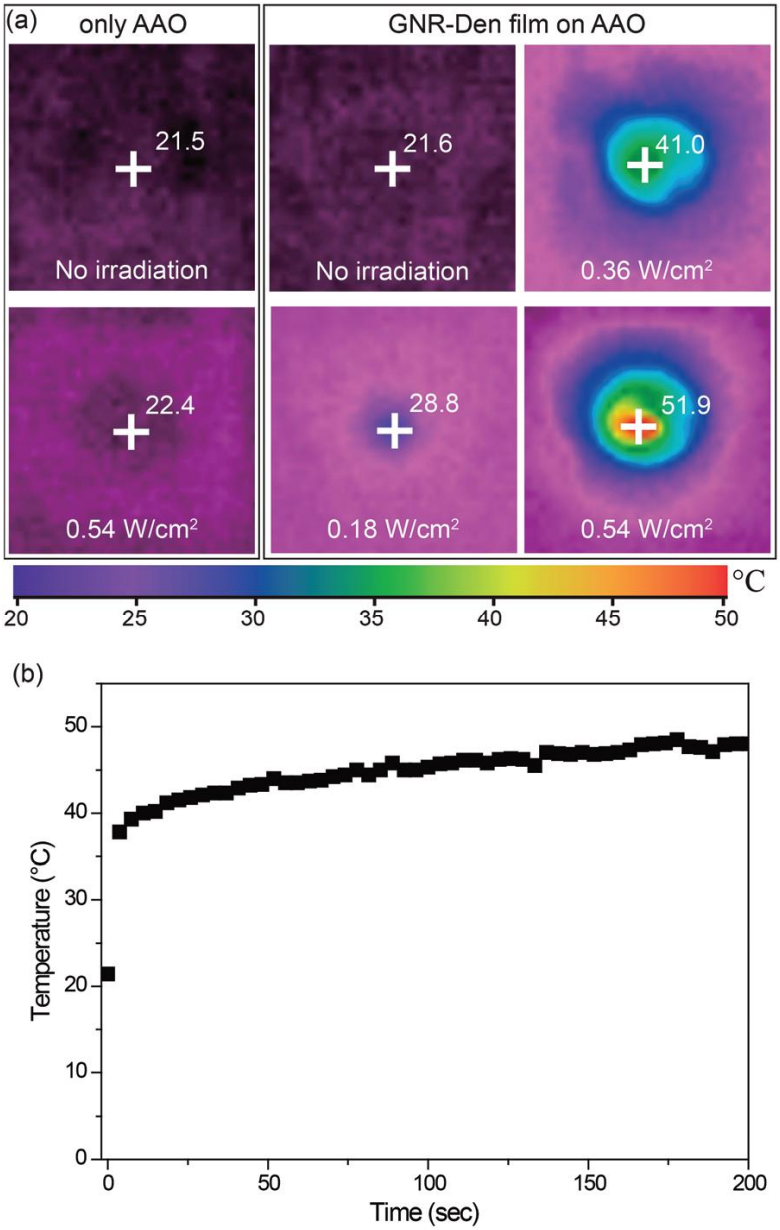


**Figure 2-7.** (a) The temperature traces with and without a GNR-Den film on AAO measured by using an infrared camera at a NIR power of 0, 0.18, 0.36, and 0.54 W $cm^{-2}$. (b) The temperature response from the device by NIR irradiation with a power of 0.54 W $cm^{-2.}$

To validate our hypothesis, temperature traces of the device containing a GNR-Den membrane upon NIR irradiation were recorded first using an infrared camera (Figure 2-4a). In the absence of NIR light, normal room temperature (21.6 and 21.5 °C) was observed in the device with and without a GNR-Den membrane, respectively. Upon continuous NIR irradiation, the device with a GNR-Den composite membrane showed the increased temperature of 28.8, 41.0, 51.9 °C depending on the energy (0.18, 0.36, 0.54 W $cm^{-2}$, respectively) of the irradiated NIR light (λ= 850 nm). No significant change in temperature was observed in the device without a composite membrane (22.4 °C) (Figure 2-4a).

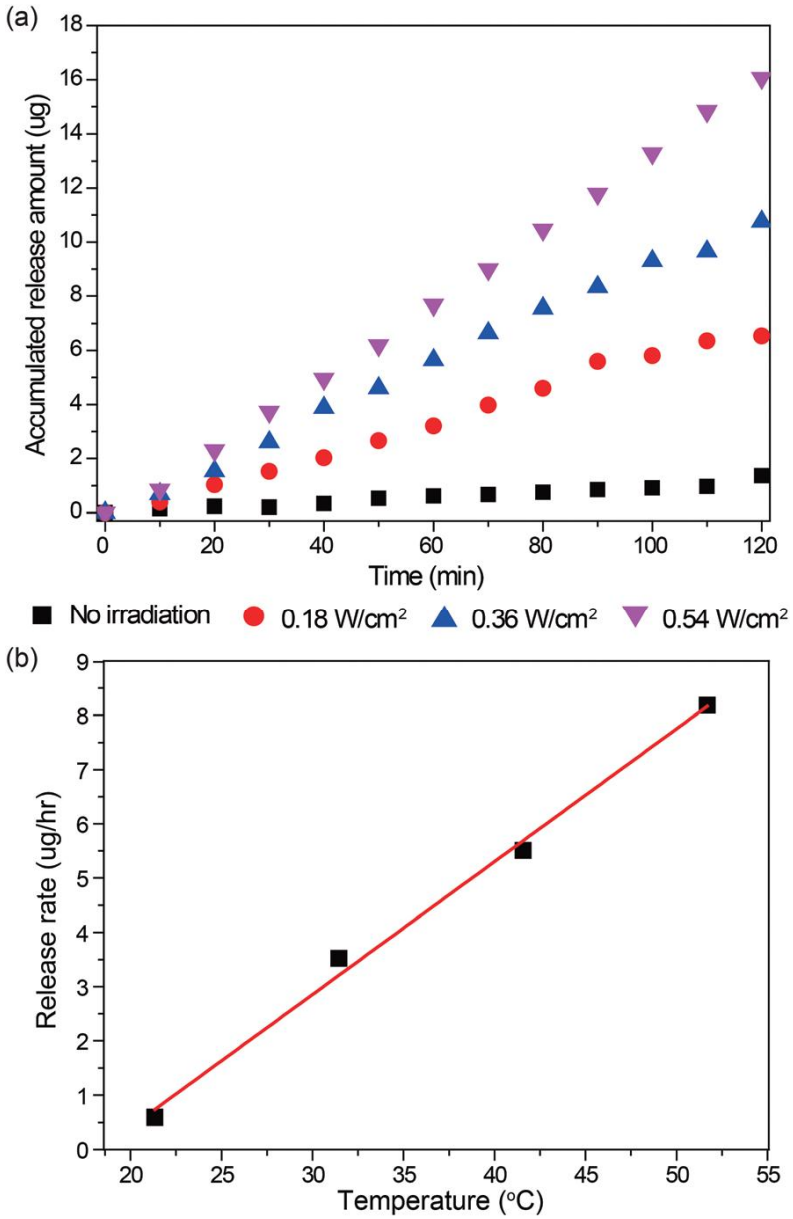


**Figure 2-8.** (a) The Dox release profiles for accumulated amounts from the device at NIR powers of 0, 0.18, 0.36, and 0.54 W $cm^{-2}$. (b) The Dox release rate profile is based on temperature controlled by a NIR power.

Figure 2-4b shows the kinetic thermal response of the composite membrane by NIR irradiation with the energy 0.54 W $cm^{-2}$. The rapid increase from 21.4 to 40 °C was seen within 10 s while a gradual increase was observed from 10 to 200 s. Because the thermal response of the GNRs upon NIR irradiation has been known to be much faster,[43] we assume that the temperature increase measured by using an infrared camera includes the water content in a drug reservoir. After investigating temperature response upon NIR irradiation, doxorubicin hydrochloride (Dox) was chosen as a model drug to investigate the on-demand release feature of the membrane. Figure 2-5 shows the cumulative amounts of Dox released from the reservoir. With the same concentration of Dox solution (850 μM, 0.4 mL) in the reservoir, on-demand, zero-order release was achieved that was directly correlated to the power of NIR irradiation. Release rates of 3.5, 5.5, and 8.2 μg $h^{-1}$ were obtained with light powers of 0.18, 0.36, and 0.54 W $cm^{-2}$, respectively, while low release (0.5 μg observed in a control experiment with no NIR. These results indicate a $h^{-1}$) was direct relationship between the amounts of released drugs, temperature, and irradiated light energy, suggesting an efficient strategy for on-demand controlled release. To demonstrate the robustness of our membrane, the collected aliquots from the accumulated drain layer after 3, 9, 12, and 36 hours in the presence of NIR light and 336 hours in the absence of NIR light were further analyzed using ICP-Mass. The negligible signals (<1 μg $L^{-1}$) concerning gold (267.594) observed with each sample indicate that our GNR-Den membrane in devices is robustly retained during light stimuli. We next integrated our membrane into a continuous flow system. The GNR-Den-AAO membrane was fitted into a PBS flow system consisting of PDMS channel and peristaltic pump, just as shown in Figure 2-5a. With a continuous PBS flow (4 mL $h^{-1}$) each fraction was collected for every 5 min. Figure 2-5b shows the Dox amounts of each fraction as analyzed using UV-Vis spectroscopy and a fluorimeter. Strikingly, rapid and strong release of Dox from the fluidic device was observed upon NIR irradiation, while slow release was shown in the absence of NIR light. This reversible phenomenon can be obtained continuously when the switch is ON/OFF and also utilized for the patients who unexpectedly require a high flux of drugs. After successfully demonstrating the light-triggered release of drugs through the GNR-Den membrane, we further investigated the ability to efficiently regulate drug amounts in cancer cells cultured in in vitro experiments. SCC-7 cancer cells were treated with drug aliquots collected in the presence of NIR irradiation (40 min (NIR1) and 120 min (NIR2)) and in the absence of NIR irradiation (80 min (NoLight1) and 160 min (NoLight2)), and cell viability was determined after 48 h and 72 h using alamar blue dye assay. The cell viability assays with both aliquots collected in the presence of NIR light revealed that Dox delivery significantly decreased cell viability to lower than 25% and 10% after 48 h and 72 h, respectively, whereas a relatively small decrease in the viability (to approximately 60-75%) was observed with the aliquots collected in the absence of NIR light (Figure 2-6c). These results suggest that our GNR-contained membrane can be used to control on-demand release of therapeutics based on the conditions of patients who require doses of drugs frequently and precisely.

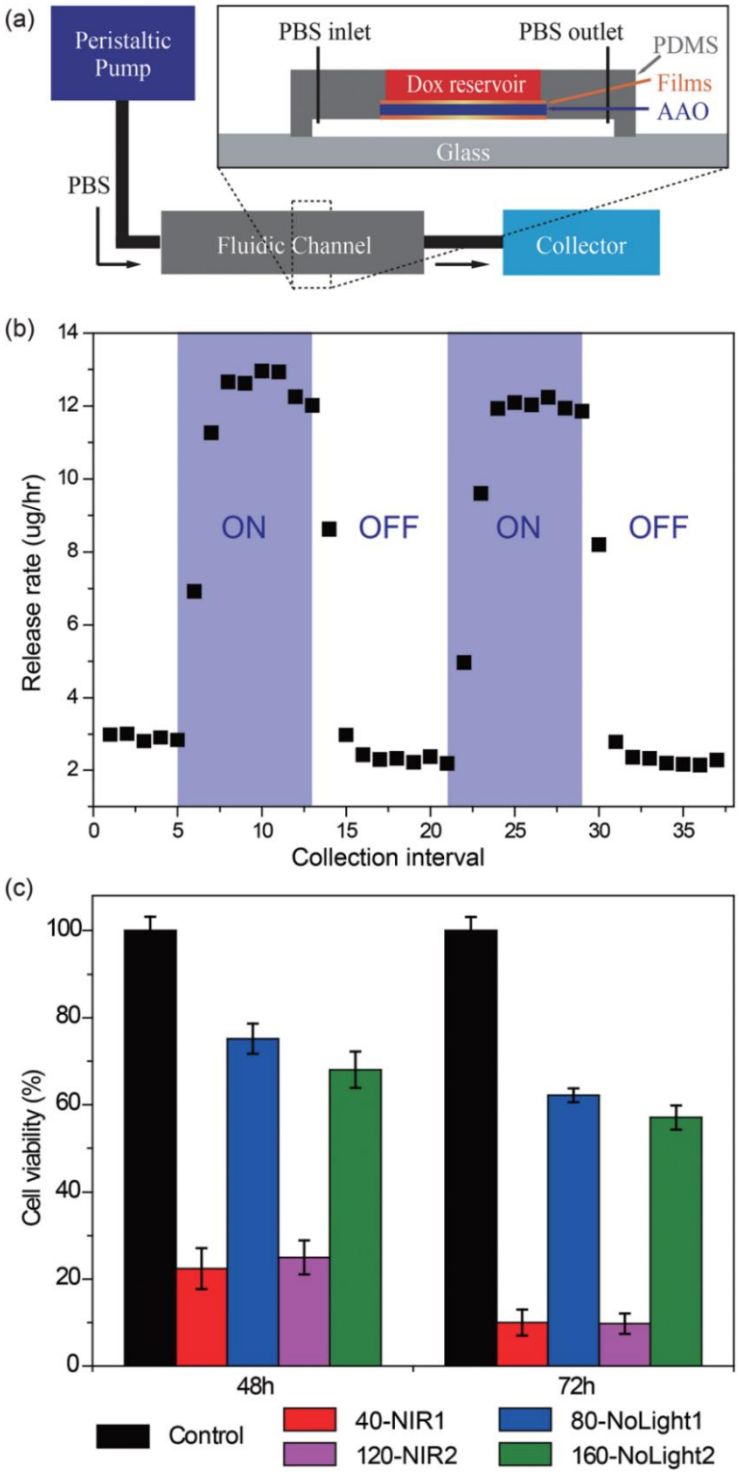


**Figure 2-9.** (a) Schematic illustration of the fluidic system experimental set-up with the GNR-Den composite membrane, (b) Dox release profile in the absence (OFF) and presence (ON) of the NIR light (850 nm, 0.54 W $cm^{-2}$, 5 min collection interval), and (c) in vitro cytotoxicity of aliquots collected at 80 (NoLight1) and 160 min (NoLight2) with no irradiation and at 40 (NIR1) and 120 min (NIR2) with NIR irradiation after 48 h and 72 h incubation.

For example, the minimum drug concentration in a therapeutic range has been retained usually depending on individual patients, however when the necessity arises, it becomes accelerated by switching ON for NIR irradiation to provide a high dosage. Previously, our research group has demonstrated the effectiveness of post-functionalized composite membranes in controlling the diffusion rate based on the analyte charge, porosity, and hydrophobicity.[44] The functionalized composite membrane capable of interacting with each analyte more selectively can efficiently control the diffusion rate of the analytes. We assumed that because both the prior and current systems are based on a diffusion release mechanism, the functionalized membrane will also provide multi-drug releases with programmable pharmacokinetics in a delivery system. This means our system can provide a controlled concentration for each drug in an each therapeutic range of relevance through not only an initial feeding ratio of multi drugs but also their chemical structure.

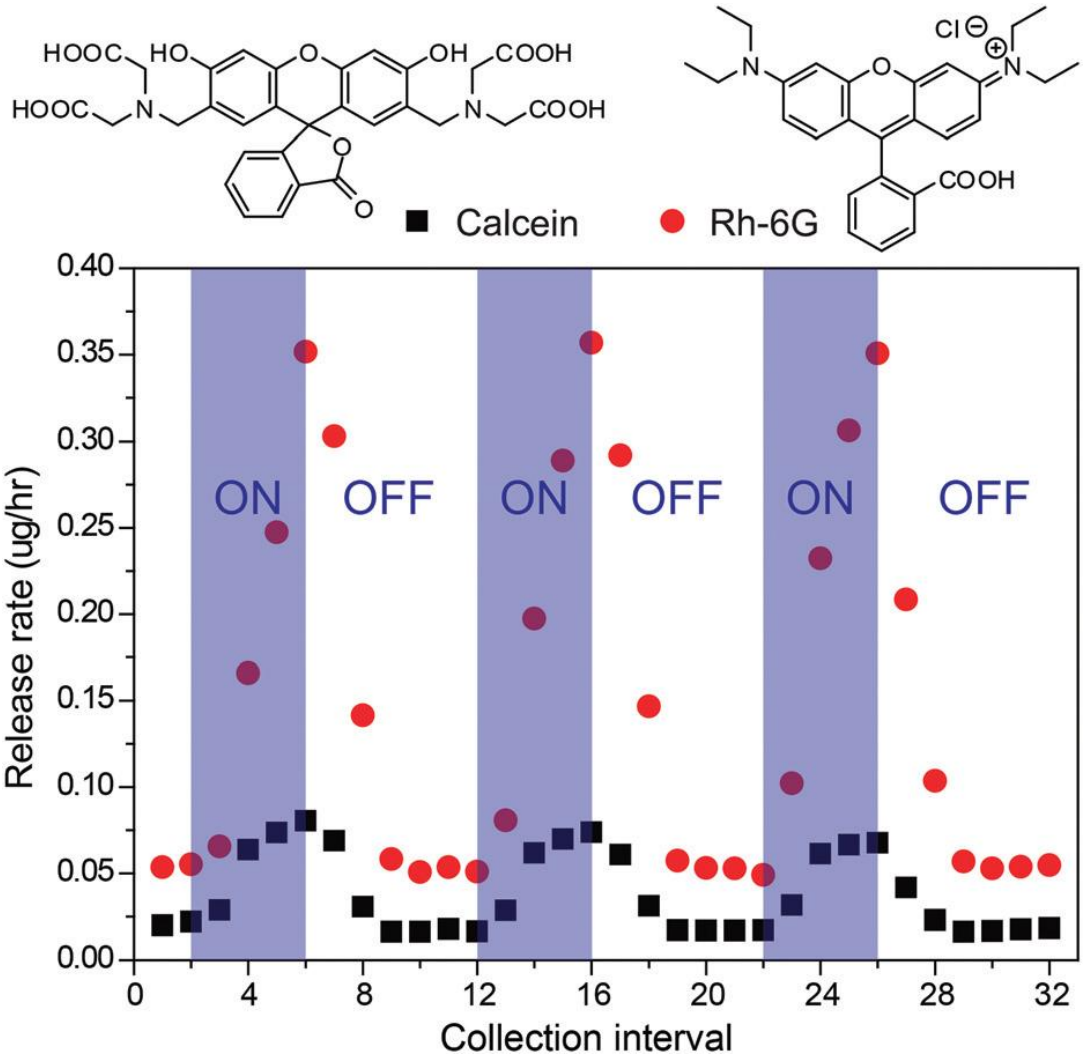


**Figure 1-10.** Molecular structures and their pulsatile release profiles from a mixture of calcein and Rh-6G from the TMA-GNR-Den membrane contained fluidic device (850 nm, 0.54 W $cm^{-2}$, 2.5 min collection interval).

As a proof-of-concept of a multi-drug delivery system with different pharmacokinetics, the positively charged composite membrane was utilized with two watersoluble organic dyes (anionic calcein and cationic rhodamine 6G (Rh-6G)) with opposite charges but similar structures. The positively charged trimethyl ammonium (TMA)-functionalized membrane was fabricated by the post-functionalization method previously mentioned[15] and fitted into the fluidic device. With a continuous PBS flow (4 mL $h^{-1}$) each fraction was collected for every 2.5 min. Initially, the different concentrations of two dyes were observed before NIR irradiation despite the same feeding ratio (Rh-6G:calcein=1:1), because the positively charged TMA membrane interacted more strongly with anionic calcein, which retarded its release, than with cationic Rh-6G. However, different diffusion responses were observed in the presence of NIR light (Figure 2-7). The localized heat caused by NIR irradiation accelerated the release rate of both dyes as mentioned above. Interestingly, Rh-6G weakly interacted with the TMA membrane showing a much faster release (7 times higher than before irradiation), while a comparatively small acceleration of calcein release (3 times higher than before irradiation) was observed because of their strong reciprocal interaction with the TMA membrane (Figure 2-7). Overall, the difference in concentration was two times in the absence of NIR light, but it becomes 4.5 times in the presence of NIR light. This phenomenon can be efficiently used when the release of multi-drugs is limited to different therapeutic ranges for each drug, opening a new way with our versatile platform.

**2.4 Summary**

The versatile platform presented in this study provides NIR triggered drug release using a GNR-contained membrane. The direct correlation ship between NIR energy and the drug release rate makes the system readily programmable for pulsatile release. We incorporated the membrane into a device containing a refillable drug reservoir for sustained release. Proof of concept biological studies using SCC-7 cancer cells demonstrate the potential utility of this system for therapeutic release. Interestingly, different responses to stimuli were obtained from each drug in the absence and presence of NIR light, indicating the versatile potential of our on-demand drug delivery system in less-invasive therapies requiring multi-drug delivery strategies. These enhanced delivery systems have the potential to improve therapeutic efficacy and reduce side effects through regulation of plasma drug profiles, providing a new direction in the design of implantable medical devices that combine microscale and macroscale technologies.

## 2.5 Experimental

| Aliquot (#) | Power ($W/cm^2$) | Duration (hr). | Sol'n Conc. (mg/L) | SD | %RSD | Intensity (c/s) |
|---|---|---|---|---|---|---|
| 1 | 0.54 | 3 | 0.000 | 0.001 | 310.0 | 19.1 |
| 2 | 0.54 | 9 | 0.001 | 0.000 | 17.0 | 37.2 |
| 3 | 0.54 | 24 | 0.001 | 0.002 | 214.2 | 30.3 |
| 4 | 0.54 | 36 | 0.001 | 0.000 | 47.2 | 31.3 |
| 5 | No | 336 | 0.001 | 0.000 | 21.2 | 79.3 |

**Table 2-1.** ICP-Mass data from each collected aliquot from the accumulated drain layer after 3(#1), 9(#2), 24(#3), and 36 hours(#4) in the presence of NIR light at a power of 0.54 W/cm2 and 336 hours(#5) without NIR light. The results indicate that our GNR-Den membrane in the device is robustly retained during light stimuli.

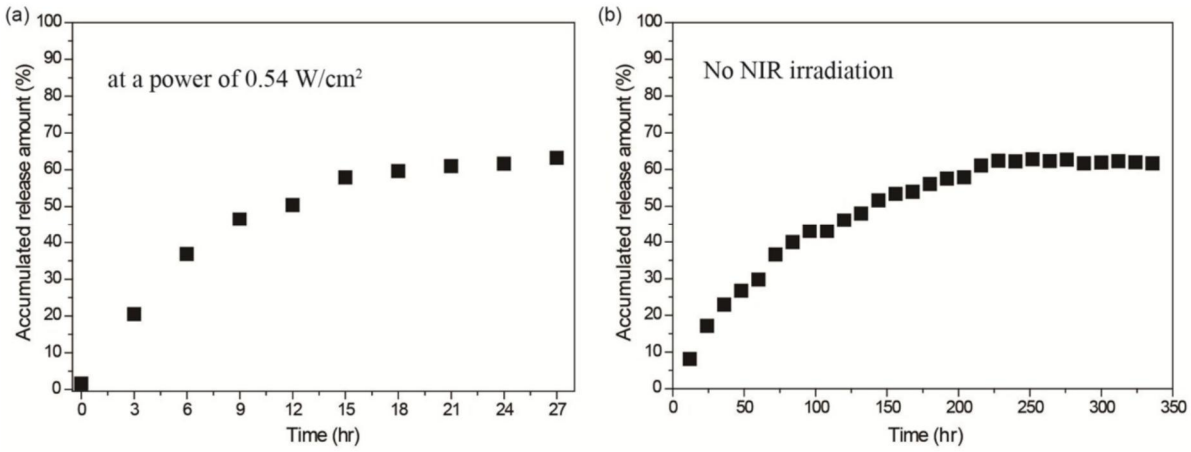


**Figure 2-8.** (a) The Dox release percent profile for accumulated amounts from the device at a NIR power of 0.54 $W/cm^2$. After 9 hours NIR irradiation at a NIR power of 0.54 $W/cm^2$, the release amount was significantly decreased with almost 50% Dox release from the total payload (180 μg) and reached a plateau during next 18 hours even in the presence of NIR. (b) The Dox release percent profile for accumulated release amounts from the device in the absence of NIR for a long time period.

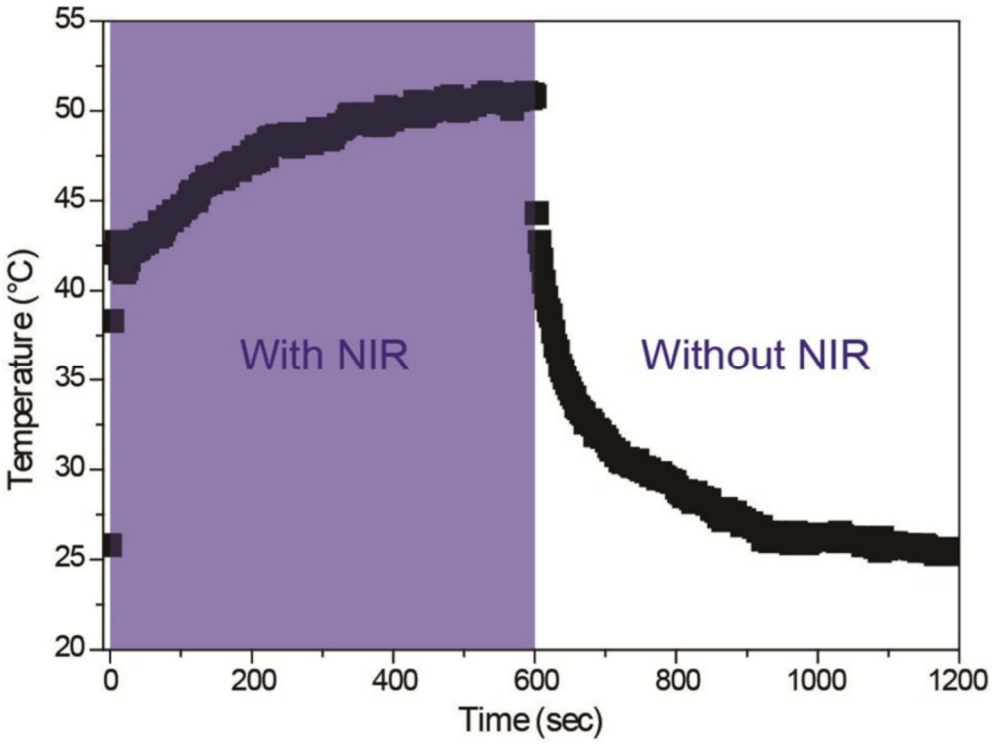


**Figure 2-9.** The temperature response from the fluidic device used for the experiment in Figure 2-6b by NIR irradiation (10 min) with a power of 0.54 W/cm$^2$. It shows a little hysteresis in light response. The media in the drug reservoir have been slowly heated with light and rapidly cooled without light, because the continuous water flow under the membrane in the fluidic device could be acted like a cooling system. We observed the fast increase in 10 sec up to 40 ℃, but the slow increase to 50 ℃ after next 10 min because the media in the drug reservoir have been heated together by the localized heat from GNRs in the presence of light. With no heat source in the absence of light, the continuous supply of fresh PBS rapidly cooled the media in drug reservoir, showing fast decease in drug release rate.

**Materials and methods:** Cetyltrimethylammonium bromide (CTAB), Gold(III) chloride trihydrate ($HAuCl_4 \cdot 3H2O$), Sodium borohydride ($NaBH_4$), ascorbic acid (AA), Silver nitrate ($AgNO_3$), rhodamine B (Rh-B), calcein, and doxorubicin (Dox) were purchased from Aldrich and used any further purification. The Sylgard 184 silicone elastomer kit, anodic aluminum oxide (AAO) membranes (Anodisc 25, 60 μm film thickness and 0.02 μm pore size), and a peristaltic pump were purchased from the Fisher Scientific. A diode laser system with a wavelength of 850 nm and 2000 mW output power was used for a light stimulus. Temperature traces were recorded using a Ti95 an infrared camera (Fluke, USA). Scanning electron microscopy and transmission electron microscopy images were acquired on a JSM-6510, JEOL, Japan, and JEOL 1000CX operating at 80 keV respectively. The concentration of the drugs that were transferred through the membrane was measured using QM-400 spectrofluorometer (PTI, USA) and Neosys-2000 a UV-Vis spectrophotometer (Scinco, USA). The concentration of gold in a drain layer was analysed using the ELAN DRC-II ICP-Mass (Perkin Elmer, USA). For in vitro cell study, squamous cell carcinoma (SCC-7) cancer cells were purchased from American Type Culture Collection. Dulbecco's Modified Eagle's Medium (DMEM, Sigma Aldrich), fetal bovine serum (FBS, Thermoscientific), and antibiotics (Cellgro) were prepared. Phosphate buffered solution 1X (PBS) was purchased from Thermo Scientific. Photoluminescence was analyzed on a Photon Technology International fluorescence spectrometer with Felix 32 and cell viability was determined on a Spectra-Max M5 microplate reader (Molecular Devices).

**Preparation of GNRs:** The CTAB coated GNRs were prepared along a known procedure using a seed-mediated growing method.[39] In a typical procedure, 0.5 mL of an 10 mM solution of $HAuCl_4$ was added to 15 mL of a aqueous 10 mM CTAB solution, followed by mild stirring until the solution became brown-yellow. Subsequently, 1.2 mL of an 10 mM $NaBH_4$ aqueous solution was quickly added with rapidly stirring until the solution turned brown-yellow. The temperature of the seed solution was maintained at 25 °C before use. A 10 mM aqueous solution of $AgNO_3$ (0.36 mL) was added to a mixture of an 10 mM solution of $HAuCl_4$ (2.4 mL) and a 100 mM solution of CTAB (57 mL) in a 50 mL Falcon tube with gentle stirring. Subsequently, 0.384 mL of 100 mM AA was added and the aqueous solution became colorless following addition and gently mixing of AA. Finally, 0.12 mL of the seed solution was rapidly added, and the reaction solution was mixed slowly for 10 s and left undisturbed state for at least 8 h in a water bath. The GNR solution was purified by centrifugation at 13,000 rpm repeatedly. The shape and size of the prepared GNRs were confirmed with TEM.

**Fabrication of the device and characterization of drug release:** A polydimethylsiloxane (PDMS) replica was fabricated by mixing a 10:1 (v/v) mixture of the Sylgard 184 elastomer and a curing reagent using a extremely flat silicon wafer channel mold. The mixture was cured for 4 h at 80 °C and

then shuck from the mold. After the fabrication of the PDMS channel mold, a GNR-Den-AAO composite membrane was fitted into the middle of the PDMS replica and then covered with another PDMS replica to form the PDMS device. After gently placing the device in a fresh phosphate buffered solution (PBS), a Dox-enriched solution (0.4 mL, 850 μM) was poured into a reservoir placed over the membrane (Figure 2-1a). During continuous agitation, 1 mL fractions in the drain were collected for an intended period and analyzed using UV-Vis spectroscopy. After collecting each fraction, 1 mL of fresh PBS was added to retain the PBS level in the drain. To prepare the fluidic device, one side of the device was linked to a peristaltic pump, which supplied a continuous flow of PBS (pH = 7.4), and the other side was fitted with sample collection containers for fluorescence quantification of the released drugs (Figure 2-4). The flow rate of PBS was retained at 4 mL $h^{-1}$ by using the peristaltic pump. After 10 min of initial flowing for wetting of a GNR-Den membrane, the samples were collected after passing through the channel including the Dox-enrich reservoir. The release profiles of Dox from the reservoir under both conditions were generated by analyzing the collected PBS samples over time using a fluorescence spectrometer.

**Post-functionalization of a GNR–Den membrane:** Post-functionalization of a GNR-Den membrane was easily achieved by placing the membrane in a solution for each reactant with mild stirring. In a typical experiment, the prepared GNR-Den membrane was immersed into a solution of 0.5 mM HCl solution for 3 h to regenerate initial amine groups onto PAMAM dendrimers. This $NH_2$-membrane was further placed in a 100 mL methanol solution of MeI (1.0 mL) in the presence of triethylamine (1.0 mL) for 12 h. After rinsing with methanol several times, the TMA-membrane was dried completely before experiments.

**In vitro analysis:** SCC-7 cells were cultured in RPMI 1640 supplemented with 10% FBS and 1% antibiotics under a humidified atmosphere of 5% $CO_2$ at 37 °C. Cells were seeded at 2 × 105 cells per wells in a 96-well plate for 24 h. SCC-7 cells were cultured with each sample for 48 h or 72 h in a $CO_2$ incubator at 37 °C. Cell viability was estimated by an alamar blue assay (alamarBlue®, AbD Serotec, UK). After 48 h or 72 h of incubation, the cells were washed three times with PBS and then incubated with fresh culture medium supplemented with 10 vol% alamarBlue® solution. Following the incubation, 0.10 mL of medium from each well was transported into a 96-well plate. Fluorescence was assessed (excitation 560 nm and emission 590 nm) by a microplate reader.

**2.6 References**

1. Mendes, P. M., Stimuli-responsive surfaces for bio-applications. *Chem Soc Rev* **2008,** *37* (11), 2512-29.

2. Stuart, M. A.; Huck, W. T.; Genzer, J.; Muller, M.; Ober, C.; Stamm, M.; Sukhorukov, G. B.; Szleifer, I.; Tsukruk, V. V.; Urban, M.; Winnik, F.; Zauscher, S.; Luzinov, I.; Minko, S., Emerging applications of stimuli-responsive polymer materials. *Nat Mater* **2010,** *9* (2), 101-13.

3. Rapoport, N., Physical stimuli-responsive polymeric micelles for anti-cancer drug delivery. *Progress in Polymer Science* **2007,** *32* (8-9), 962-990.

4. Jeon, G.; Yang, S. Y.; Byun, J.; Kim, J. K., Electrically actuatable smart nanoporous membrane for pulsatile drug release. *Nano Lett* **2011,** *11* (3), 1284-8.

5. Raeburn, J.; Alston, B.; Kroeger, J.; McDonald, T. O.; Howse, J. R.; Cameron, P. J.; Adams, D. J., Electrochemically-triggered spatially and temporally resolved multi-component gels. *Mater. Horiz.* **2014,** *1* (2), 241-246.

6. Hoare, T.; Timko, B. P.; Santamaria, J.; Goya, G. F.; Irusta, S.; Lau, S.; Stefanescu, C. F.; Lin, D.; Langer, R.; Kohane, D. S., Magnetically triggered nanocomposite membranes: a versatile platform for triggered drug release. *Nano Lett* **2011,** *11* (3), 1395-400.

7. Gao, W.; Chan, J. M.; Farokhzad, O. C., pH-Responsive nanoparticles for drug delivery. *Mol Pharm* **2010,** *7* (6), 1913-20.

8. Yoon, H. J.; Kozminsky, M.; Nagrath, S., Emerging role of nanomaterials in circulating tumor cell isolation and analysis. *ACS Nano* **2014,** *8* (3), 1995-2017.

9. Delcea, M.; Mohwald, H.; Skirtach, A. G., Stimuli-responsive LbL capsules and nanoshells for drug delivery. *Adv Drug Deliv Rev* **2011,** *63* (9), 730-47

10. Satarkar, N. S.; Hilt, J. Z., Magnetic hydrogel nanocomposites for remote controlled pulsatile drug release. *J Control Release* **2008,** *130* (3), 246-51.

11. Liu, T.-Y.; Hu, S.-H.; Liu, D.-M.; Chen, S.-Y.; Chen, I. W., Biomedical nanoparticle carriers with combined thermal and magnetic responses. *Nano Today* **2009,** *4* (1), 52-65.

12. Timko, B. P.; Dvir, T.; Kohane, D. S. Remotely triggerable drug delivery systems. *Advanced materials*, 2010 *22* (44), 4925-4943.

13. Ganta, S.; Devalapally, H.; Shahiwala, A.; Amiji, M., A review of stimuli-responsive nanocarriers for drug and gene delivery. *J Control Release* **2008,** *126* (3), 187-204.

14. Hoffman, A. S., The origins and evolution of "controlled" drug delivery systems. *J Control Release* **2008,** *132* (3), 153-63.

15. Timko, B. P.; Kohane, D. S., Drug-Delivery Systems for Tunable and Localized Drug Release. *Israel Journal of Chemistry* **2013**, 53, 728-736;

16. Liu, G.; Zhou, L.; Guan, Y.; Su, Y.; Dong, C. M., Multi-responsive polypeptidosome: characterization, morphology transformation, and triggered drug delivery. *Macromol Rapid Commun*

**2014,** *35* (19), 1673-8.

17. Mura, S.; Nicolas, J.; Couvreur, P., Stimuli-responsive nanocarriers for drug delivery. *Nat Mater* **2013,** *12* (11), 991-1003.

18. Zhao, X.; Kim, J.; Cezar, C. A.; Huebsch, N.; Lee, K.; Bouhadir, K.; Mooney, D. J., Active scaffolds for on-demand drug and cell delivery. *Proc Natl Acad Sci U S A* **2011,** *108* (1), 67-72.

19. Brayden, D. J. Controlled release technologies for drug delivery. *Drug discovery today*, **2003** *21* (8), 976-978.

20. Cohen-Karni, T.; Langer, R.; Kohane, D. S., The smartest materials: the future of nanoelectronics in medicine. *ACS Nano* **2012,** *6* (8), 6541-5.

21. Sun, T.; Zhang, Y. S.; Pang, B.; Hyun, D. C.; Yang, M.; Xia, Y., Engineered nanoparticles for drug delivery in cancer therapy. *Angew Chem Int Ed Engl* **2014,** *53* (46), 12320-12364.

22. Ruiz-Hernandez, E.; Baeza, A.; Vallet-Regi, M., Smart drug delivery through DNA/magnetic nanoparticle gates. *ACS Nano* **2011,** *5* (2), 1259-66.

23. Santini Jr, J. T.; Richards, A. C.; Scheidt, R.; Cima, M. J.; Langer, R. Microchips as controlled drug-delivery devices. *Angewandte Chemie International Edition*, 2000, *39* (14), 2396-2407.

24. Timko, B. P.; Arruebo, M.; Shankarappa, S. A.; McAlvin, J. B.; Okonkwo, O. S.; Mizrahi, B.; Stefanescu, C. F.; Gomez, L.; Zhu, J.; Zhu, A.; Santamaria, J.; Langer, R.; Kohane, D. S., Near-infrared-actuated devices for remotely controlled drug delivery. *Proc Natl Acad Sci U S A* **2014,** *111* (4), 1349-54.

25. Hribar, K. C.; Metter, R. B.; Ifkovits, J. L.; Troxler, T.; Burdick, J. A., Light-induced temperature transitions in biodegradable polymer and nanorod composites. *Small* **2009,** *5* (16), 1830-4.

26. Huschka, R.; Zuloaga, J.; Knight, M. W.; Brown, L. V.; Nordlander, P.; Halas, N. J., Light-induced release of DNA from gold nanoparticles: nanoshells and nanorods. *J Am Chem Soc* **2011,** *133* (31), 12247-55.

27. Weissleder, R. A clearer vision for *in vivo* imaging. *Nature Biotechnology* 2001, 19 316–317.

28. Yan, B.; Boyer, J. C.; Habault, D.; Branda, N. R.; Zhao, Y. Near infrared light triggered release of biomacromolecules from hydrogels loaded with upconversion nanoparticles. *Journal of the American Chemical Society*, **2012** *134* (40), 16558-16561.

29. Li, W.; Cai, X.; Kim, C.; Sun, G.; Zhang, Y.; Deng, R.; Yang, M.; Chen, J.; Achilefu, S.; Wang, L. V.; Xia, Y., Gold nanocages covered with thermally-responsive polymers for controlled release by high-intensity focused ultrasound. *Nanoscale* **2011,** *3* (4), 1724-30.

30. Lim, D. K.; Barhoumi, A.; Wylie, R. G.; Reznor, G.; Langer, R. S.; Kohane, D. S., Enhanced photothermal effect of plasmonic nanoparticles coated with reduced graphene oxide. *Nano Lett* **2013,** *13* (9), 4075-9.

31. Hribar, K. C.; Lee, M. H.; Lee, D.; Burdick, J. A., Enhanced release of small molecules from near-infrared light responsive polymer-nanorod composites. *ACS Nano* **2011,** *5* (4), 2948-56.

32. You, J.; Shao, R.; Wei, X.; Gupta, S.; Li, C., Near-infrared light triggers release of Paclitaxel from biodegradable microspheres: photothermal effect and enhanced antitumor activity. *Small* **2010,** *6* (9), 1022-31.

33. Sortino, S., Photoactivated nanomaterials for biomedical release applications. *J. Mater. Chem.* **2012,** *22* (2), 301-318.

34. Hirsch, L. R.; Stafford, R. J.; Bankson, J. A.; Sershen, S. R.; Rivera, B.; Price, R. E.; Hazle, J. D.; Halas, N. J.; West, J. L. Nanoshell-mediated near-infrared thermal therapy of tumors under magnetic resonance guidance. *Proceedings of the National Academy of Sciences*, **2003***100* (23), 13549-13554.

35. Zhong, Y.; Wang, C.; Cheng, L.; Meng, F.; Zhong, Z.; Liu, Z., Gold nanorod-cored biodegradable micelles as a robust and remotely controllable doxorubicin release system for potent inhibition of drug-sensitive and -resistant cancer cells. *Biomacromolecules* **2013,** *14* (7), 2411-9.

36. Zhong, Y.; Wang, C.; Cheng, R.; Cheng, L.; Meng, F.; Liu, Z.; Zhong, Z., cRGD-directed, NIR-responsive and robust AuNR/PEG-PCL hybrid nanoparticles for targeted chemotherapy of glioblastoma in vivo. *J Control Release* **2014,** *195*, 63-71.

37. Park, M. H.; Agasti, S. S.; Creran, B.; Kim, C.; Rotello, V. M. Controlled and sustained release of drugs from dendrimer–nanoparticle composite films. *Advanced Materials*, **2011** *23* (25), 2839-2842.

38. Park, M.-H.; Ofir, Y.; Samanta, B.; Arumugam, P.; Miranda, O. R.; Rotello, V. M., Nanoparticle Immobilization on Surfaces via Activatable Heterobifunctional Dithiocarbamate Bond Formation. *Advanced Materials* **2008**, *20,* 4185-4188.

39. Sau, T. K.; Murphy, C. J., Seeded high yield synthesis of short Au nanorods in aqueous solution. *Langmuir* **2004,** *20* (15), 6414-20.

40. Park, M. H.; Kim, S. T.; Rana, S.; Solfiell, D.; Jeong, Y.; Duncan, B.; Yan, B.; Aksoy, B.; Rotello, V. M., Replenishable dendrimer-nanoparticle hybrid membranes for sustained release of therapeutics. *Nanoscale* **2013,** *5* (17), 7805-7808.

41. Park, M.-H.; Ofir, Y.; Samanta, B.; Rotello, V. M., Robust and Responsive Dendrimer-Gold Nanoparticle Nanocomposites via Dithiocarbamate Crosslinking. *Advanced Materials* **2009,** *21* (22), 2323-2327.

42. Wu, G.; Mikhailovsky, A.; Khant, H. A.; Fu, C.; Chiu, W.; Zasadzinski, J. A., Remotely triggered liposome release by near-infrared light absorption via hollow gold nanoshells. *J Am Chem Soc* **2008,** *130* (26), 8175-7.

43. Petrova, H.; Perez Juste, J.; Pastoriza-Santos, I.; Hartland, G. V.; Liz-Marzan, L. M.; Mulvaney, P., On the temperature stability of gold nanorods: comparison between thermal and ultrafast laser-induced heating. *Phys Chem Chem Phys* **2006,** *8* (7), 814-21.

44. Park, M. H.; Subramani, C.; Rana, S.; Rotello, V. M., Chemoselective nanoporous membranes via chemically directed assembly of nanoparticles and dendrimers. *Adv Mater* **2012,** *24* (43), 5862-6.

# Chapter 3. Dual responsive drug release of polymer coated GNR@MS nanoparticle for cancer therapy.

## 3.1 Abstract

Nanoparticles has been considerable as a drug delivery system to deliver hydrophobic drugs. However, premature drug release during the delivery process, occurs drug side effect. To overcome this challenge, we developed a stimuli responsive gatekeeper system. This system blocks the pore to keep the drug in the nanoparticle and open the pore by responding to internal (pH, enzyme, hypoxia, redox) or external stimuli (temperature, sonication, magnetic, light). The system responding to internal and external signals can regulate the space and timing of drug release, increasing the effects of cancer therapy. Glutathione (GSH) polymer-coated gold nanorod (GNR) mesoporous silica (MS) core shell structure (GNR@MS) respond to the internal and external stimuli and can control the drug release. In particular, GNR@MS increases the cancer therapy effect by combined chemo and photothermal therapy.

## 3.2 Introduction

Nanoparticles facilitate the delivery of hydrophobic drugs and selective cancer accumulation through the EPR effect.[1] However, as a result of low encapsulation stability, a significant amount of the loaded drug is released upon circulation, and the drug cannot be readily released from the nanoparticle after reaching the target cancer cell. Recently, gatekeeper systems have been studied to control the release of drugs to prevent unexpected drug release during drug delivery, to reduce the side effects and increase the therapeutic effect.[2-6] Gatekeeper system blocks the nanoparticle pores by a stimuli-responsive material to control the drug release.[5-6] Drug release in these systems is controlled by internal stimuli (pH, enzyme, hypoxia, redox) and external stimuli (temperature, sonication, magnetic, light).[7-9] These internal stimuli-responsive materials have the advantages of self-controlled drug release and facile application in clinical settings at the targeted cancer cell.[10-11] The external stimuli-responsive nanoparticles, on the other hand, offer obvious merits of precision space and timing as well as dose control over drug release through a remote apparatus, in which drug release might be switched on and off at will.[12-13] Thus, internal stimuli enable spatial control and external stimuli enable temporal control. The system responding to internal and external signals can regulate the spatial and temporal of drug release, increasing the cancer therapy effect.[7, 14-17]

We developed PEG-PDS-coated gold nanorod (GNR) mesoporous silica (MS) core shell structure, a GNR@MS@PDS dual-stimuli system. The drug encapsulation was induced bynoncovalent interaction such as the Van der waals interaction, and physical absorbance.[18-19] Theporous MS shell induces an increase in loading capacity as the interaction with the drug increases. GNR@MS shows higher drug loading capacity than drug modification of GNR.[20-21] Thus, GNR@MS induces the local

temperature increase by the surface plasmon resonance (SPR) effect under the near infrared (NIR) light irradiation. Increasing the temperature not only promotes drug release by inducing drug diffusion but also facilitates photo thermal therapy (PTT) by generating heat.[22] The PEG-PDS used to block the open pore of the nanoparticle is degraded by glutathione (GSH). Therefore, GNR@MSN@PDS induces drug releases in response to GSH (internal) and light (external) stimuli.[18, 20, 23] In addition, chemo and photothermal combined therapies increase the cancer cell therapy effect (Figure 3-1).

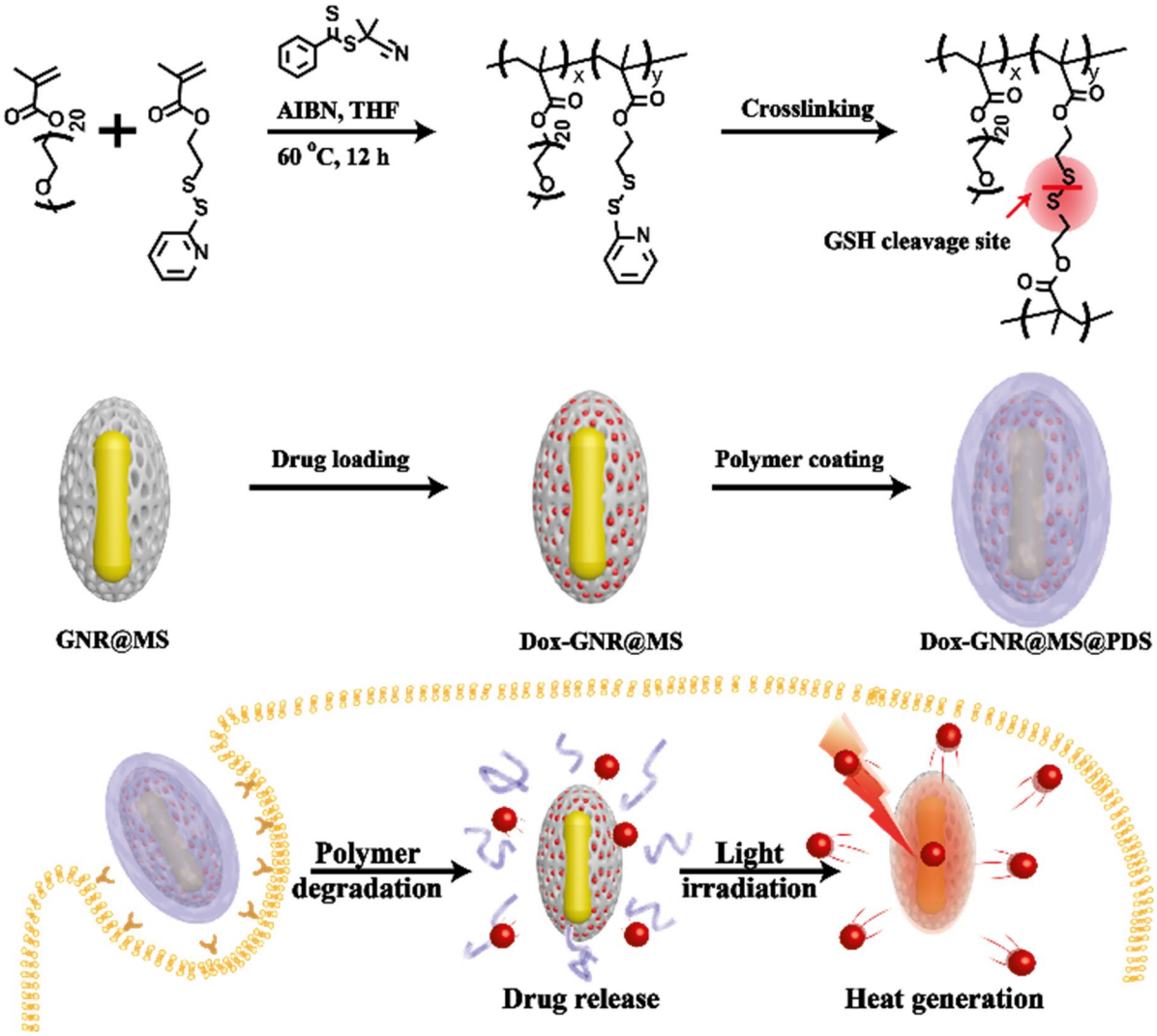


**Figure 3-1.** Schematic illustration of preparation of GNR@MS@PDS and dual-stimuli responsive chemo and PTT combined therapy procedure.

### 3.3 Results and discussion

GNR@MS was synthesized according to a reported protocol.[24] Synthesized GNR showed that length and width were respectively 37 nm and 12 nm (aprox. 3:1 aspect ratio). After coating the silica to the GNR, 10 nm thickness of mesoporous silica shell (MS) was observed in TEM image (Figure 3-2b). Comparing the absorption band of GNR, the absorption band of GNR@MS red sifted about 30 nm upon the silica coating (Figure 3-2a). This phenomenon is explained by the fact that the local refractive index of the silica shell is larger than that of water.

GNR@MS can be used as a drug-delivery system because it can load drugs to a MS shell. Dox loading capacity was 5% when the concentration of supernatant was calculated by Beer's law after loading GNR@MS. After loading Dox to the GNR@MS, polymer-coated GNR@MS (GNR@MS0@PDS) was synthesized according to a reported protocol.[20] For polymer coating, Pyridine of PEG-PDS polymer was protonated by the added hydrochloric acid. Protonated pyridine endows the plus charge to the polymer that facilitates the approach of polymer to the GNR@MS surface. After attachments of polymer, Dithiolthreitol (DTT) was added to immobilize the polymer on the nanoparticle surface. The morphology of GNR@MS@PDS was confirmed by TEM and had a core shell morphology of GNR@MS.

Meanwhile, the surface charge of GNR@MS@PDS was increased from -35.0 mV to -22.4 mV after polymer coating (Figure 3-2c). These results suggest that the polymer was well-coated on the nanoparticle surface without destruction of structure. Coated polymer with a disulfide bond is selectively cleaved by GSH. Synthesized GNR@MS@PDS exhibits an SPR effect under light stimuli and increases the temperature in the surrounding solution. Figure 3-2d shows the temperature change of the GNR@MS@PDS. As the concentration of GNR increased so did the maximum temperature of the solution, with a maximum temperature of 58°C at 0.8 nM. The maximum temperature increases as a linear function of the nanoparticle concentration (Figure 3-2e).

PEG-PDS polymer-coating prevents the unexpected release of drugs by blocking the pores and increases the biocompatibility of nanoparticles. Drug-loaded GNR@MS@PDS facilitates the controlled drug-release in response to GSH and light stimuli. As shown in Figure 3-2f, encapsulated drugs are released in the presence of GSH or light irradiation. Meanwhile, Dox release is effectively prevented in absence of stimuli. GSH induces the degradation of the polymer that blocks the pore of GNR@MS and facilitates drug release. Light stimuli that leads to local temperature increase induces the drug release by polymer swelling. Thus, GNR@MS@PDS effectively regulates drug release in response to dual stimuli.

Dox-loaded GNR @MS@PDS was cultured in SCC7 cells for 3 hours, and the cell uptake ability was confirmed by observing the location of the nanoparticles using a confocal microscope. As shown in Figure 3-3a, Dox fluorescence well colocalize with Lysotracker, suggesting the existence of in the lysosome by the endocytosis of the cell.

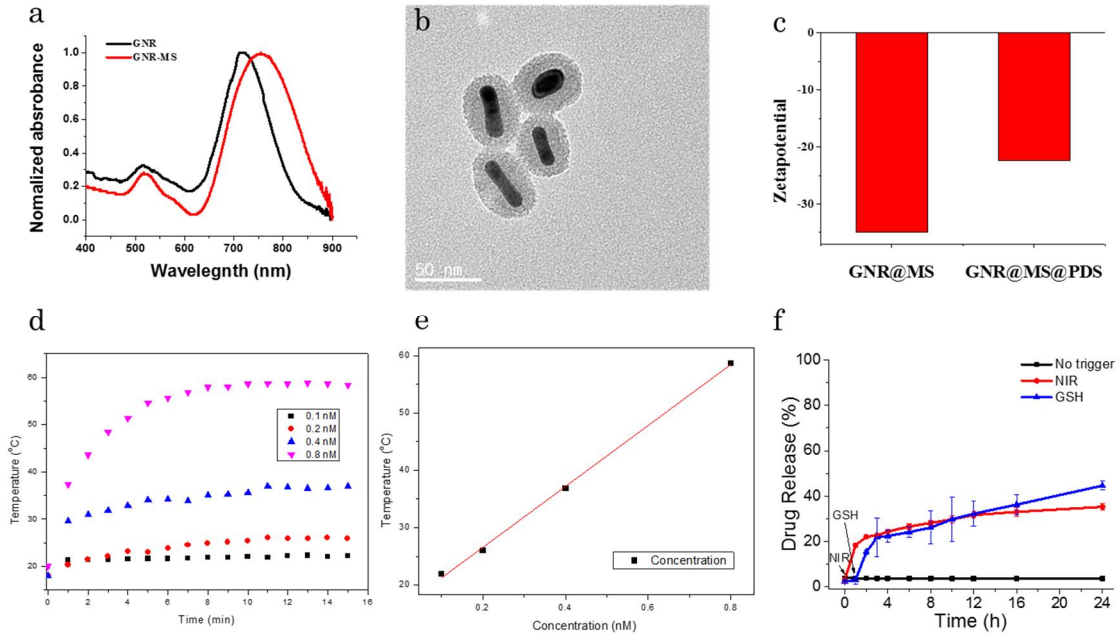


**Figure 3-2.** Characterization of GNR@MS@PDS a) UV-visible spectra for GNR and GNR@MS; b) TEM images of GNR@MS; c) Zeta potential measurements of GNR@MS and GNR@MS@PDS; d); e) heat generation effect of GNR@MS at different concentration; f) Drug release profile analysis in presence and absence of light and GSH.

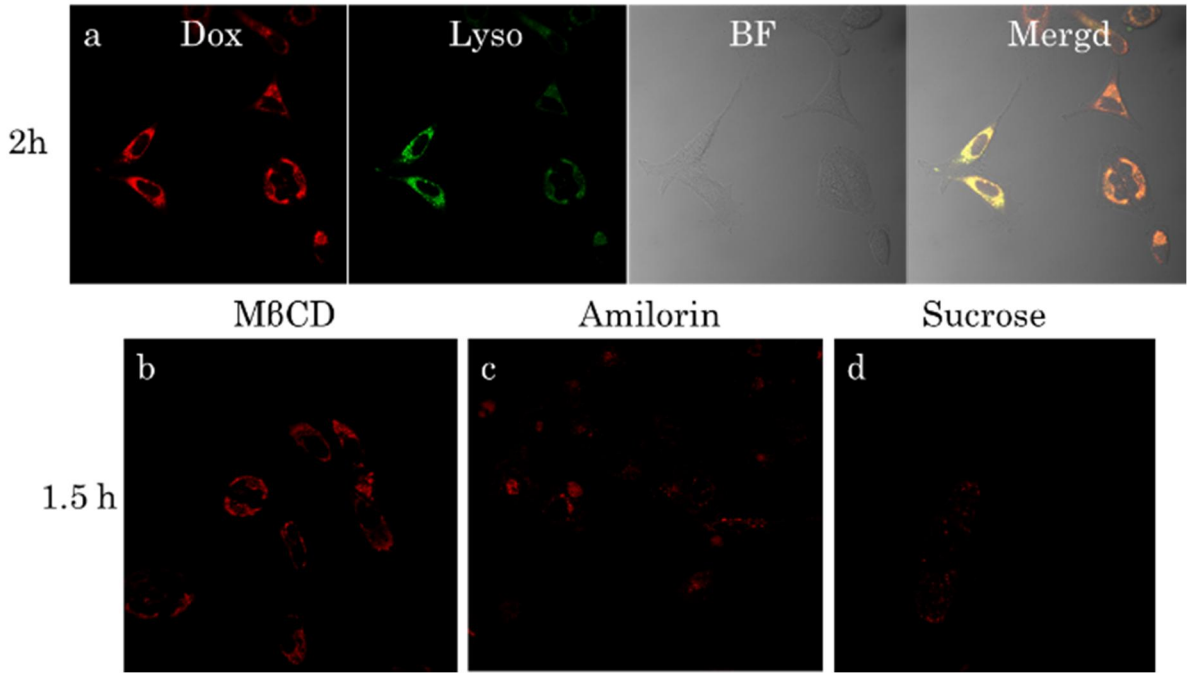


**Figure 3-3.** Cellular uptake analysis for Dox loaded PGNRMS in SCC7 cells at different time points of incubation. Uptake pathway analysis for Dox-PGNRMS in presence of uptake pathway inhibitors b) Sucrose - caveolae, b) amilorin – macropinocytosis and c) methyl beta cyclo dextrin

To confirm the cellular uptake pathway, GNR@MS@PDS was added to cells pretreated with various inhibitors, namely sucrose (clathrin-mediated uptake), methyl-beta cytodextrin (caveolae mediated uptake) and amilorin (macropinocytosis). An inhibitor-treated SCC7 cell was incubated with a Dox-loaded nanoparticle for 3 hours, after which a methyl beta cytodextrin and amilorin pretreated cell line showed a strong Dox fluorescence. Meanwhile, a sucrose-treated cell showed low fluorescence, suggesting that the cellural uptake mechanismof GNR@MS@PDS relates with clathrin-mediated uptake pathway (Figure 3-3b).

To verify the biocompatability and PTT effect, GNR@MS@PDS, calceinAM, and ethdiumbromide was incubated to the scc7cell. Living cells show green fluorescence by Calcein AM and dead cells show red fluorescence by propidium iodide (PI). As shown in Figure 3-4, the control displayed a green fluorescence regardless of light irradiation. On the other hand, red fluorescence was increased when light was irradiated to GNR@MS@PDS incubated cell, suggesting that nanoparticles treat the cancer cell by inducing PTT under the light irradiation. In order to investigate the effect of cancer treatment by controlled drug release, SCC-7 cells were incubated with GNR@MS@PDS and Dox-loaded GNR@MS@ PDS for 24 hours.

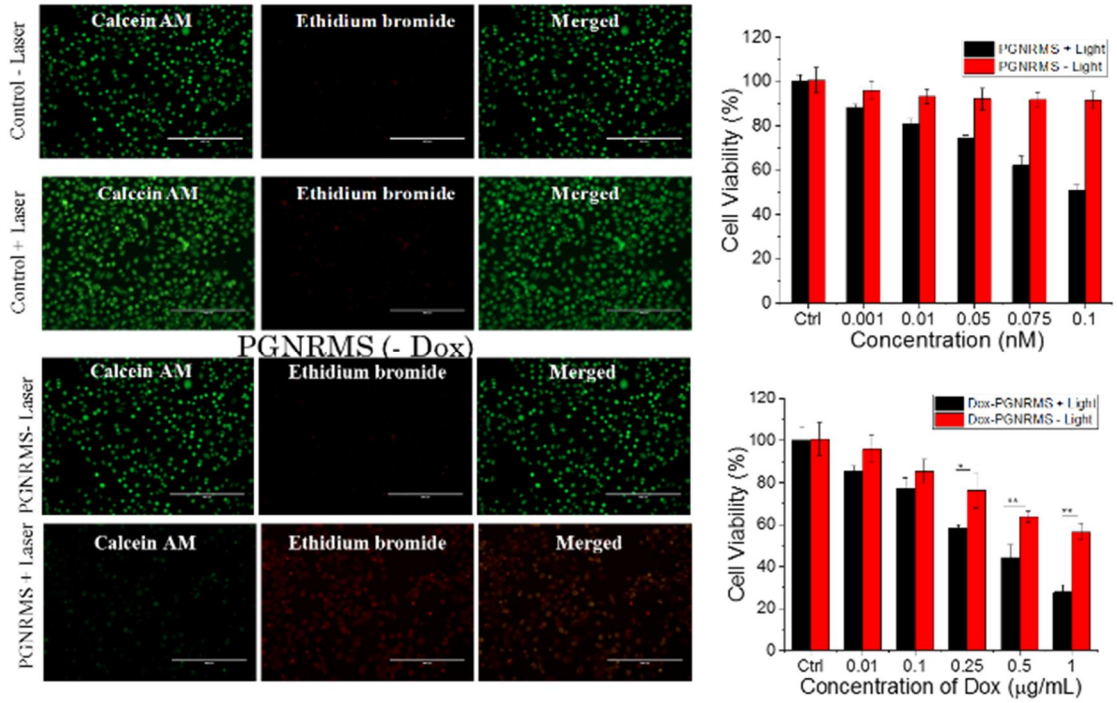


**Figure 3-4.** a) Laser irradiation-mediated apoptosis measured by PI/calcein staining assay after incubation for 12h in SCC7 cells for GNR@MS in presence and absence of laser. b) Cell viability analysis for Dox loaded GNR@MS@PDS nanoparticles in SCC7 cells in the presence and absence of laser irradiation after 24 h incubation, nanoparticles were incubated for 12h, replaced and wash with fresh media. Laser power set at 1.6 W/cm$^2$ for 5 min

As shown in Figure 3-4b, the drug-free GNR@MS@PDS showed low toxicity up to 0.1 nM concentration and treated cancer cells in the presence of light irradiation. This implies that the PTT effect was induced by light irradiation. The drug-loaded GNR@MS@PDS was found to be toxic without light irradiation because the polymer is cleaved by GSH and releases the drug to enable chemotherapy. Dox-loaded GNR@MS@PDS was shown the toxicity in absence light irradiation, implying that the drug was released from the nanoparticle because of polymer degradation by the GSH. Furthermore, under light irradiation, the cancer cell therapy effect was increased by chemo and photodynamic-combined therapy.

### 3.4 Summary

In summary, we developed the internal and external stimulus responsive gatekeeper system on GNR@MS for combined chemo & photothermal therapy. GNR coated with MS facilitates Dox loading through physical adsorption due to the increased surface area of nanoparticles. The PEG-PDS polymer blocks the pore of the MS to prevent premature release of the drug. Drug release of the GNR@MS@PDS system was triggered by responding the GSH and NIR light irradiation. Invitro experiment show the increased therapy effect by combined chemo and photo thermal therapy. Thus, our GNR@MS@PDS, dual stimuli responsive controlled drug release system increases the cancer therapy effect.

### 3.5 Experimental

**General information:** All chemicals and reagents were purchased from Sigma-Aldrich, TCI and Alfa Aesar, Korea unless otherwise specified and used without further purifications. Doxorubicin hydrochloride was obtained from Ontario Chemicals Inc, Canada. Deionized (DI) water was produced by the Millipore Milli-Q system (18.2 MΩ cm).

**Synthesis of PEG−PDS Random Copolymer:** The PEG−PDS random copolymer was synthesized using the RAFT polymerization method. In detail, 2-cyano-2-propyl benzodithioate (0.05 mmol), PDSEMA (3.92 mmol), poly(ethylene glycol) methacrylate (0.98 mmol), and AIBN (0.0146 mmol) were mixed together in a round-bottom flask containing THF and degassed by purging with Ar under sealed condition. Under constant stirring at 70 °C for 24 h, the samples were collected, precipitated thrice in ice-cold diethyl ether, and vacuum-dried. The synthesized samples were analyzed by NMR spectroscopy.

**Synthesis of mesoporous silica capped gold nanorod (GNR@MS)**: GNR@MS were synthesized according to a reported protocol.[24] 0.25 mL of an aqueous $10 \times 10^{-3}$ M solution of $HauCl_4$ was added to 7.5 mL of a $10 \times 10^{-3}$ M CTAB solution, followed by gentle stirring until the solution became bright brown-yellow. Subsequently, 0.6 mL of an aqueous $10 \times 10^{-9}$ M $NaBH_4$ solution was quickly

added with vigorous stirring until the solution turned pale brown-yellow. The temperature of the seed solution was retained at 25 ℃ before use. A $10 \times 10^{-3}$ M solution of $AgNO_3$ (0.18 mL) was added to a mixture of an aqueous $10 \times 10^{-3}$ M solution of $HAuCl_4$ (1.2 mL) and a $100 \times 10^{-3}$ M solution of CTAB (28.5 mL) in a 50 mL Falcon tube with mild stirring. Subsequently, 0.192 mL of $100 \times 10^{-3}$ M AA was slowly added and mixed, after which it became colorless. After addition of 0.06 mL of the seed solution, the reaction mixture was gently mixed for 10 s and left undisturbed for at least 8 h in a water bath at 35 °C. After 8 h, the as-synthesized GNR was centrifuged and washed with Milli-Q water twice at 11,000 rpm for 25 min to remove excess CTAB. Then, the precipitate was redispersed in 100 mL of DI water followed by adding 1 mL of NaOH (0.1 M) solution. Thereafter, 300 μL TEOS/MeOH (20%, v/v) was injected three times under gentle stirring at 30 min intervals. After gentle stirring for another 6 h, GNR@MS was obtained and washed with DI water twice to remove the unreacted species.

Syntehsis of PEG-PDS modified GNR@MS: GNR@MS were capped using the PEG−PDS copolymer following method. About 0.1 ml of GNR@MS was dispersed in 0.9 mL of DI water containing 10 mg of PEG−PDS polymer and continuously stir for a period of 12 h at room temperature. To cross-link the polymer shell, partial amount of DTT was added (50 mol % against PDS group) and again stir for a period of 3 h at RT to allow in situ cross-linking. Then the polymer capped GNR@MS were collected by centrifugation, washed thrice with DI water.

### 3.6 References

1. Lammers, T.; Hennink, W. E.; Storm, G., Tumour-targeted nanomedicines: principles and practice. Br J Cancer 2008, 99 (3), 392-7.

2. Zhang, X.; Yang, P.; Dai, Y.; Ma, P. a.; Li, X.; Cheng, Z.; Hou, Z.; Kang, X.; Li, C.; Lin, J., Multifunctional Up-Converting Nanocomposites with Smart Polymer Brushes Gated Mesopores for Cell Imaging and Thermo/pH Dual-Responsive Drug Controlled Release. Advanced Functional Materials 2013, 23 (33), 4067-4078.

3. Gil, E.; Hudson, S., Stimuli-reponsive polymers and their bioconjugates. Progress in Polymer Science 2004, 29 (12), 1173-1222.

4. de Las Heras Alarcon, C.; Pennadam, S.; Alexander, C., Stimuli responsive polymers for biomedical applications. Chem Soc Rev 2005, 34 (3), 276-85.

5. Guillet-Nicolas, R.; Popat, A.; Bridot, J. L.; Monteith, G.; Qiao, S. Z.; Kleitz, F., pH-responsive nutraceutical-mesoporous silica nanoconjugates with enhanced colloidal stability. Angew Chem Int Ed Engl 2013, 52 (8), 2318-22.

6. Singh, N.; Karambelkar, A.; Gu, L.; Lin, K.; Miller, J. S.; Chen, C. S.; Sailor, M. J.; Bhatia, S. N., Bioresponsive mesoporous silica nanoparticles for triggered drug release. J Am Chem Soc 2011, 133 (49), 19582-5.

7. Cheng, R.; Meng, F.; Deng, C.; Klok, H. A.; Zhong, Z., Dual and multi-stimuli responsive polymeric nanoparticles for programmed site-specific drug delivery. Biomaterials 2013, 34 (14), 3647-57.

8. Bawa, P.; Pillay, V.; Choonara, Y. E.; du Toit, L. C., Stimuli-responsive polymers and their applications in drug delivery. Biomed Mater 2009, 4 (2), 022001.

9. Meng, F.; Zhong, Z.; Feijen, J., Stimuli-responsive polymersomes for programmed drug delivery. Biomacromolecules 2009, 10 (2), 197-209.

10. Liu, M.; Du, H.; Zhang, W.; Zhai, G., Internal stimuli-responsive nanocarriers for drug delivery: Design strategies and applications. Mater Sci Eng C Mater Biol Appl 2017, 71, 1267-1280.

11. Gupta, P.; Vermani, K.; Garg, S., Hydrogels: from controlled release to pH-responsive drug delivery. Drug discovery today 2002, 7 (10), 569-579.

12. Chan, A.; Orme, R. P.; Fricker, R. A.; Roach, P., Remote and local control of stimuli responsive materials for therapeutic applications. Adv Drug Deliv Rev 2013, 65 (4), 497-514.

13. Ghosh, P.; Han, G.; De, M.; Kim, C. K.; Rotello, V. M., Gold nanoparticles in delivery applications. Adv Drug Deliv Rev 2008, 60 (11), 1307-15.

14. Chen, C.; Geng, J.; Pu, F.; Yang, X.; Ren, J.; Qu, X., Polyvalent nucleic acid/mesoporous silica nanoparticle conjugates: dual stimuli-responsive vehicles for intracellular drug delivery. Angew Chem Int Ed Engl 2011, 50 (4), 882-6.

15. Chen, Y.; Pang, X.-H.; Dong, C.-M., Dual Stimuli-Responsive Supramolecular Polypeptide-Based Hydrogel and Reverse Micellar Hydrogel Mediated by Host-Guest Chemistry. Advanced Functional Materials 2010, 20 (4), 579-586.

16. Stoffelen, C.; Voskuhl, J.; Jonkheijm, P.; Huskens, J., Dual stimuli-responsive self-assembled supramolecular nanoparticles. Angew Chem Int Ed Engl 2014, 53 (13), 3400-4.

17. Zhang, L.; Guo, R.; Yang, M.; Jiang, X.; Liu, B., Thermo and pH Dual-Responsive Nanoparticles for Anti-Cancer Drug Delivery. Advanced Materials 2007, 19 (19), 2988-2992.

18. Palanikumar, L.; Kim, H. Y.; Oh, J. Y.; Thomas, A. P.; Choi, E. S.; Jeena, M. T.; Joo, S. H.; Ryu, J. H., Noncovalent Surface Locking of Mesoporous Silica Nanoparticles for Exceptionally High Hydrophobic Drug Loading and Enhanced Colloidal Stability. Biomacromolecules 2015, 16 (9), 2701-14.

19. Vallet-Regi, M.; Balas, F.; Arcos, D., Mesoporous materials for drug delivery. Angew Chem Int Ed Engl 2007, 46 (40), 7548-58.

20. Palanikumar, L.; Choi, E. S.; Cheon, J. Y.; Joo, S. H.; Ryu, J.-H., Noncovalent Polymer-Gatekeeper in Mesoporous Silica Nanoparticles as a Targeted Drug Delivery Platform. Advanced Functional Materials 2015, 25 (6), 957-965.

21. Zhang, Z.; Wang, L.; Wang, J.; Jiang, X.; Li, X.; Hu, Z.; Ji, Y.; Wu, X.; Chen, C., Mesoporous silica-coated gold nanorods as a light-mediated multifunctional theranostic platform for cancer

treatment. Adv Mater 2012, 24 (11), 1418-23.

22. Shen, S.; Tang, H.; Zhang, X.; Ren, J.; Pang, Z.; Wang, D.; Gao, H.; Qian, Y.; Jiang, X.; Yang, W., Targeting mesoporous silica-encapsulated gold nanorods for chemo-photothermal therapy with near-infrared radiation. Biomaterials 2013, 34 (12), 3150-8.

23. Palanikumar, L.; Choi, E. S.; Oh, J. Y.; Park, S. A.; Choi, H.; Kim, K.; Kim, C.; Ryu, J. H., Importance of Encapsulation Stability of Nanocarriers with High Drug Loading Capacity for Increasing in Vivo Therapeutic Efficacy. Biomacromolecules 2018, 19 (7), 3030-3039.

24. Luo, G.-F.; Chen, W.-H.; Lei, Q.; Qiu, W.-X.; Liu, Y.-X.; Cheng, Y.-J.; Zhang, X.-Z., A Triple-Collaborative Strategy for High-Performance Tumor Therapy by Multifunctional Mesoporous Silica-Coated Gold Nanorods. Advanced Functional Materials 2016, 26 (24), 4339-4350.

# Chapter 4. MOF X Biopolymer: Collaborative Combination of Metal-Organic Framework and Biopolymer for Advanced Anticancer Therapy.

## 4.1 Abstract

Metal-Organic Framework (MOFs) nanoparticles with high porosity and greater tunability have emerged as new drug delivery vehicles. However, premature drug release still remains a challenge in MOF delivery system. Here, we report enzyme responsive polymer coated MOF gatekeeper system using hyaluronic acid (HA) and PCN-224 nanoMOF. The external surface of nanoMOF can be stably covered by HA through multivalent coordination bonding between Zr-cluster and multiple carboxylic acid of HA, which acts as a gatekeeper. HA allows the selective accumulation of drug carriers in CD44 overexpressed cancer cells and the enzyme response drug release in the cancer cell environment. In particular, inherent characteristics of PCN-224, which is used as a drug carrier, facilitate transfer the drug to cancer cells more stably and allows photodynamic therapy. This HA-PCN system enables dual therapy of chemotherapy and photodynamic therapy to enhance cancer therapy effect.

## 4.2 Introduction

Cancer is a public health threat worldwide, responsible for 609,940 deaths in the United State alone in 2018.[1] Although chemotherapy is a popular cancer treatment therapy, direct administration of anticancer drugs often causes severe side effects.[2] Development of drug delivery vehicles, which regulate drug release while minimizing side effects and maintaining therapeutic efficacy, is highly desirable.[3-5] Drug delivery systems have developed for the past few decades include inorganic mesoporous silica,[6] quantum dots,[7] metal nanoparticles,[8-10] polymer nanoparticle[11] and organic dendrimers.[10, 12] However, these systems are still far from ideal drug delivery systems, difficult to satisfy the following important requirements simultaneously, including large drug loading capacity, colloidal stability, low toxicity, and bio-degradability.[13-15]

Metal-organic frameworks (MOFs), a new class of porous materials, are now emerging as new drug delivery vehicles,[16-18] due to their high porosity and their greater tunability compared to conventional porous materials,[19, 20] providing multifunctionalities based on size,[20] composition,[21] topology[22, 23] and chemical properties.[24, 25] However, controlled drug release has not been investigated extensively in these MOF-based systems.[26, 27] Most of reported nanoMOFs has lack of colloidal stability in aqueous environment and premature drug release behavior even without any stimuli as the surface of nanoMOFs is not fully covered. To stably deliver drug molecules into cancer cells without undesired drug leakage before reaching target site and increase therapeutic effect by releasing the drug molecules inside the cancer cells, it is necessary to regulate drug release precisely by introducing the stable stimuli-sensitive system into the surface of nanoMOFs.

To achieve this goal, we design an enzyme responsive polymer gatekeeper on nanoscale MOF (nanoMOF). First, we choose a nanoscale, Zr-based porphyrinic MOF, PCN-224, for a main component for the drug delivery system.[28] This MOF is robust, yet biodegradable, with large surface area, and stable over wide range of pH.[29] Furthermore, it can generate $^1O_2$, an essential feature for photodynamic cancer therapy.[30] After loading drug molecules inside MOF, the nanoscale MOFs are covered with a gatekeeper, blocking the pore entrance to preserve drug molecules inside the pore to prevent premature release.[31, 32] Hyaluronic acid (HA), a natural polysaccharide with good biocompatibility, is chosen as a polymer gatekeeper. NanoMOFs covered with HA gatekeeper several significant advantages; (i) the multiple coordination bonds between HA and the MOF make stable surface modification and keep the drug molecules inside pore, ii) hydrophilic HA on the MOFs provides a good colloidal stability in the water, (iii) HA acts as a cancer-targeting ligand for selective drug delivery because it can interact with CD44 which is overexpressed in many cancer cells, and (iv) HA is degraded by HAdase in cancer cells so that the drug molecules can be only released inside the cancer cell. We hypothesize that such a carefully designed HA-nanoMOF system would be a highly efficient drug delivery system for multimodal anticancer therapy. Herein, we report that HA-nanoMOF system loaded with anticancer drug doxorubicin (Dox) is indeed highly efficient for cancer therapy. This approach is one step closer to precision medicine, providing multifunctional capabilities, including cancer-targeting, on-site drug release, and photodynamic therapy (Figure 4-1). This combined therapy,[33, 34] chemotherapy and PDT, demonstrated here is highly efficient for targeting multi-drug resistant cancer cells.

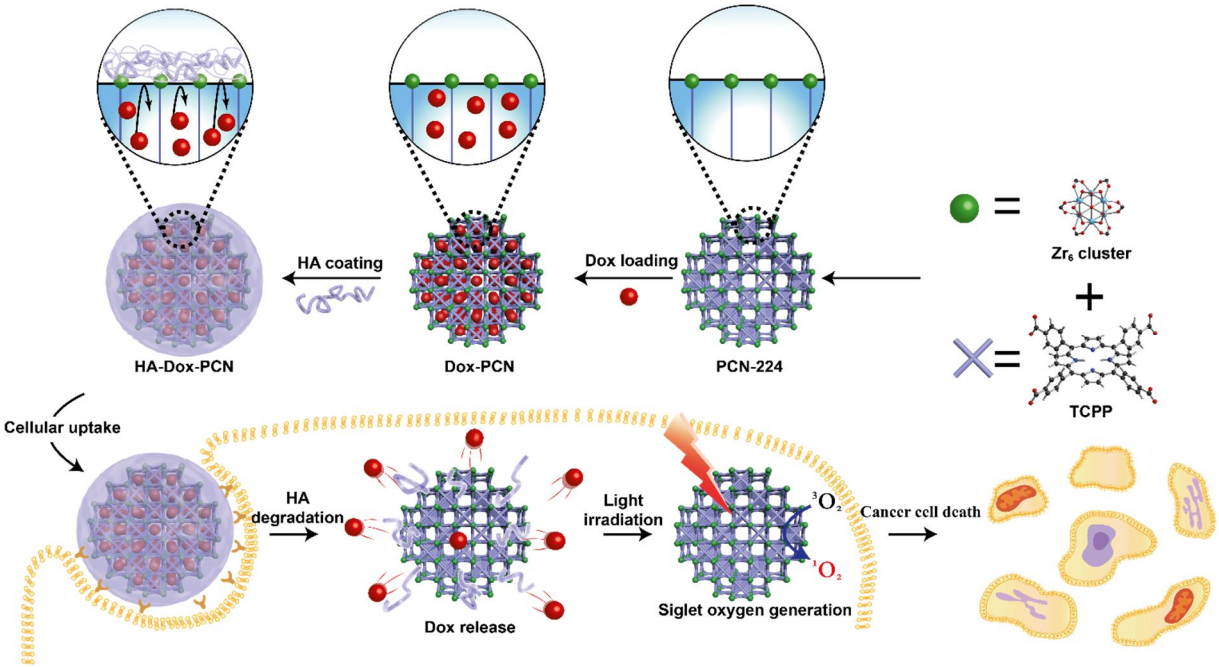


**Figure 4-1.** Illustration of preparation of HA gate keeper metal organic frame work nanosystem and chemo and PDT combined therapy procedure

### 4.3 Results and discussion

The crystal structure of PCN-224 has a **she** topology with *Im-3m* space group which contains three-dimensional open channels with 1.9 nm.[28] As biocompatibile Zr (IV) has strong interaction with the carboxylate linker, Zr nodes provide the framework robustness and thus ensures that the drug is delivered to cancer cells stably. In addition, the porphyrinic linker in the MOF framework allows efficient PDT without aggregation in the aqua solution. PCN-224 nanoparticles were synthesized using a synthetic method described in the previous report.[30] Synthesized PCN-224 nanoparticle was observed spherical morphology with 100 nm by TEM and SEM (Figure 4-2a, b). The structure of synthesized nanoparticles was confirmed by powder X-ray diffraction (PXRD). Experimental PXRD pattern of the MOF nanoparticle is well matched the PCN-224 simulation (Figure 4-2c) and still maintains crystallinity after HA coating, implying MOF structure remain during the synthesis process. The nanoMOF has a large Brunauer-Emmett-Teller (BET) surface area of 2296(8) $m^2/g$ and three-dimensional channels with 1.8 nm pore size those were measured by $N_2$ adsorption studies at 77K (Figure 4-2d, 4-5). This high surface area and porosity allow the drug loading in large quantities, demonstrating the potential of the PCN-224 nanoparticle as a drug delivery carrier. We investigated the loading capacity of the hydrophobic Dox in unmodified PCN-224 through physical entrapment. The drug encapsulation mechanism is caused by noncovalent interactions such hydrogen bonding and van der Waals interactions, allowing the high surface area of PCN-224 to interact more effectively with the drug molecule.[48] As showing in Figure 4-6, PCN-224 shows high loading capacity ability (108%, weight ratio between Dox and nanoMOFs).

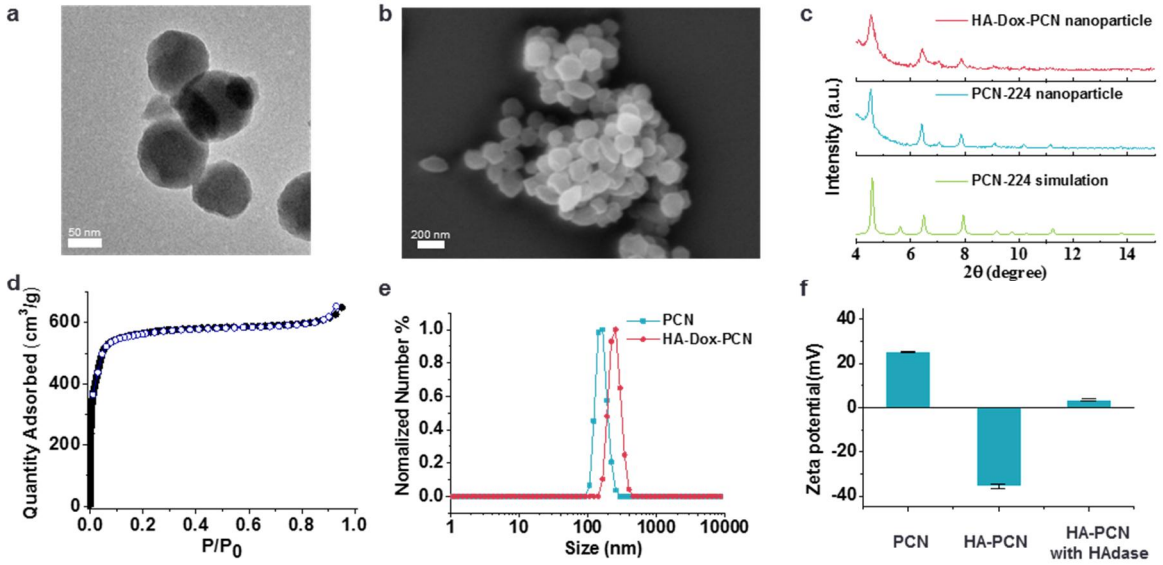


**Figure 4-2.** a) TEM and b) SEM image of PCN-224 that size is around 90nm. c) PXRD pattern of PCN-224 (graph change to arbitrary unit) d) $N_2$ sorption data of PCN-224 e) DLS size of PCN-224 and HA-Dox-PCN. f) Surface charge was measured by Zetasizer

Along with major limitation in MOF drug delivery system, the hydrophobicity of the particle surface and opened pore of Dox-PCN can cause low colloidal stability and premature drug release. To overcome such drawbacks, the Dox-PCN has been modified by HA biopolymer through the coordination interaction with Zr cluster and carboxylic acid of HA. The DLS experiment indicated an increase in the hydrodynamic radius of HA-Dox-PCN (~250 ± 20 nm) compared with that of PCN-224 (~164 ± 20 nm) (Figure 4-2e). After HA coating, MOF still have the spherical morphology (Figure 4-7). Furthermore, surface properties of PCN-224 and HA-Dox-PCN were measured by zeta potential in aqueous solution. The zeta potential experiment indicated a change of the surface charge from positive potential of PCN-224 (+27 mV) to negative potential of HA-Dox-PCN (-34 mV) (Figure 4-2f). Size and surface charge change indicate that HA was coated successfully on PCN-224 surface. HA-Dox-PCN colloidal stability was studied by measuring the size change by varying the time in media.

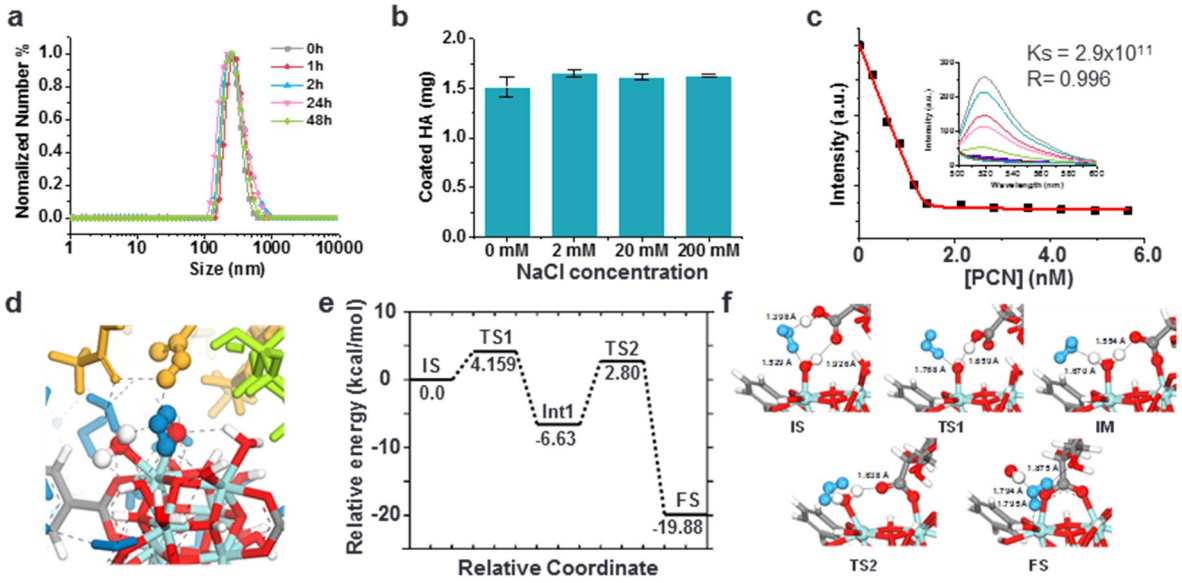


**Figure 4-3.** a) HA-Dox-PCN colloidal stability measured by DLS in cell media over 48 h. b) Modified HA amount to PCN at different concentration of NaCl. c) Fluorescence titration graph d) Enlarged snapshots of interacting structures between HA decamers and PCN-224 surface with water molecules. Black dashed lines represent hydrogen bond. e) Energy diagram of the reaction path on the formation mechanism of coordination bond between HA monomer and Zr6 cluster model in surface region. The acronyms IS, TS, IM and FS represent the initial, transition, intermediate and final states, respectively. The numbers represent the relative energies of each state based on that of the IS. f) Atomic configurations of each state in reaction coordinate. The atoms in bond formation reaction are shown by ball-and-stick, while the remaining atoms are presented by sticks. Except for water molecule colored in blue, the Zr, C, H, and O atoms are colored in cyan, gray, white, and red, respectively.

As shown Figure 4-3a, particle size didn't show any significant different for 48 h, indicative of high colloidal stability. NP colloidal stability is important for the safe and effective nanomedicine since low colloidal stability of NPs can lead to capillary blockage in vivo and are likely to be rapidly removed by the body's reticuloendothelial system (RES).

There are two possible driving forces of HA coatings; i) by electrostatic interactions since the highly negative charged HA can interact with the highly positive surface potentials of PCN-224, ii) by the coordination bond of HA with Zr-cluster. To investigate the main driving force of HA-coating, we observed the effect of salt concentration in HA-coating process. We hypothesized that if the main driving force is the electrostatic interaction, the coating of HA onto PCN-224 will be influenced by ionic strength of the solution, since increasing ionic strength weaken the electrostatic interactions. Modified amount of HA was confirmed at different sodium chloride concentrations by the carbazole assay, which is commonly used to measure the amount of HA.

As shown in Figure 4-3b, the amount of HA is independent on the concentration of sodium chloride. More interestingly, the HA coating is quite satbleeven at high salt concentration (2 M). These results imply that the coating of HA might be happened by the coordination bonds, along with simple electrostatic interaction. To further investigate binding between HA and PCN-224, fluorescence titration was performed.[49] Different molecular weight of FITC-modified HA (high molecular weight HA (1,500~2,200 kDa), and low molecular weight HA (8~15 kDa) ) were prepared to compare the binding constant. The fluorescence of FITC-modified HA (FITC-HA) was significantly quenched when PCN-224 nanoparticles were added, probably due to the energy transfer from FITC to porphyrin framework (Figure 4-3c, Figure 4-8). The normalized fluorescence intensities of FITC-HA at 520 nm were plotted against the ratio of nanoparticle to polymer. The binding constants ($K_s$) were obtained through nonlinear least-squares curve-fitting analysis. $K_s$ of high molecular weight HA-FITC with PCN-224 is 2.9 x $10^{11}$ $M^{-1}$. Meanwhile, that of low molecular weight HA-FITC with PCN-224 is significantly decreased to 3.19 x $10^{7}$ $M^{-1}$. These results suggest that number of carboxylate groups of HA affect to the binding force. Therefore, polyvalent coordination bonds with Zr-clusters on the surface of PCN-224 nanoparticle is very important for a robust and stable gatekeeper system.

HA-coating on nanoMOF, we observed physical adsorption of HA on the surface of PCN-224 via molecular dynamics simulations. (see Theoretical methods). At the low HA coverage systems with 2 decamers in the coating layer in the dry and hydrated conditions, HA's became adsorbed along the pore edge of the PCN-224 due to the formation of hydrogen bonds (Figure 4-12). However, as the number of HA decamers increased to 6 to thickening the HA-coating, amorphous coating layer was formed, resulting in the blocking of pore structure in nanoMOF. More specifically, at the outermost surface of nanoMOF with HA's in the dry condition, -OH in HA (e.g. carboxylic acid and hydroxyl group) stably interacted with terminal hydroxyl group of the $Zr_6$ nodes (Figure 4-13a) and amine group of the TCPP linkers.

Even in the hydrated condition, similar molecular configuration was observed while the hydroxyl groups and the water molecules interacting with each other, as shown in the Figure 4-3d and 4-13b, contributing to stably locating HA-coating layer near the surface. We conjectured the formation of coordination bond between HA and nanoMOF would be driven by this strong hydrogen bonding force.

To verify the formation of coordination bond between HA and $Zr_6$ node, thermodynamic mechanism was calculated via density functional theory (DFT) calculation (Figure 4-3e, f and 4-14). By considering molecular configurations observed at hydrated condition in MD simulation, HA monomer and water molecule were placed near the terminal -OH group of the $Zr_6$ cluster. To make coordination bond between HA and nanoMOF, we assumed that the reaction would occur at the structure interconnected by hydrogen bonding interactions, i.e. water molecule, carboxyl acid in HA, and terminal -OH group of the $Zr_6$ cluster. At the initial reaction, hydrogen atom was transferred from carboxylic acid in HA to terminal -OH group in $Zr_6$ node, which was stabilized by adjacent water molecule. Subsequently, remaining carboxylate was coordinated to open Zr site, accompanying 4.16 kcal/mol of activation energy ($E_a$), and -6.63 kcal/mol of heat of reaction($\Delta$E). From IM1 to FS, as-made water molecule was readily detached from Zr atom, and concurrently carboxylate was coordinated to the Zr atom with 9.42 kcal/mol of $E_a$ and -13.25 kcal/mol of $\Delta E$. Considering this relatively low $E_a$, if the HA polymer was closely located to the $Zr_6$ metal node of the PCN-224, the polymer was expected to construct new coordination bond with the PCN-224 even at room temperature.[50]

Due to high expression of HAdase in cancer cells, the gatekeeper, HA can be degraded inside cancer cells to trigger the release of the drug molecules. We first monitored HA degradation by HAdase in aqueous solution by observing the change of the surface charge. As shown in Figure 1f, the surface charge of HA-PCN was changed from -34 mV to +4 mV after incubation with HAdase. This indicates that coated HA on the PCN-224 was degraded by HAdase. HAdase triggered drug release was investigated by measuring the emission of released Dox from HA-Dox-PCN.

As shown Figure 4-4a, when HAdase (400 U/ml) was added to the HA-Dox-PCN aqueous suspension after 3h incubation, Dox fluorescence intensity was gradually increased, implying that HAdase induce the drug release by degrading the HA which attached to PCN-224 surface. Meanwhile, only HA-Dox-PCN indicated stable encapsulation of Dox without unwanted drug release. It suggests that HA efficiently blocked the PCN-224 pore entrance before degradation by HAdase.

To facilitate the dual therapy, we chose the water stable PCN-224 consisting of Zr and porphyrinic organic ligand which is used as a sensitizer for photo dynamic therapy. The (4-carboxyphenyl) porphyrin photosensitizer that constitutes PCN-224 can make use of the light to produce $^1O_2$. $^1O_2$ generation was investigated by measuring ABDA absorption decrease under photo-irradiation. As shown Figure 4-4b and 4-17, ABDA absorbance consistently decreases by increasing illumination time. Additional advantage of HA coating is selective targeting cancer and controlled drug release by

HAdase inside the cancer cells. The cancer targeting ability is confirmed by monitoring cellular uptake experiments. Prepared HA-Dox-PCN was incubated with Hek 293T (Human embryonic kidney 293 cells, CD44 negative cell), MDA-MB-231 (human mammary gland -breast cancer cells), and SCC7 ((Murine squamous cell carcinoma, CD44 positive cells). After 2h incubation, cellular uptake ability of HA-Dox-PCN was observed by confocal microscopy. MDA-MB231 and SCC-7 cell was shown higher intensity of Dox compare with Hek 293T cell (Figure 4-4c). It is well known that CD44 is over expressed on the surface of cancer cell. Thus, these results suggest that HA-Dox-PCN nanoparticles can selectively uptake into CD44 receptor expressing cancer cells. Cellular uptake pathway experiment was conducted to confirm the more accurate invasion mechanism of HA-Dox-PCN. Figure 4-16 shows that cellular uptake of HA-Dox-PCN is associated with clathrin mediated endocytosis. The therapy effect of PCN, HA-PCN, and HA-Dox-PCN were investigated by measuring cellular viability. Hek 293T (CD44 negative), MDA-MB-231(CD44 positive), and SCC-7(CD44 positive) cell was incubated with PCN-224, HA-PCN, and HA-Dox-PCN. Only PCN-224 showed toxicity to CD44 negative cells under light irradiation (Figure 4-4d, 4-18). Meanwhile, HA-PCN showed toxicity under light irradiation in CD44 positive cells (Figure 4-19). In addition, HA-Dox-PCN showed increased toxicity in existence light irradiation (Figure 4-4e, 4-20). These results suggest that HA facilitate the selective cancer cells uptake and combined chemo-photodynamic therapy increase the cancer therapy effect under light irradiation. Furthermore, MCF-7/ADR cell (multidrug-resistant (MDR) human breast cancer) was prepared to observe the HA-Dox-PCN therapy effect in the MDR cell. MCF-7/ADR cell show low cell viability when incubate with HA-Dox-PCN with light irradiation (Figure 4-21).

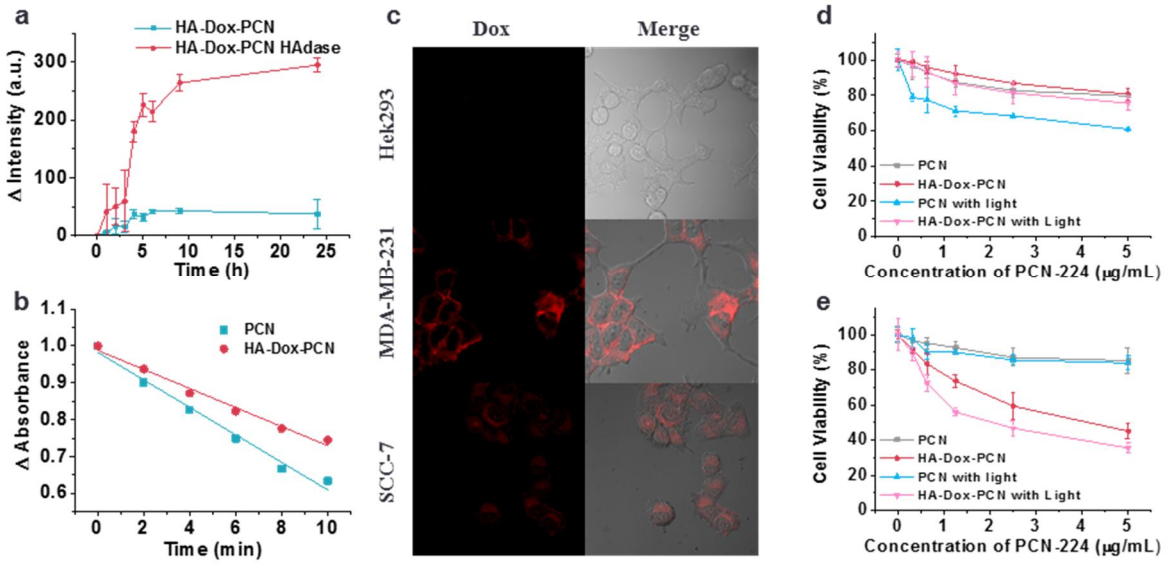


**Figure 4-4.** a) Drug release profile of HA-Dox-PCN. b) ABDA assay analysis of PCN-224 and HA-Dox-PCN. c) Confocal imaging to check the cellular uptake of Dox loaded HA-PCN nanoparticles after 2h incubation. Cell viability analysis at different cell line at PCN-224 5 μg/ml d) Hek 293T, e) MDA-MB-231

### 4.4 Summary

In summary, we developed the enzyme responsive polymer gatekeeper system on nanoMOF for combined chemo & photodynamic therapy. NanoMOF, PCN-224, has very high loading capacity for hydrophobic Dox through physical adsorption due to a large surface area of nanoMOF. The polymer gatekeeper, HA blocks the pore entrance to preserve drug molecules inside the pore and prevent premature release through polyvalent coordination bonds along with electrostatic interaction. Drug release of HA-Dox-PCN system was triggered by responding HAdase enzyme stimulation and can specifically target the cancer cells. In vitro experiment of combination chemo and photodynamic therapy showed higher therapeutic efficacy under the light irradiation. Moreover, this system effectively treats the MCF-7/ADR drug resistant cell compare dox chemotherapy. Thus, our HA-Dox-PCN, controlled drug release system, expand role of the nanoMOF as drug carrier.

**4.5 Experimental**

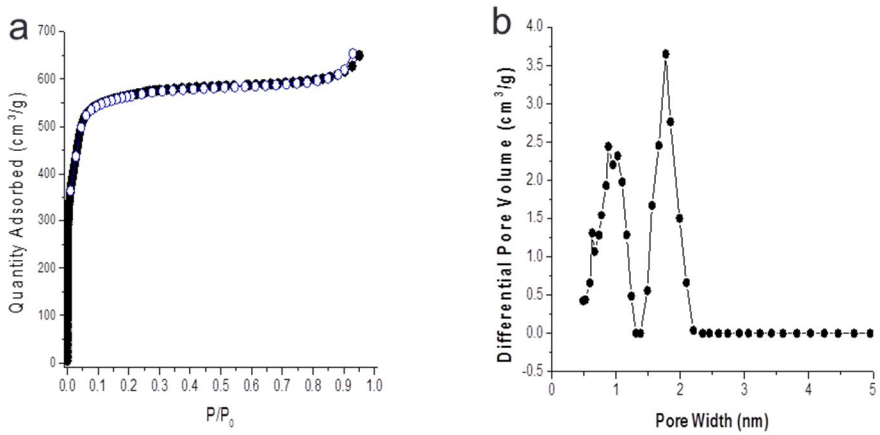


**Figure 4-5.** a) $N_2$ sorption and b) pore size distribution of PCN.

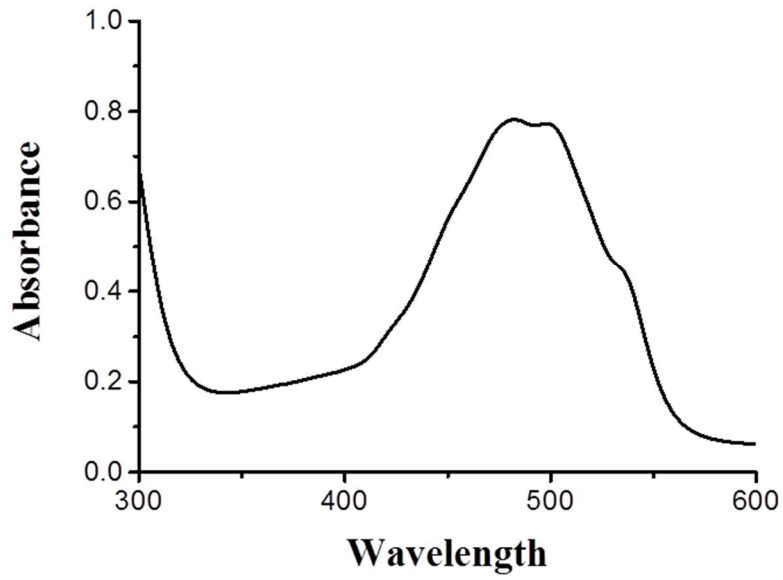


**Figure 4-6.** 100times diluted supernatant UV-Vis spectra after drug loading to PCN (Initial dox concentration is 8 mg/mL in DMSO).

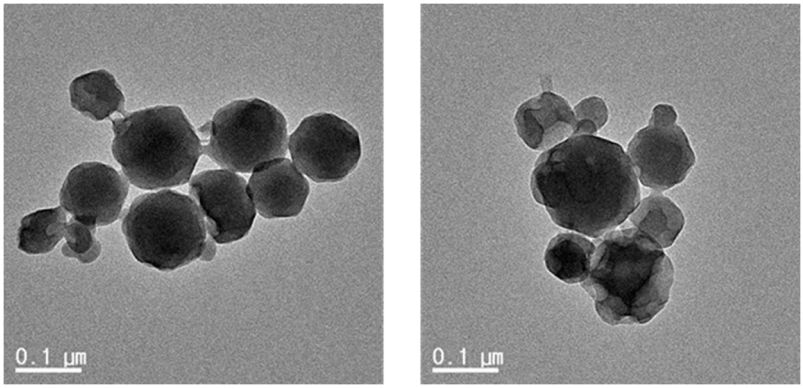


**Figure 4-7.** TEM image of HA-Dox-PCN nanoparticle that size is around 90 nm

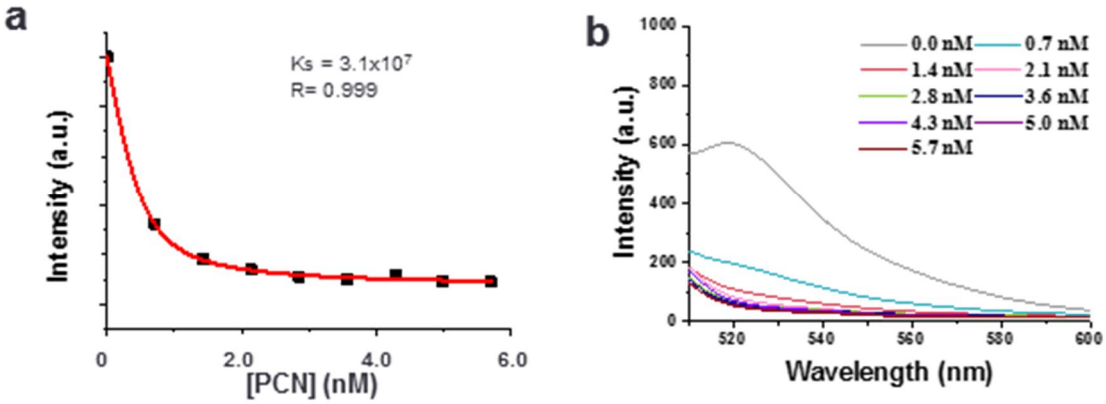


**Figure 4-8.** a,b) Fluorescence titration graph ( HA molecular weight: 8,000 ~ 15,000 )

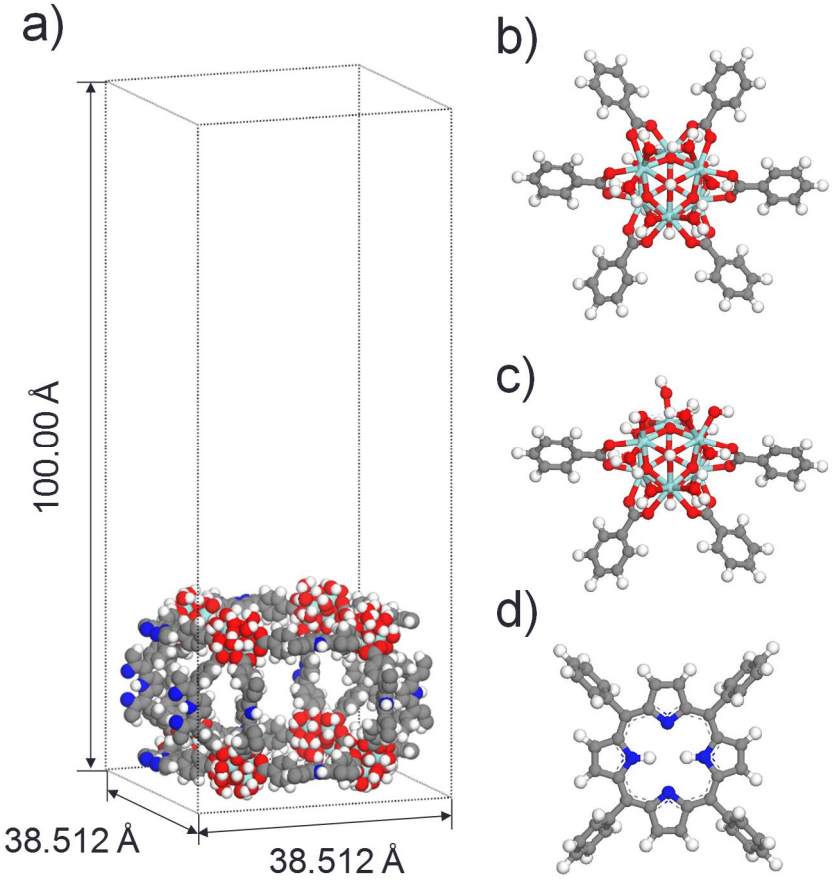


**Figure 4-9.** a) Slab models of PCN-224 MOF. Fragmented Zr6 cluster model in b) bulk and c) surface region. d) Fragmented TCPP ligand cluster. For the clear view, the slab model is presented by space-filling model, whereas cluster models are presented by ball-and-stick. The Zr, C, H, O, and N atoms are colored in cyan, gray, white, red, and blue, respectively.

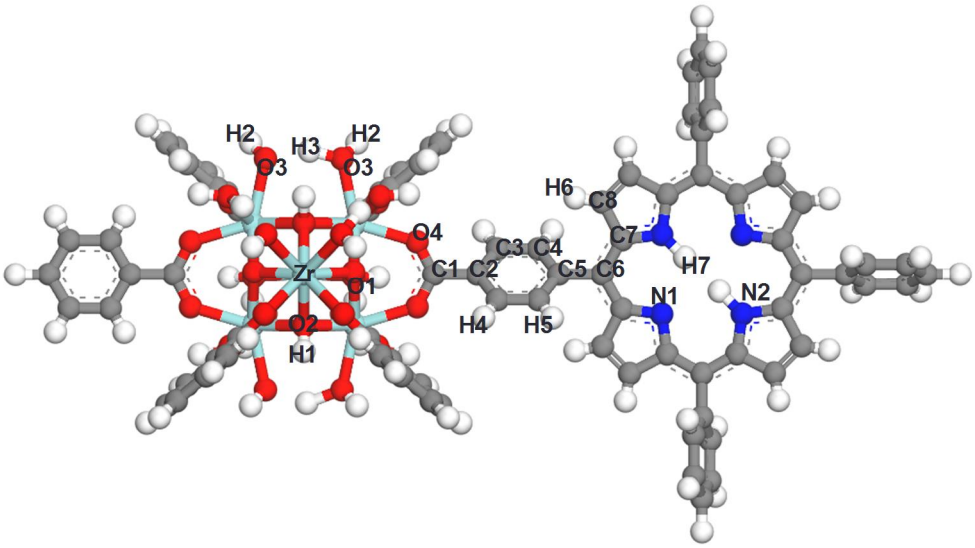


**Figure 4-10.** Atomic type representation of PCN-224 (see Table 4-1). Color scheme is same as Figure 4-9.

**Table 4-1.** Partial charges for atomic types in PCN-224 (as labeled in Figure 4-10).

| Atom | Charge (*e*) | Atom | Charge (*e*) |
|---|---|---|---|
| C1 | 0.600 | H1 | 0.317 |
| C2 | -0.032 | H2 | 0.290 |
| C3 | -0.088 | H3 | 0.373 |
| C4 | -0.097 | H4 | 0.112 |
| C5 | 0.035 | H5 | 0.069 |
| C6 | 0.047 | H6 | 0.071 |
| C7 | 0.160 | H7 | 0.248 |
| C8 | -0.132 | O1 | -0.938 |
| Zr | 1.964 | O2 | -0.792 |
| N1 | -0.260 | O3 | -0.702 |
| N2 | -0.410 | O4 | -0.600 |
| Hs (Surface) | 0.171 | Os (Surface) | -0.742 |

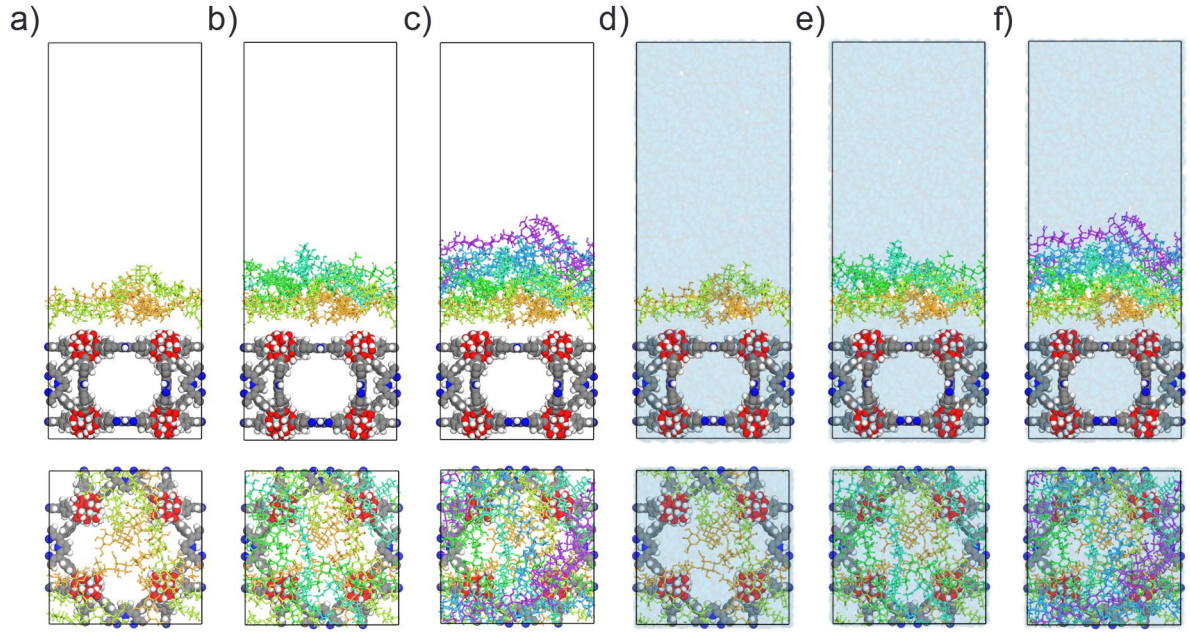


**Figure 4-11.** Initial models employed in MD simulations. Slab models with a) 2, b) 4, and c) 6 HA decamers. Slab models with d) 2, e) 4, f) 6 HA decamers in hydrated condition. For the clear view, the slab models are presented by space-filling model, whereas HA decamers are shown by stick with each different color (from orange to purple). Water molecules are presented by transparent blue space-filling model. Color scheme of the atoms in the slab models is same as Figure 4-9.

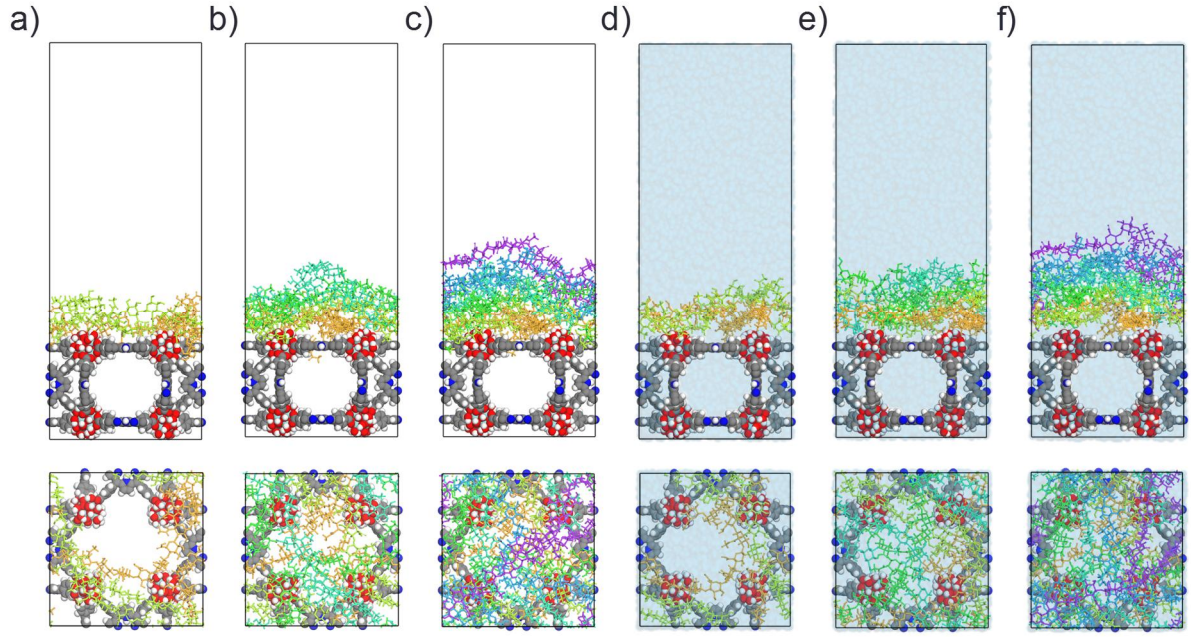


**Figure 4-12.** Equilibrated structures of HA-coating on PCN-224 surface after 3ns MD simulations. Slab models with a) 2, b) 4, and c) 6 HA decamers. Slab models with d) 2, e) 4, f) 6 HA decamers in hydrated condition. Color scheme and presented styles are same as Figure 4-11.

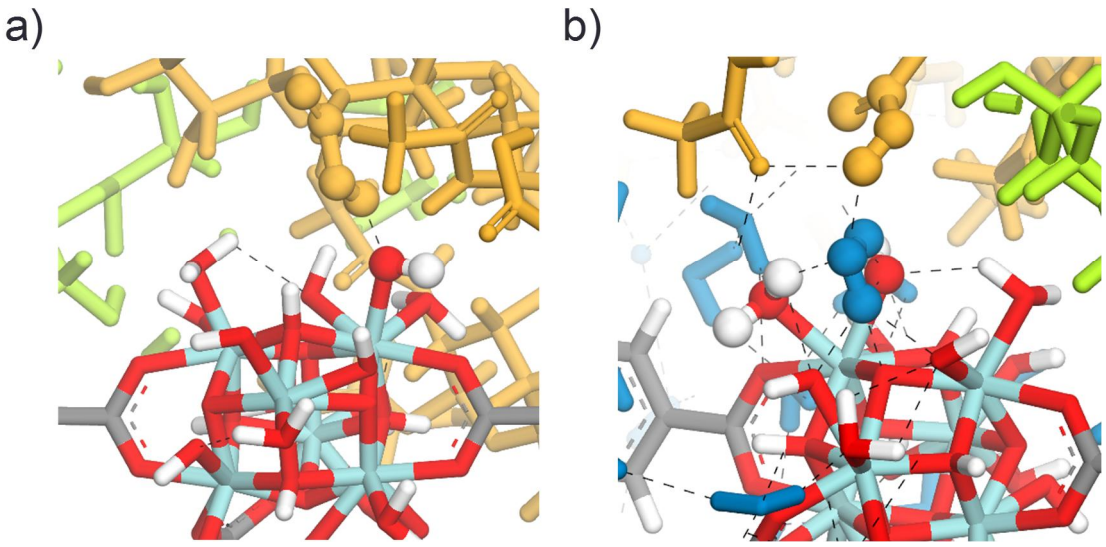


**Figure 4-13.** Enlarged snapshots of interacting structures between HA decamers and PCN-224 surface a) without and b) with water molecules. Black dashed lines represent hydrogen bond. For the clear view, some selected atoms are shown by ball-and-stick to show hydrogen bonding between HA and PCN-224 with water. Except for these atoms, all atoms are shown by stick, and color scheme is same as Figure 4-11.

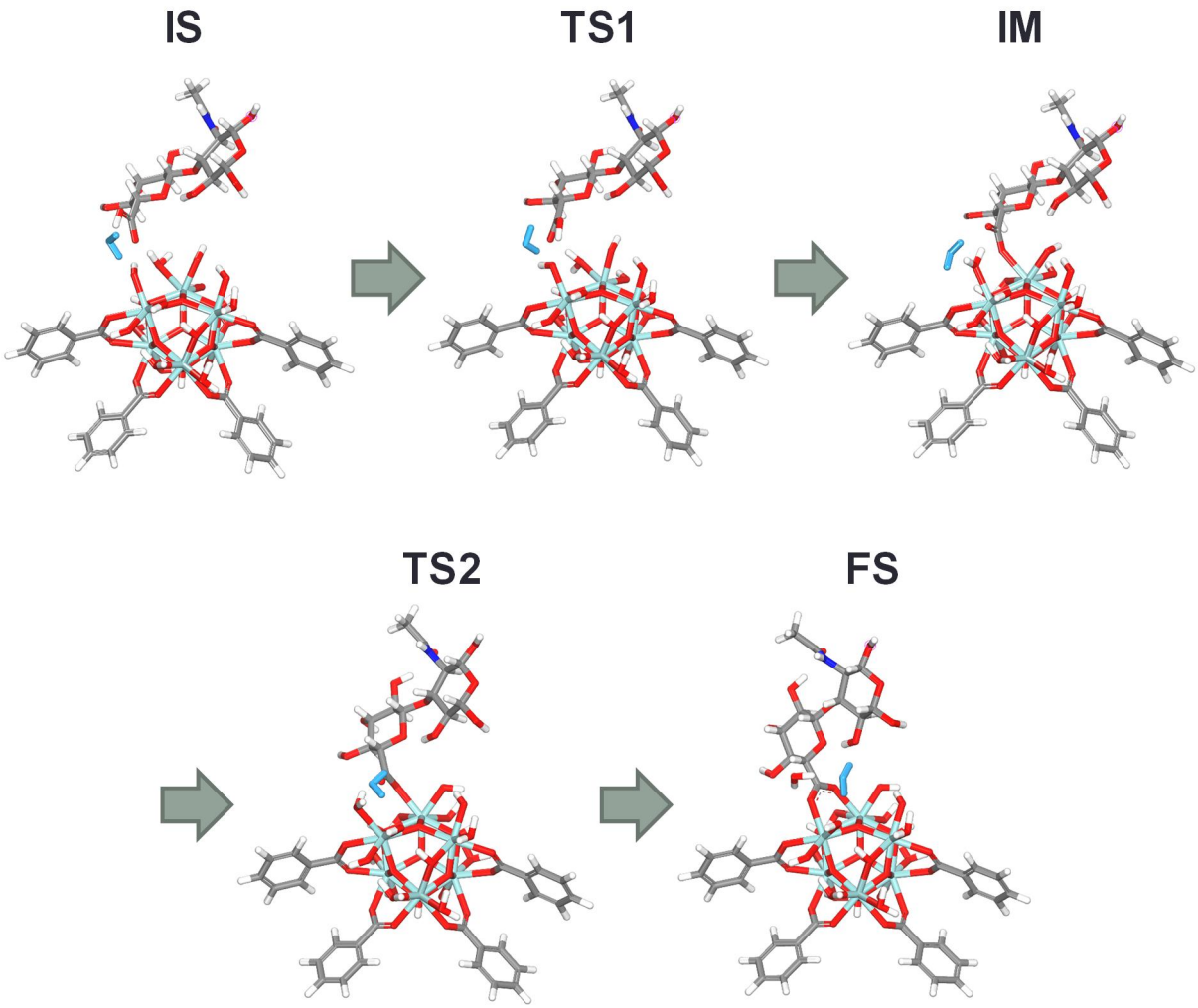


**Figure 4-14.** Extended atomic configurations of the formation mechanism of coordination bond between HA monomer and Zr6 cluster model in surface region. The acronyms IS, TS, IM and FS represent the initial, transition, intermediate, and final states, respectively. Except for water molecule in blue, all atoms are presented by stick, and color scheme is same as Figure 4-9.

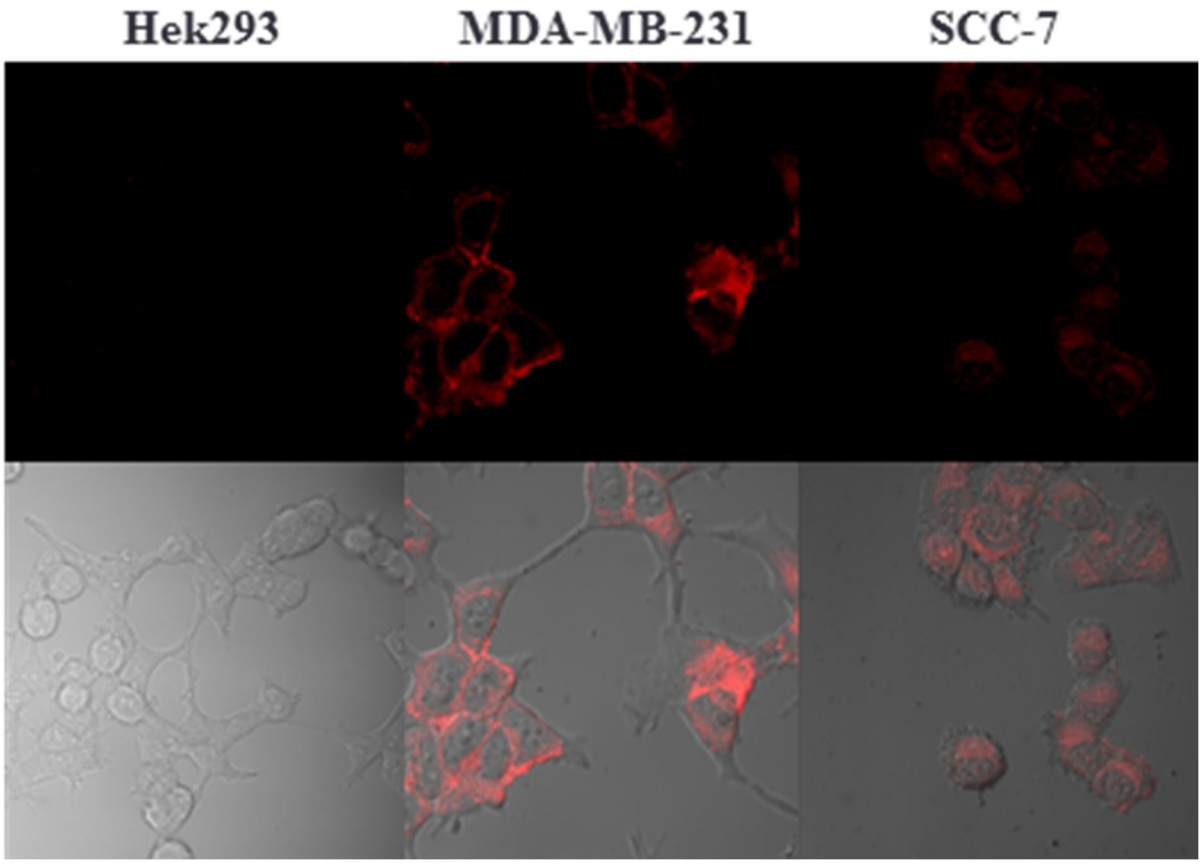


**Figure 4-15.** Confocal microscope images of of HeK 293T, MDA-MB-231 and SCC7 to check the cellular uptake of HA-Dox-PCN nanoparticles after 2h incubation.

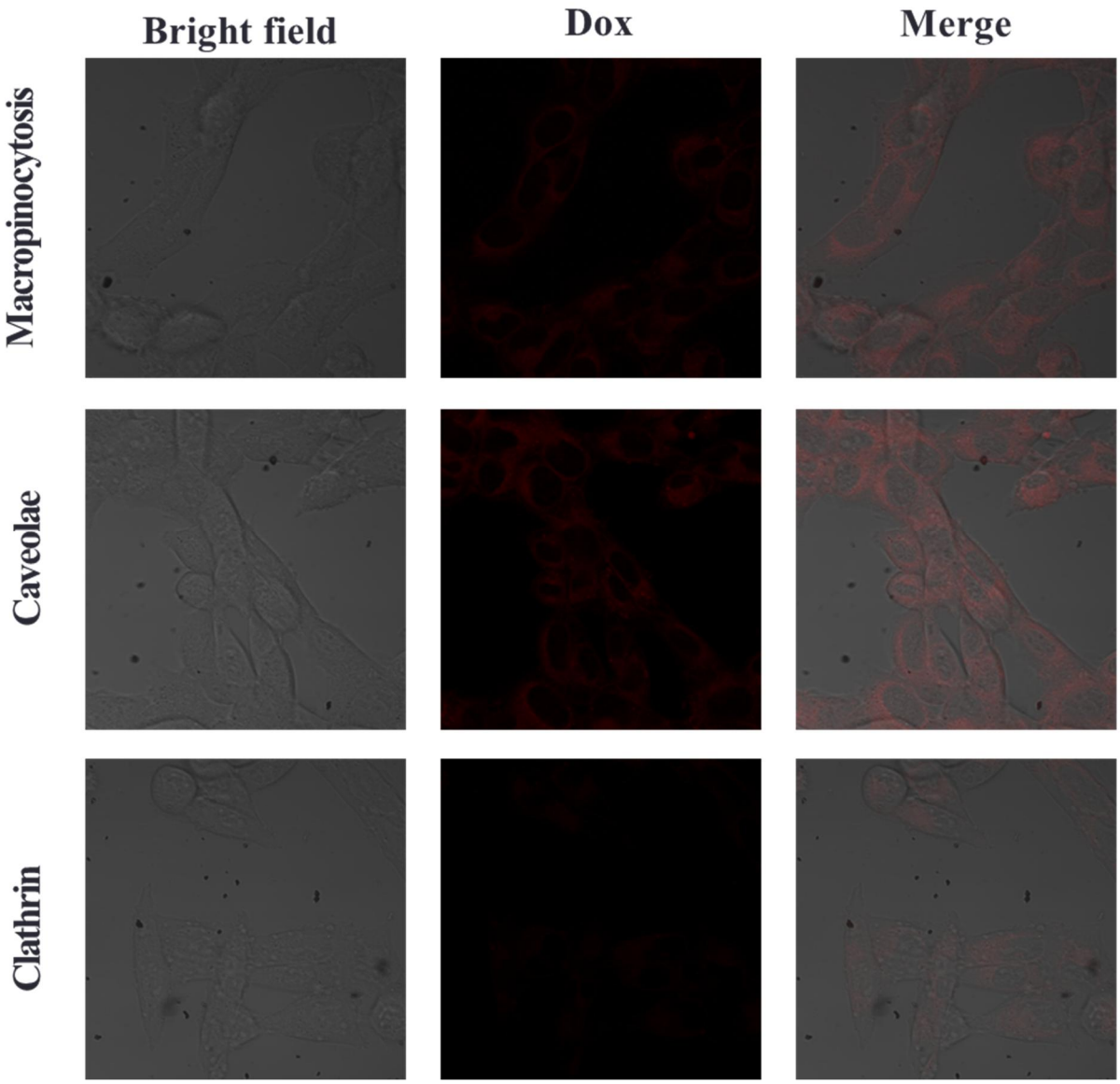


**Figure 4-16.** Confocal microscope images of SCC7 cells incubated in presence of uptake pathway inhibitors to check the uptake pathway of HA-Dox-PCN nanoparticles after 2h incubation.

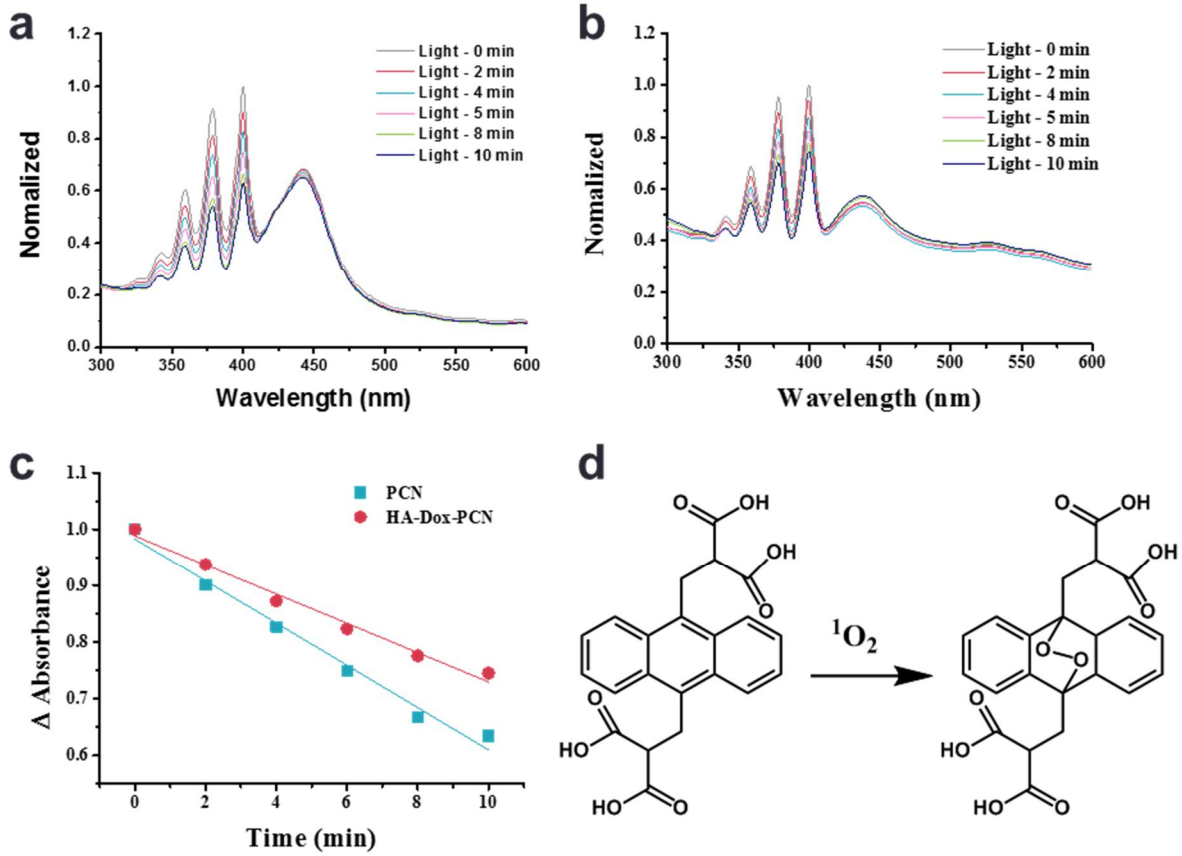


**Figure 4-17.** ABDA assay analysis of a) PCN-224 and b) HA-Dox-PCN for checking singlet oxygen generation. c) Absorbance decrease of ABDA by generation of singlet oxygen d) d) ABDA reaction mechanism with singlet oxygen.

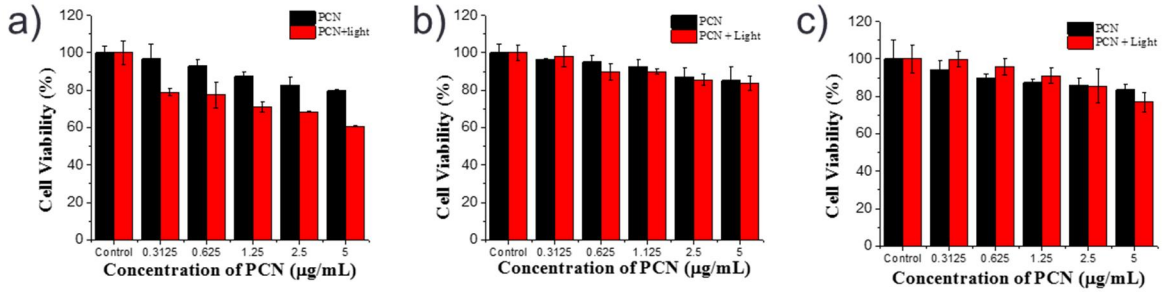


**Figure 4-18.** Cell viability analysis of PCN at different cell line a) Hek 293T, b) MDA-MB-231, and c) SCC7.

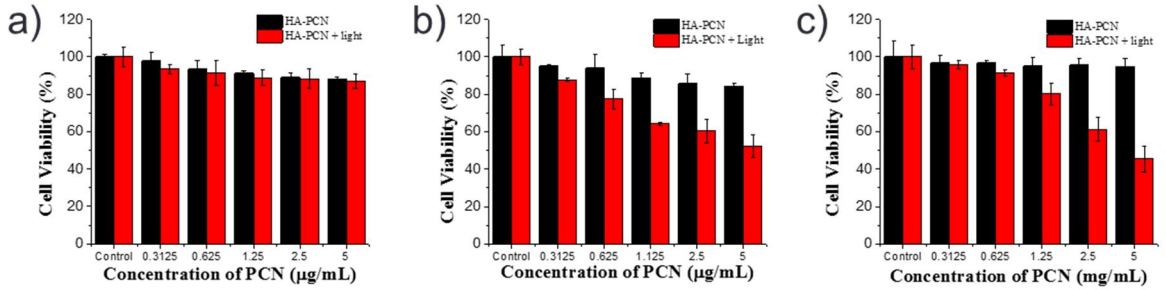


**Figure 4-19.** Cell viability analysis of HA-PCN at different cell line a) Hek 293T, b) MDA-MB-231, and c) SCC7.

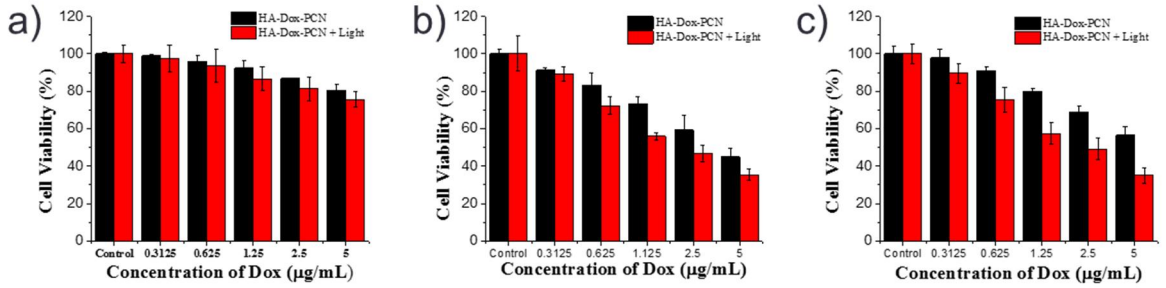


**Figure 4-20.** Cell viability analysis of HA-Dox-PCN at different cell line a) Hek 293T, b) MDA-MB-231, and c) Scc7.

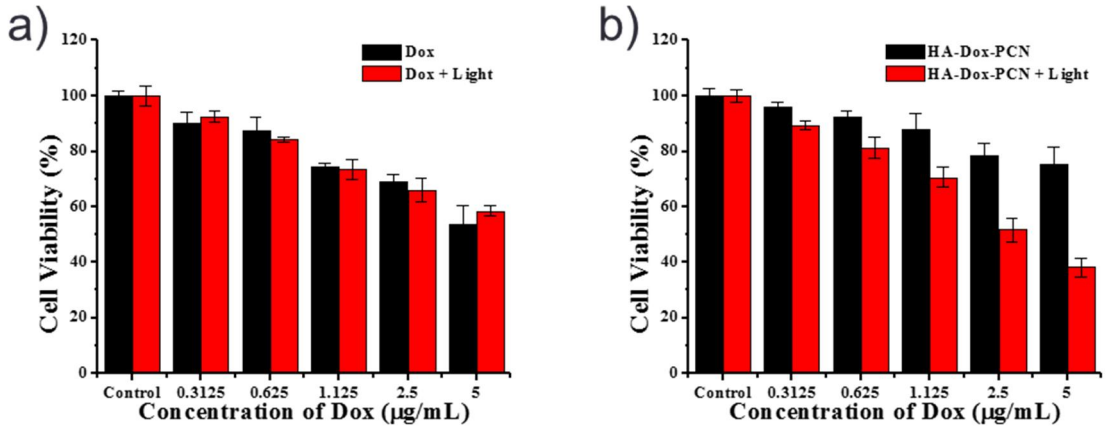


**Figure 4-21.** Cell viability analysis of HA-Dox-PCN at MCF-7/ADR cell a) free Dox, b) HA-Dox-PCN.

**Material and method**

General information: All chemicals and reagents were purchased from Sigma-Aldrich, TCI and Alfa Aesar, Korea unless otherwise specified and used without further purifications. Sodium hyaluronate was purchased from Acros Organic (Belgium). Doxorubicin hydrochloride was obtained from Ontario Chemicals Inc, Canada. Deionized (DI) water was produced by the Millipore Milli-Q system (18.2 MΩ cm).

**Preparation of PCN-224 (100 nm):** PCN-224 nanoparticles were synthesized in a solvothermal condition as reported.[30] Meso-Tetra(4-carboxyphenyl)porphine (TCPP) (100mg, 0.13mmol), $ZrOCl_2 \cdot 8H_2O$ (300mg, 0.93mmol), benzoic acid (2.8g, 23mmol) and DMF (100mL) were combined in a 250mL round-bottom flask. The mixture was heated to 90 °C for 5hours with 300rpm stirring and then cooled to room temperature. The product was collected by centrifugation with 15000rpm for 30min and washed by fresh DMF and acetone. The synthesized PCN-224 sample was characterized by powder X-ray diffraction (PXRD).

**Characterizations of PCN:** Before gas adsorption measurement, 90 nm-PCN-224 samples were thoroughly washed with DMF for three times and acetone for twice. After decanting acetone, samples were dried under vacuum for 3 hours. And the dried powder was activated at 85 °C for 30 min and 120 °C for 5hours on ASAP 2020 for $N_2$ adsorption measurement. BET surface area for PCN-224 is 2296(8) $m^2/g$. Corresponding pore size distribution was analyzed by the non-local density functional theory (NLDFT).

**Preparation of Dox-PCN:** About 4 mg of PCN-224 were dispersed in 8mg of Dox were dissolved in 1 mL of DMSO and stir for 24 hours at room temperature. Then the Dox loaded PCN-224 was collected by centrifugation and dried under high vacuum. Then dried samples were redispersed in DI water. The supernatant solution containing unloaded Dox were analyzed under UV-Visible spectra using molar absorption coefficient.

Drug loading capacity (%): Mass of the drug in PCN-224/Mass of PCN-224 * 100

**Preparation of HA-Dox-PCN:** About 1 mg of Dox loaded PCN were dispersed in 20 mL of DI water containing 2 mg of Hyaluronic acid (HA) and stir for 24 hours at room temperature. Then HA coated Dox-PCN was collected by centrifugation and redispersed in DI water. HA-Dox-PCN was washed 3 times by repeated centrifugation and redispersion. The supernatant solution containing unmodified HA were analyzed by carbazole assay.

**Synthesis of Amine modified FITC:** Amine functional group was modified to fluorescein isothiocyanate (FITC) to prepare FITC-HA. FITC (5 mg, 12 μmol) and ethylenediamine (1 μL, 18

μmol) were dissolved in 2 mL of DMSO. The mixture was stirred at room temperature for 12 hours. The solvents and ethylenediamine was removed by freeze drier.

**Synthesis of FITC-HA:** Hyaluronic acid (20 mg) was dissolved in 10 mL of DI water. Then, EDC (15mg, 97 μmol) and NHS (11mg, 96 μmol) was added in HA solution. The mixture was stirred at room temperature for 4 hours. Then, Amine modified FITC (2.2 mg, 5 μmol) was added in the mixture solution. After stirring at room temperature for 24 hours, the mixture was purified by dialysis by using 2.5K dialysis bag for 1 week. After dialysis, solution was removed by the freeze drier.

**Drug Release Profile:** Release kinetics of HA-Dox-PCN was analyzed by Shimadzu RFPC 5430 spectrophotometer. Nanoparticle was dispersed in phosphate-buffered saline (pH 7.4). After dispersion, Dox fluorescence intensity was measured on a at excitation wavelengths of 480 nm. To determine the induced drug release profile, HAdase (400 U/ml) was added to the nanoparticle solution at 4 hours and the release profile was analyzed using a fluorescence.

**Singlet oxygen generation analysis:** Newport IQE-200 solar simulator (Irvine, CA, USA) was used as a light source. The power density for light was 40 $mW/cm^2$. To measure the generated singlet oxygen ($^1O_2$), 9,10-anthracenediyl bis(methylene)malonic acid (ABDA) and nanoparticle (100 μM and 20 μM) was prepared in distilled water. The absorbance of ABDA is attenuated after reaction with $^1O_2$ from PCN-224. The degree of absorbance changes before/after photo-irradiation implies absolute amount of generated $^1O_2$. Absorbance was obtained for every 2 minutes under the irradiation. Binding constant analysis: 1 mL HA-FITC solution (2.5 nM) was placed in the vial. Different volume of PCN-224 (8.55 nM) and D.I water were subsequently added to the HA-FITC solution. Mixture solution volume adjust to 3 mL. Emission spectrum of sample was recorded with excitation at 470 nm. After measurement, The normalized fluorescence intensities calibrated by respective controls at 520 nm were plotted against the concentration of PCN-224. Nonlinear least-squares curve-fitting analysis was conducted to estimate the complex stability.

**Cell culture:** Murine squamous carconoma cell SCC-7, Human breast cancer cell lines MDA-MB-231, Human breast cancer MCF-7/ADR cells and non-cancerous fibroblast HeK293T cells were obtained as a gift from Prof. Sebuyang Kang lab at UNIST and Prof. Ick Chan Kwon at KIST, Korea. The cells were cultured (using RPMI 1640 and DMEM medium, respectively) while supplemented with 10% fetal bovine serum (FBS), 100 μg $mL^{-1}$ streptomycin and 100 U $mL^{-1}$ penicillin under incubation at 37 °C and humidified with 5% $CO_2$.

**Cell viability analysis:** Cells ($5 \times 10^3$ cells/well) were cultured in sterile 96-well Nunc (Thermo

Scientific Inc.) plates for 24 hours and treated with different concentrations of PCN, HA-Dox-PCN (1.0, 2.0, 3.0, 4.0 and 5.0 μg/mL) for 12 hours in dark, then media was replaced with fresh media and the cells were irradiated for 30 min at 1 sun light (100 mW $cm^{-2}$ ) using the solar simulator. Cells were incubated for another 12 hours before checking the cell cytotoxicity using Alamar blue dye assay following the manufacturer's protocol (DAL 1025, Invitrogen).

**Endocytic pathway analysis:** To check the endocytosis mediated uptake pathway of HA-Dox-PCN, MDA-MB231 cells were seeded in four well chambered cover glass (Lab Tek II, Thermo Scientific Inc.) and pretreated with different inhibitors including sucrose (clathrin-mediated uptake, 400 nM), methyl-beta cytodextrin (caveolae mediated uptake) and amilorin (macropinocytosis) in serum-free DMEM for 1 hour and replaced with fresh media. [35] Afterwards, HA-Dox-PCN were added to the medium for another 1 h incubation. Then the cells were analyzed under the confocal microscope (Olympus FV1000) connected to $CO_2$ incubator.

**Cellular uptake analysis:** The cellular uptake of HA-Dox-PCN nanoparticles in HeK293T, MDA-MB-231 and SCC-7 cells were investigated by live confocal microscope images (Olympus FV 1000 series). The cells were seeded at a density of 2 x $10^5$ cells/well in two well chambered cover glass (Lab Tek II, Thermo Scientific. After 24 hours incubation, cells were treated with HA-Dox-PCN at a final concentration of Dox at 10 μg/mL at different time points and analyzed using the confocal microscope.

**Theoretical methods**

**Molecular modeling:** To investigate the interfacial structure between HA-coating and PCN-224 surface via molecular dynamics (MD) simulation and density functional theory (DFT) calculation, we modelled two kinds of model systems for PCN-224 MOF, *i.e.* slab and cluster models. Each model was taken from crystal structure of PCN-224, which was obtained from experimental XRD analysis. For the charge balance around the Zr(IV) atom, half of $\mu_3$-OH and μ-OH in each $Zr_6$ node were substituted by $\mu_3$-O and μ-$H_2O$, respectively, as suggested by Park *et al.*'s work.[30] The slab model was modeled as thin monolayer slab perpendicular to (100) surface, which was composed of 8 $Zr_6$ nodes and 8 TCPP ligands, with about 70 Å of vacuum region (Figure 4-9a). Dangling bonds and charge imbalance due to (100) surface cleavage were compensated by adding two hydroxyl groups to each $Zr_6$ node, *i.e.* $(Zr_6(\mu_3\text{-}O)_4(\mu_3\text{-}OH)_4(\mu\text{-}OH)_8(\mu\text{-}H_2O)_6)_8TCPP_8$. For the cluster model, we employed 3 fragmented cluster models to represent the structure around $Zr_6$ node in the bulk and surface regions as well as TCPP ligand, respectively (Figure 4-9b-d). The TCPP ligand was so bulky that it was replaced by carboxy phenyl functional group in $Zr_6$ cluster. Thus, the $Zr_6$ cluster model in bulk region

was composed of $Zr_6(\mu_3\text{-}O)_4(\mu_3\text{-}OH)_4(\mu\text{-}OH)_6(\mu\text{-}H_2O)_6(C_6H_5COO)_6$, whereas that in surface region was composed of $Zr_6(\mu_3\text{-}O)_4(\mu_3\text{-}OH)_4(\mu\text{-}OH)_8(\mu\text{-}H_2O)_6(C_6H_5COO)_4$. These cluster models were employed for calculating partial charges of PCN-224 (Figure 4-10 and Table 4-1), and for calculating formation mechanism of coordination bond.

**Molecular Dynamics:** To observe physical adsorption of HA polymers on nanoMOF, we employed slab model and HA decamer, whose length was about 2 to 3 times longer than one side of the slab model. In the MD simulation, we modelled HA-MOF systems with three different numbers of HA decamers (i.e. 2, 4, and 6 HA decamers, respectively) near one side of the surface (Figure 4-11). In addition, to apply hydrated condition in HA-coating, hydrated models were also considered, where water molecules were packed in all void region of each system. In the MD simulation, the PCN-224 slab was regarded as a rigid body, whereas HA and water molecules were free to move. To observe relaxed configuration of HA, we carried out thermal annealing in the range of temperatures between 298K and 500 K for 3 ns. For the non-bonding interaction energy parameters of slab model, universal forcefield[36] and mulliken charges[37] obtained from DFT were employed. Atomic charges employed in MD simulation are summarized in Table S1. For HA polymers and water molecules, consistent-valence forcefield (CVFF)[38] was applied to describe bonding and non-bonding interaction parameters. Lorentz-Berthelot combination rule[39, 40] was applied for the van der Waals parameters between slab model and HA or water in the system.

**Density Functional Theory (DFT):** We investigated the formation mechanism of coordination bond between HA and $Zr_6$ metal node using DMol$^3$ program.[41, 42] The mechanism was predicted to be a dehydration condensation reaction by the interaction between the carboxylic acid functional group of HA and the hydroxyl group coordinated to the metal node. For the DFT calculation, we employed the Perdew-Burke-Ernzerhof (PBE) exchange-correlation functional[43] and DNP 4.4 basis set with the all-electron relativistic core treatment. The convergence criteria for energy, force, and displacement were set to $1\times10^{-5}$ Ha, 0.002 Ha/Å, and 0.005 Å, respectively. To include the dispersion correction of the van der Waals effect, the Tkatchenko-Scheffler scheme was used.[44] The electrostatic contribution in hydrated condition was considered by applying the Conductor-like Screening Model (COSMO) method[45], with the dielectric constants of water ($\varepsilon$ = 78.54). To calculate transition states in the formation mechanism of the coordination bond between Ha and $Zr_6$ metal node, we employed complete single linear synchronous transit (LST) and quadratic synchronous transit (QST) methods[46, 47], and the convergence criteria of the root mean square (RMS) force was set as 0.002 Ha/Å

**4.6 References**

1. Siegel, R. L.; Miller, K. D.; Jermal, A. Cancer statistics, 2018. A. Jemal, *CA Cancer J. Clin.* **2018**, *68*, 7-30.

2. Allen, T. M.; Cullis, P. R. Drug delivery systems: entering the mainstream. *Science* **2004**, *303*, 1818-1822.

3. Park, K. Facing the truth about nanotechnology in drug delivery. *ACS nano* **2013**, *7*, 7442-7447.

4. Peer, D.; Karp, J. M.; Hong, S.; Farokhzad, O. C.; Margalit, R.; Langer, R. Nanocarriers as an emerging platform for cancer therapy. *Nat. Nanotechnol.* **2007**, *2*, 751-760;

5. Wong, P. T.; Choi, S. K.; Mechanisms of drug release in nanotherapeutic delivery systems. *Chem. Rev.* **2015**, *115*, 3388-3432.

6. Slowing, I.I.; Vivero-Escoto, J. L.; Wu, C. W.; Lin, V. S. -Y. Mesoporous silica nanoparticles as controlled release drug delivery and gene transfection carriers. *Adv. Drug Deliv. Rev.* **2008**, *60*, 1278-1288.

7. Matea, C. T.; Mocan, T.; Tabaran, F.; Pop, T.; Mosteanu, O.; Puia, C.; Iancu, C.; Mocan, L. Quantum dots in imaging, drug delivery and sensor applications. *Int. J. Nanomedicine* **2017**, *12*, 5421-5431.

8. Ghosh, P.; Han, G.; De, M.; Kim, C. K.; Rotello, V. M. Gold nanoparticles in delivery applications. *Adv. Drug Deliv. Rev.* **2008**, *60*, 1307-1315;

9. Sun, C.; Lee, J. S. H.; Zhang, M. Magnetic nanoparticles in MR imaging and drug delivery. *Adv. Drug Deliv. Rev.* **2008**, *60*, 1252-1265;

10. Sun, T.; Zhang, Y. S.; Pang, B.; Hyun, D. C.; Yang, M.; Xia, Y. Engineered nanoparticles for drug delivery in cancer therapy. *Angew. Chem. Int. Ed.* **2014**, *53*, 12320-12364

11. Kumari, A.; Yadav, S. K.; Yadav, S. C. Biodegradable polymeric nanoparticles based drug delivery systems. *Colloids Surf. B: Biointerfaces* **2010**, *75*, 1-18.

12. Medina, S. H.; El-Sayed, M. E. H. Dendrimers as carriers for delivery of chemotherapeutic agents. *Chem. Rev.* **2009**, *109*, 3141-3157

13. Kim, I. -Y.; Joachim, E.; Choi, H.; Kim, K. Toxicity of silica nanoparticles depends on size, dose, and cell type. *Nanomedicine* **2015**, *11*, 1407-1416;

14. Moore, T. L.; Rodriguez-Lorenzo, L.; Hirsch, V.; Balog, S.; Urban, D.; Jud, C.; Rothen-Rutishauser, B.; Lattuada, M.; Petri-Fink, A. Nanoparticle colloidal stability in cell culture media and impact on cellular interactions. *Chem. Soc. Rev.* **2015**, *44*, 6287-6305;

15. Tong, R.; Cheng, J. Paclitaxel-initiated, controlled polymerization of lactide for the formulation of polymeric nanoparticulate delivery vehicles. *Angew. Chem.* **2008**, *120*, 4908-4912.

16. Wu, M. -X.; Yang, Y. -W. Metal–organic framework (MOF)-based drug/cargo delivery and cancer therapy. *Adv. Mater.* **2017**, *29,* 1606134;

17. Rocca, J. D.; Liu, D.; Lin, W. Nanoscale metal–organic frameworks for biomedical imaging and

drug delivery. *Acc. Chem. Res* **2011**, *44*, 957-968;

18. Lu, K.; He, C.; Lin, W.; Nanoscale metal–organic framework for highly effective photodynamic therapy of resistant head and neck cancer. *J. Am. Chem. Soc.* **2014**, *136*, 16712-16715.

19. Lu, W.; Wei, Z.; Gu, Z. -Y.; Liu, T. -F.; Park, J.; Park, J.; Tian, J.; Zhang, M.; Zhang, Q.; Gentle III, T.; Bosch, M.; Zhou, H. -C. Tuning the structure and function of metal–organic frameworks via linker design. *Chem. Soc. Rev.* **2014**, *43,* 5561-5593.

20. Furukawa, H.; Cordova, K. E.; O'Keeffe, M.; Yaghi, O. M. The chemistry and applications of metal-organic frameworks. *Science* **2013**, *341*, 1230444.

21. Zhang, M.; Bosch, M.; Gentle III, T.; Zhou, H.-C. Rational design of metal–organic frameworks with anticipated porosities and functionalities. *CrystEngComm* **2014**, *16*, 4069-4083.

22. Kim, D.; Liu, X.; Lah, M. S. Topology analysis of metal–organic frameworks based on metal–organic polyhedra as secondary or tertiary building units. *Inorg. Chem. Front.* **2015**, *2*, 336-360;

23. Guillerm, V.; Kim, D.; Eubank, J. F.; Luebke, R.; Liu, X.; Adil, K.; Lah, M. S.; Eddaoudi, M. A supermolecular building approach for the design and construction of metal–organic frameworks. *Chem. Soc. Rev.* **2014**, *43*, 6141-6172.

24. Li, B.; Wen, H. -M.; Cui, Y.; Zhou, W.; Qian, G.; Chen, B. Emerging multifunctional metal–organic framework materials. *Adv. Mater.* **2016**, *28*, 8819-8860.

25. Ricco, R.; Pfeiffer, C.; Sumida, K.; Sumby, C. J.; Falcaro, P. Furukawa, S.; Champness, N. R.; Doonan, C. J. Emerging applications of metal–organic frameworks. *CrystEngComm* **2016**, *18*, 6532-6542.

26. Cunha, D.; Yahia, M. B.; Hall, S.; Miller, S. R.; Chevreau, H.; Elkaïm, E.; Maurin, G.; Horcajada, P.; Serre, C. Rationale of drug encapsulation and release from biocompatible porous metal–organic frameworks. *Chem. Mater.* **2013**, *25*, 2767-2776;

27. Horcajada, P.; Chalati, T.; Serre, C.; Gillet, B.; Sebrie, C.; Baati, T.; Eubank, J. F.; Heurtaux, D.; Clayette, P.; Kreuz, C.; Chang, J. S.; Hwang, Y. K.; Marsaud, V.; Bories, P. -N.; Cynober, L.; Gil, S.; Ferey, G.; Couvreur, P.; Gref, R. Porous metal–organic-framework nanoscale carriers as a potential platform for drug delivery and imaging. *Nat. Mater.* **2010**, *9*, 172-178.gpa

28. Feng, D.; Chung, W. -C.; Wei, Z.; Gu, Z. -Y.; Jiang, H. -L.; Chen, Y. -P.; Darensbourg, D. J.; Zhou, H. -C. Construction of ultrastable porphyrin Zr metal–organic frameworks through linker elimination. *J. Am. Chem. Soc.* **2013**, *135*, 17105-17110.

29. Bosch, M.; Zhang, M.; Zhou, H.-C. Increasing the stability of metal-organic frameworks. *Adv. Chem.* **2014**, *2014*, 182327.

30. Park, J.; Jiang, Q.; Feng, D.; Mao, L.; Zhou, H. -C. Size-controlled synthesis of porphyrinic metal–organic framework and functionalization for targeted photodynamic therapy. *J. Am. Chem. Soc.* **2016**, *138*, 3518-3525.

31. Tan, L. -L.; Li, H.; Zhou, Y.; Zhang, Y.; Feng, X.; Wang, B.; Yang, Y. -W. $Zn^{2+}$-Triggered Drug

Release from Biocompatible Zirconium MOFs Equipped with Supramolecular Gates. *Small* **2015**, *11*, 3807-3813;

32. Meng, X.; Gui, B.; Yuan, D.; Zeller, M.; Wang, C. Mechanized azobenzene-functionalized zirconium metal-organic framework for on-command cargo release. *Sci. Adv.* **2016**, *2*, e1600480.

33. Zhang, W.; Li, Y.; Sun, J. -H.; Tan, C. -P.; Ji, L. -N.; Mao, Z. -W. Supramolecular self-assembled nanoparticles for chemo-photodynamic dual therapy against cisplatin resistant cancer cells. *Chem. Commun.* **2015**, *51*, 1807-1810;

34. Khdair, A.; Chen, D.; Patil, Y.; Ma, L.; Dou, Q. P.; Shekhar, M. P. V.; Panyam, J. Nanoparticle-mediated combination chemotherapy and photodynamic therapy overcomes tumor drug resistance. *J. Control. Release* **2010**, *141*, 137-144

35. Palanikumar, L.; Kim, H. Y.; Oh, J. Y.; Thomas, A. P.; Choi, E. S.; Jeena, M.T.; Joo, S. H.; Ryu, J-. H. Noncovalent surface locking of mesoporous silica nanoparticles for exceptionally high hydrophobic drug loading and enhanced colloidal stability. *Biomacromolecules* **2015**, *16*, 2701-2714.

36. Rappe, A. K.; Casewit, C. J.; Colwell, K. S.; Goddard, W. A.; Skiff, W. M. UFF, a full periodic table force field for molecular mechanics and molecular dynamics simulations. *J. Am. Chem. Soc.* **1992**, *114*, 10024-10035.

37. Mulliken, R. S. Electronic population analysis on LCAO–MO molecular wave functions. I. *J. Chem. Phys.* **1955**, *23*, 1833-1840.

38. Dauber-Osguthorpe, P.; Roberts, V. A.; Osguthorpe, D. J.; Wolff, J.; Genest, M.; Hagler, A. T. Structure and energetics of ligand binding to proteins: Escherichia coli dihydrofolate reductase-trimethoprim, a drug-receptor system. *Proteins: Struct., Function Genetics* **1988**, *4*, 31-47.

39. Lorentz, H. A. Ueber die Anwendung des Satzes vom Virial in der kinetischen Theorie der Gase. *Ann. Phys.* **1881**, *12*, 127-136.

40. Berthelot, D.Sur le mélange des gaz. *C. R. Hebd. Seances Acad. Sci., Paris* **1898**, *126*, 1703-1706.

41. Delley, B. An all-electron numerical method for solving the local density functional for polyatomic molecules. *J. Chem. Phys*. **1990**, *92*, 508-517.

42. Delley, B. From molecules to solids with the $DMol^3$ approach. *J. Chem. Phys.* **2000**, *113*, 7756-7764.

43. Perdew, J. P.; Burke, K.; Ernzerhof, M. Generalized gradient approximation made simple. *Phys. Rev. Lett.* **1996**, *77*, 3865-3868.

44. Tkatchenko, A.; Scheffler, M. Accurate molecular van der Waals interactions from ground-state electron density and free-atom reference data. *Phys. Rev. Lett.* **2009**, *102*, 073005.

45. Klamt, A.; Schüürmann, G. COSMO: a new approach to dielectric screening in solvents with explicit expressions for the screening energy and its gradient. *J. Chem. Soc. Perkin Trans. 2*, **1993**, *5*, 799-805.

46. Bell, S.; Crighton, J. S. Locating transition states. *J. Chem. Phys*. **1984**, *80*, 2464-2475.

47. Halgren, T. A.; Lipscomb, W. N. The synchronous-transit method for determining reaction pathways and locating molecular transition states. *Chem. Phys. Lett.* **1977**, *49*, 225-232.

48. Palanikumar, L.; Choi, E. S.; Cheon, J. Y.; Joo, S. H.; Ryu, J.-H. Noncovalent polymer-gatekeeper in mesoporous silica nanoparticles as a targeted drug delivery platform. *Adv. Funct. Mater.* **2015**, *25*, 957-965.

49. You, C. -C.; Miranda, O. R.; Gider, B.; Ghosh, P. S.; Kim, I. -B.; Erdogan, B.; Krovi, S. A.; Bunz, U. H. F.; Rotello, V. M. Detection and identification of proteins using nanoparticle–fluorescent polymer 'chemical nose'sensors. *Nat. Nanotechnol.* **2007**, *2*, 318-323.

50. Zhang, H.; Li, D.; Cheng, J.; Lin, F.; Mao, J.; Jen, A. K. -Y.; Grätzel, M.; Choy, W. C. H. Room temperature formation of organic–inorganic lead halide perovskites: design of nanostructured and highly reactive intermediates. J. Mater. Chem. A 2017, 5, 3599-3608

# Chapter 5. Polyvalent interaction between MOF and polymer for effective cancer therapy.

## 5.1 Abstract

NanoMOF, with a high surface, porous and easily adjustable structure, has attracted much attention in drug delivery systems. In particular, the unsaturated metal clusters present on the MOF surface can easily form coordination bonds with Lewis compounds for post-functionalization. Various nanoMOF drug delivery systems utilize this feature to modify cancer-targeting ligands or DNA on the MOF surface, but various proteins and bio chemical with Lewis bases are present in the body, and these substances induce the detachment of the modified ligand on the MOF surface. Therefore, in order to prevent the above detachment and to enhance its therapeutic effects in cancer treatment, we studied a stable system in the body by combining multivalent coordination of MOF with polymer.

## 5.2 Introduction

The metal organic framework (MOF), characterized by a simple manufacturing method, high surface area, porosity, and structure controllability, consists of an inorganic building block (metal ion or metal oxide cluster) and an organic linker.[1] It is used in catalysis,[2-4] gas storage,[5-7] separation,[8-10] or sensing[11-13] industrial fields.

Recently, nanosized MOF (nanoMOF) has been used as a carrier of drugs,[14-16] nucleic acids,[17] peptdies, and proteins[18-19] in bio application and also as in photodynamic therapy[20-21] and as a MRI contrast agent[20-21] using its inherent characteristics. The surface of MOF was functionalized with various functional groups for more effective use, such as cancer-targeting ability and increase of body stability of nanoparticles.[21-23] Several post-synthetic modification procedures, such as surface adsorption,[24-25] lipid coating,[26-27] and covalent conjugation,[28-29] have been reported. However, these methods have various problems, such as weak interaction with MOF, additional chemical reaction for modification.[19, 30] To solve this problem, coordination bonding between MOF and Lewis base are used for ligand modification.

Cancer-targeting ligands, DNA, and peptides were modified using a coordination bond.[21, 31-32] However, various proteins and biochemicals with Lewis base functional groups are endogenous,[33] and may competitively interact with the functional groups attached to the surface of the MOF, which may cause ligand detachment from the MOF. This phenomenon limits the use of MOF but has not been studied extensively.

In this paper, we investigate the interaction between PCN-224, which has high stability in aqueous solutions, and cancer-targeting ligands with Lewis base functional groups. Folic acid with carboxylic acid functional group and polyacrylic acid with modified folic acid (Folic-PAA) are modified on the MOF surface by forming monovalent and polyvalent coordination bond, respectively. To observe the

stability of nanoparticles, PCN-224 modified with Folic acid and Folic-PAA was incubated in a cell culture media containing fetal bovine serum albumin (FBS), and the detachment of folic acid was quantified by high performance liquid chromatography (HPLC). The monovalent binding of folic acid showed unstable ligand modification in the culture medium resulting in decreased cancer-targeting ability. Meanwhile, Folic-PAA with polyvalent bonding showed stable modification ability and high cancer-targeting ability.

### 5.3 Results and discussion

PCN-224 was synthesized according to a previously published paper.[21] The synthesized nanoparticles were identified by TEM and SEM. The nanoparticles have 100 nm size and sphere morphology (Figure 5-1a, b). PCN-224 of this size has higher cellular uptake capability than PCN-224 of other sizes. Folic acid and folic acid-modified polyacrylic acid were modified on the MOF surface by stirring with PCN-224 in the solution state. The carboxylic acid group of folic acid forms a monovalent coordination bond with MOF, and the remaining carboxylic acid group of PAA forms a polyvalent coordination bond with MOF. After modification of Folic acid and Folic-PAA ligand to the MOF, the hydrodynamic size changed from 106 nm to 140 nm when PAA-folic acid was modified and did not change significantly when folic acid was modified (Figure 5-1c).

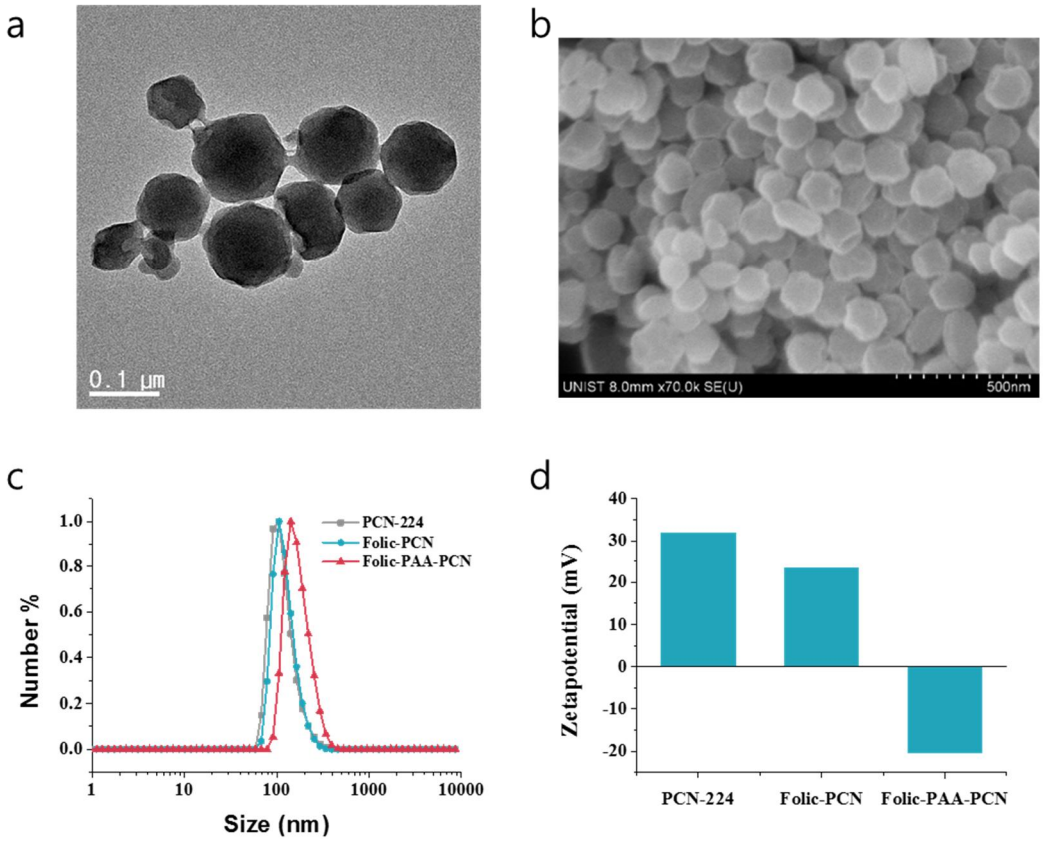


**Figure 5-1.** a) TEM and b) SEM image of PCN-224. c)DLS data and d) zeta potential of PCN-224, Folic-PCN, and Folic-PAA-PCN

This that modification of the small molecule Folic acid does not affect the size of the nanoparticle, but relatively bulky PAA modification affects the hydrodynamic size of the nanoparticle. In contrast, the surface charge of nanoparticles modified with Folic acid and Folic-PAA changed from 31.8 mV to 23.3 and -20.4, respectively (Figure 5-1d). The above results indicate that Folic acid and Folic-PAA were modified on MOF surface.

To determine the amount of folic acid modified on the surface of MOF, the amount of folic acid was calculated by measuring the amount of folic acid in the supernatant obtained by modifying Folic acid in PCN-224. The supernatant was analyzed by HPLC and it was confirmed that about 11 μg of folic acid was modified on 137 μg of PCN-224.

In order to confirm the stability of Folic-PCN, it was incubated for 1, 2, and 4 hours in cell culture media containing 10% PBS. After media incubation, the hydrodynamic size of nanoparticles increased from 106 nm to 122 nm by about 15 nm (Figure 5-2a). Folic acid detached from MOF was analyzed by HPLC and folic acid was observed at about 7 min (Figure 5-2b). The amount of detached Folic acid from MOF were 2.5, 2.8, and 4.8 μg at 1, 2, and 4 hours, respectively, corresponding to 22, 25, and 44% of the modified amounts (Table 5-1).

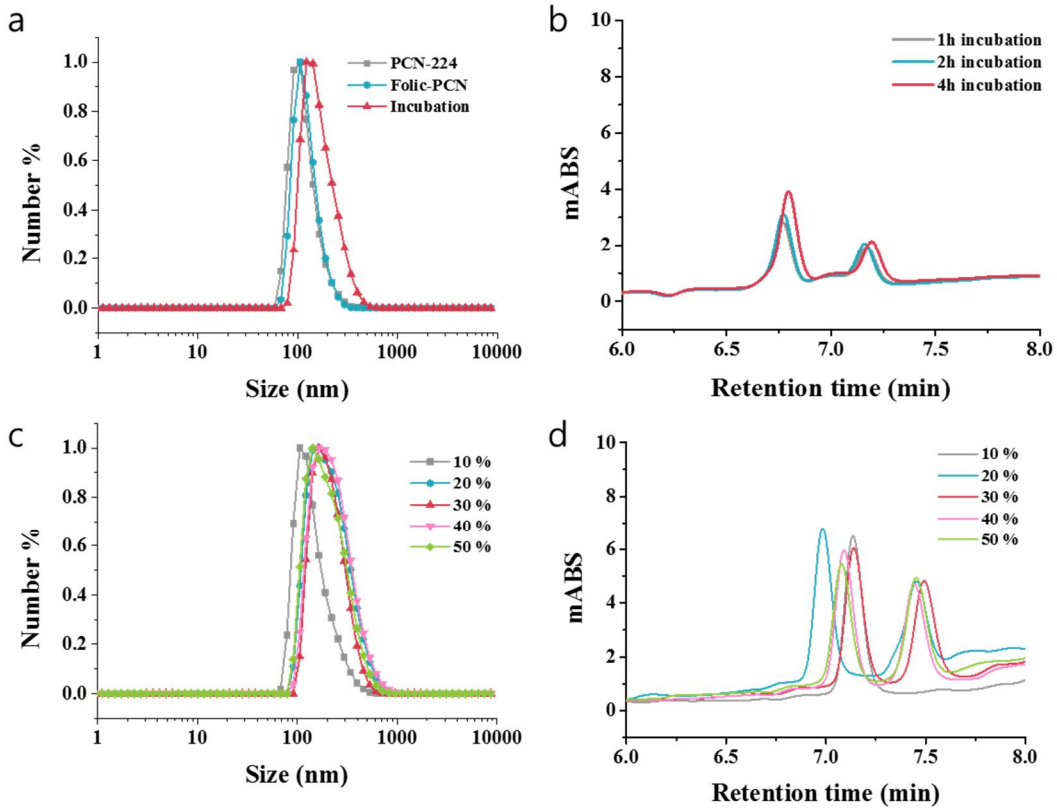


**Figure 5-2.** a) DLS data of PCN-224, Folic-PCN and media incubated Folic-PCN; b) HPLC chromatogram of Folic-PCN incubated media supernatant at different incubation time; c) DLS data of Folic-PCN after incubated different FBS concentration media; d) HPLC chromatogram of Folic-PCN incubated media supernatant at different FBS concentration

**Table 5-1.** Calculated detached amount of folic acid from PCN-224 surface.

| Time | 1 h | 2 h | 4 h |
|---|---|---|---|
| Detached Folic acid (μg) | 2.5 | 2.8 | 4.8 |
| Detached/ Modified (%) | 22 | 25 | 44 |
| Zeta potential (mV) | -21.1 | -22.1 | -21.0 |

| FBS % | 10 | 20 | 30 | 40 | 50 |
|---|---|---|---|---|---|
| Detached Folic acid (μg) | 5.2 | 4.7 | 4.4 | 4.4 | 3.7 |
| Detached/ Modified (%) | 48 | 43 | 40 | 40 | 34 |
| Zeta potential (mV) | -25 | -24.1 | -24.2 | -24.1 | -25.1 |

When the Folic-PCN was incubated in cell culture media with different FBS concentrations, the hydrodynamic size of the nanoparticles increased to 148 nm in 10% FBS and increased to approximately 220 nm in 20, 30, 40, and 50% FBS. The detachment of folic acid was analyzed by HPLC. The amount of detached folic acid was 5.2, 4.7, 4.4, 4.4 and 3.7 μg at 10, 20, 30, 40, and 50%, respectively, with an average of about 40% of folic acid detached from MOF (Table 5-1). The above results show that modified folic acid was detached by protein and biochemical present in the body, and the amount of detached folic acid is increased as the time of circulation in the body increases.

To observe the cellular uptake ability of nanoparticles by the effect of Folic acid detachment, Nile red-loaded folic-PCN and Folic-PAA-PCN was incubated to cell culture media containing 10% PBS for 4 hours (Figure 5-3). After incubation, the nanoparticles were added to Hela cells and the cellular uptake ability was confirmed by confocal microscopy (Figure 5-3). Folic-PAA-PCN showed a higher red fluorescence than Folic-PCN even without media incubation. After incubation, the fluorescence of Folic-PCN was decreased while the fluorescence of folic-PAA-PCN was still strong. The results show that folic-PAA-PCN penetrates cancer cells more effectively than folic-PCN and folic acid is losing the cellular uptake ability by biomaterials, while folic-PAA-PCN is not significantly affected.

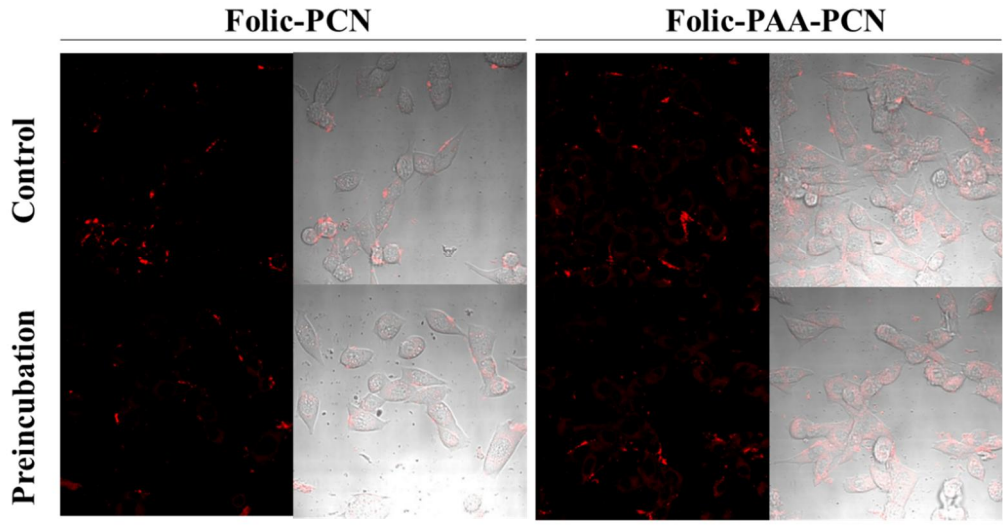


**Figure 5-3.** Confocal microscopy image of Folic-PCN and Folic-PAA-PCN (nanoparticles were incubated in media for 4 h)

### 5.4 Summary

In summary, folic acid is easily modified through monovalent coordination bonds with PCN-224. However, various proteins and biochemicals containing a Lewis base in the body competitively interact with MOF to induce the detachment of folic acid, decreasing the cellular uptake ability of Folic-PCN. In order to prevent this, folic-PAA, which can be stably modified through polyvalent coordination, was modified on the surface of PCN-224. Unlike folic-PCN, Folic-PAA-PCN showed high cell uptake ability after cell culture media incubation. These results suggest that modifying the ligand through polyvalent interaction with MOF can be used more effectively as a drug delivery system.

### 5.5 Experimental

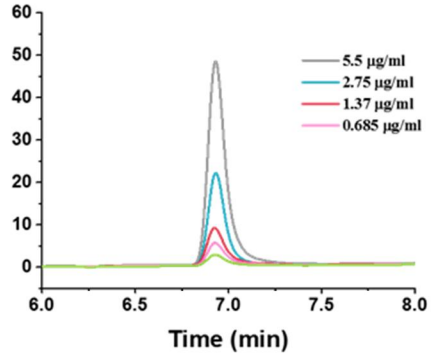


| | Area | Height |
|---|---|---|
| 5.50 μg/ml | 333 | 48 |
| 2.75 μg/ml | 148 | 21.9 |
| 1.38 μg/ml | 67 | 8.8 |
| 0.68 μg/ml | 42 | 5.3 |
| 0.34 μg/ml | 18 | 2.5 |

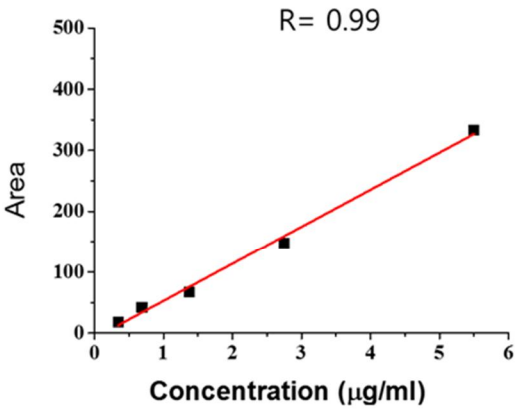


[Area]= 60.8 x [Folic] - 8.1

**Figure 5-4.** HPLC calibration curve of folic acid

**General information:** All chemicals and reagents were purchased from Sigma-Aldrich, TCI and Alfa Aesar, Korea unless otherwise specified and used without further purifications. Doxorubicin hydrochloride was obtained from Ontario Chemicals Inc, Canada. Deionized (DI) water was produced by the Millipore Milli-Q system (18.2 MΩ cm).

**Preparation of PCN-224 (90 nm):** PCN-224 nanoparticles were synthesized in a solvothermal condition as reported.[30] Meso-Tetra(4-carboxyphenyl)porphine (TCPP) (100mg, 0.13mmol), $ZrOCl_2 \cdot 8H_2O$ (300mg, 0.93mmol), benzoic acid (2.8g, 23mmol) and DMF (100mL) were combined in a 250mL round-bottom flask. The mixture was heated to 90 °C for 5hours with 300rpm stirring and then cooled to room temperature. The product was collected by centrifugation with 15000rpm for

30min and washed by fresh DMF and acetone. The synthesized PCN-224 sample was characterized by powder X-ray diffraction (PXRD).

**Preparation of Nlie red-PCN:** About 4 mg of PCN-224 were dispersed in 1mg of Nile red were dissolved in 1 mL of DMSO and stir for 24 hours at room temperature. Then the Nile red loaded PCN-224 was collected by centrifugation and dried under high vacuum. Then dried samples were redispersed in DI water.

**Preparation of Folic-PAA:** To a stirred solution of 2,2-(ethylenedioxy)-bis- (ethylamine) (1.48 g, 10 mmol) in 10 ml anhydrous $CHCl_3$, $BoC_2O$ (0.218 g, 1 mmol) in 5 ml $CHCl_3$ was added dropwise at 0 ◦C under argon atmosphere. The reaction mixture was warmed to room temperature and stirred for 24 h. Then the solvent was removed under reduced pressure and the thick oil so obtained was diluted with $CH_2Cl_2$. The organic layer was washed with brine, dried over anhydrous NaSO, and concentrated under reduced pressure. To a stirred solution of folic acid (330 mg, 0.75 mmol) in 20 ml anhydrous DMSO and pyridine (8 ml), was added synthesized chemical (216 mg, 0.87 mmol) and dicyclohexyl carbodiimide (410 mg, 2 mmol) at room temperature under argon atmosphere. The reaction mixture was stirred for 18 h at room temperature and the resulting precipitate was filtered. The filtrate was gradually poured into a vigorously stirred $Et_2O$ (50 ml) at 0 ˚C. The yellow precipitate thus obtained was collected and washed with cold $Et_2O$ several times to remove trace of DMSO. Then the solvent was removed under reduced pressure to give 2 (450 mg, 90%) as a yellow solid.

**Preparation of Folic-PCN, Folic-PAA-PCN:** About 1.38 mg of PCN were dispersed in 0.95 mL of DI water and add the 50 µl folic acid or Folic-PAA solution (2.21 mg/ml in DMSO)) and stir for 24 hours at room temperature. Then folic acid modified PCN-224 was collected by centrifugation and redispersed in DI water. The supernatant solution containing unmodified Folic acid were analyzed by HPLC.

**Cellular uptake analysis:** The cellular uptake of Folic-PCN and Folic-PAA-PCN nanoparticles in hela cells were investigated by live confocal microscope images (Olympus FV 1000 series). The cells were seeded at a density of 2 x $10^5$ cells/well in two well chambered cover glass (Lab Tek II, Thermo Scientific. After 24 hours incubation, cells were treated with Folic-PCN or Folic-PAA-PCN at a final concentration of 10 µg/mL at different time points and analyzed using the confocal microscope.

**5.6 References**

1. Moghadam, P. Z.; Li, A.; Wiggin, S. B.; Tao, A.; Maloney, A. G.; Wood, P. A.; Ward, S. C.; Fairen-Jimenez, D., Development of a Cambridge Structural Database subset: a collection of metal–organic frameworks for past, present, and future. *Chemistry of Materials* **2017,** *29* (7), 2618-2625.

2. Lee, J.; Farha, O. K.; Roberts, J.; Scheidt, K. A.; Nguyen, S. T.; Hupp, J. T., Metal–organic framework materials as catalysts. *Chemical Society Reviews* **2009,** *38* (5), 1450-1459.

3. Rogge, S. M.; Bavykina, A.; Hajek, J.; Garcia, H.; Olivos-Suarez, A. I.; Sepúlveda-Escribano, A.; Vimont, A.; Clet, G.; Bazin, P.; Kapteijn, F., Metal–organic and covalent organic frameworks as single-site catalysts. *Chemical Society Reviews* **2017,** *46* (11), 3134-3184.

4. Zhu, L.; Liu, X.-Q.; Jiang, H.-L.; Sun, L.-B., Metal–organic frameworks for heterogeneous basic catalysis. *Chemical reviews* **2017,** *117* (12), 8129-8176.

5. He, Y.; Zhou, W.; Qian, G.; Chen, B., Methane storage in metal–organic frameworks. *Chemical Society Reviews* **2014,** *43* (16), 5657-5678.

6. Ma, S.; Zhou, H.-C., Gas storage in porous metal–organic frameworks for clean energy applications. *Chemical Communications* **2010,** *46* (1), 44-53.

7. Mason, J. A.; Veenstra, M.; Long, J. R., Evaluating metal–organic frameworks for natural gas storage. *Chemical Science* **2014,** *5* (1), 32-51.

8. Chen, B.; Liang, C.; Yang, J.; Contreras, D. S.; Clancy, Y. L.; Lobkovsky, E. B.; Yaghi, O. M.; Dai, S., A Microporous Metal–Organic Framework for Gas-Chromatographic Separation of Alkanes. *Angewandte Chemie International Edition* **2006,** *45* (9), 1390-1393.

9. Li, J.-R.; Kuppler, R. J.; Zhou, H.-C., Selective gas adsorption and separation in metal–organic frameworks. *Chemical Society Reviews* **2009,** *38* (5), 1477-1504.

10. Li, J.-R.; Sculley, J.; Zhou, H.-C., Metal–organic frameworks for separations. *Chemical reviews* **2011,** *112* (2), 869-932.

11. Chen, B.; Wang, L.; Xiao, Y.; Fronczek, F. R.; Xue, M.; Cui, Y.; Qian, G., A luminescent metal–organic framework with Lewis basic pyridyl sites for the sensing of metal ions. *Angewandte Chemie International Edition* **2009,** *48* (3), 500-503.

12. Hu, Z.; Deibert, B. J.; Li, J., Luminescent metal–organic frameworks for chemical sensing and explosive detection. *Chemical Society Reviews* **2014,** *43* (16), 5815-5840.

13. Kreno, L. E.; Leong, K.; Farha, O. K.; Allendorf, M.; Van Duyne, R. P.; Hupp, J. T., Metal–organic framework materials as chemical sensors. *Chemical reviews* **2011,** *112* (2), 1105-1125.

14. Horcajada, P.; Chalati, T.; Serre, C.; Gillet, B.; Sebrie, C.; Baati, T.; Eubank, J. F.; Heurtaux, D.; Clayette, P.; Kreuz, C., Porous metal–organic-framework nanoscale carriers as a potential platform for drug delivery and imaging. *Nature materials* **2010,** *9* (2), 172.

15. Horcajada, P.; Serre, C.; Maurin, G.; Ramsahye, N. A.; Balas, F.; Vallet-Regi, M.; Sebban, M.; Taulelle, F.; Férey, G., Flexible porous metal-organic frameworks for a controlled drug delivery.

*Journal of the American Chemical Society* **2008,** *130* (21), 6774-6780.

16. Horcajada, P.; Serre, C.; Vallet-Regí, M.; Sebban, M.; Taulelle, F.; Férey, G., Metal–organic frameworks as efficient materials for drug delivery. *Angewandte Chemie International Edition* **2006,** *45* (36), 5974-5978.

17. He, C.; Lu, K.; Liu, D.; Lin, W., Nanoscale metal–organic frameworks for the co-delivery of cisplatin and pooled siRNAs to enhance therapeutic efficacy in drug-resistant ovarian cancer cells. *Journal of the American Chemical Society* **2014,** *136* (14), 5181-5184.

18. Lyu, F.; Zhang, Y.; Zare, R. N.; Ge, J.; Liu, Z., One-pot synthesis of protein-embedded metal–organic frameworks with enhanced biological activities. *Nano letters* **2014,** *14* (10), 5761-5765.

19. Röder, R.; Preiß, T.; Hirschle, P.; Steinborn, B.; Zimpel, A.; Höhn, M.; Rädler, J. O.; Bein, T.; Wagner, E.; Wuttke, S., Multifunctional nanoparticles by coordinative self-assembly of His-tagged units with metal–organic frameworks. *Journal of the American Chemical Society* **2017,** *139* (6), 2359-2368.

20. Lu, K.; He, C.; Lin, W., Nanoscale metal–organic framework for highly effective photodynamic therapy of resistant head and neck cancer. *Journal of the American Chemical Society* **2014,** *136* (48), 16712-16715.

21. Park, J.; Jiang, Q.; Feng, D.; Mao, L.; Zhou, H.-C., Size-controlled synthesis of porphyrinic metal–organic framework and functionalization for targeted photodynamic therapy. *Journal of the American Chemical Society* **2016,** *138* (10), 3518-3525.

22. Deng, K.; Hou, Z.; Li, X.; Li, C.; Zhang, Y.; Deng, X.; Cheng, Z.; Lin, J., Aptamer-mediated up-conversion core/MOF shell nanocomposites for targeted drug delivery and cell imaging. *Scientific reports* **2015,** *5*, 7851.

23. Wuttke, S.; Braig, S.; Preiss, T.; Zimpel, A.; Sicklinger, J.; Bellomo, C.; Radler, J. O.; Vollmar, A. M.; Bein, T., MOF nanoparticles coated by lipid bilayers and their uptake by cancer cells. *Chem Commun (Camb)* **2015,** *51* (87), 15752-5.

24. Agostoni, V.; Horcajada, P.; Noiray, M.; Malanga, M.; Aykaç, A.; Jicsinszky, L.; Vargas-Berenguel, A.; Semiramoth, N.; Daoud-Mahammed, S.; Nicolas, V., A “green” strategy to construct non-covalent, stable and bioactive coatings on porous MOF nanoparticles. *Scientific reports* **2015,** *5*, 7925.

25. Hidalgo, T.; Giménez-Marqués, M.; Bellido, E.; Avila, J.; Asensio, M.; Salles, F.; Lozano, M.; Guillevic, M.; Simón-Vázquez, R.; González-Fernández, A., Chitosan-coated mesoporous MIL-100 (Fe) nanoparticles as improved bio-compatible oral nanocarriers. *Scientific reports* **2017,** *7*, 43099.

26. Liu, D.; Poon, C.; Lu, K.; He, C.; Lin, W., Self-assembled nanoscale coordination polymers with trigger release properties for effective anticancer therapy. *Nature communications* **2014,** *5*, 4182.

27. Wuttke, S.; Braig, S.; Preiß, T.; Zimpel, A.; Sicklinger, J.; Bellomo, C.; Rädler, J. O.; Vollmar, A. M.; Bein, T., MOF nanoparticles coated by lipid bilayers and their uptake by cancer cells. *Chemical*

*Communications* **2015,** *51* (87), 15752-15755.

28. Hintz, H.; Wuttke, S., Postsynthetic modification of an amino-tagged MOF using peptide coupling reagents: a comparative study. *Chemical communications* **2014,** *50* (78), 11472-11475.

29. Zimpel, A.; Preiß, T.; Röder, R.; Engelke, H.; Ingrisch, M.; Peller, M.; Rädler, J. O.; Wagner, E.; Bein, T.; Lächelt, U., Imparting functionality to MOF nanoparticles by external surface selective covalent attachment of polymers. *Chemistry of Materials* **2016,** *28* (10), 3318-3326.

30. Zimpel, A.; Al Danaf, N.; Steinborn, B.; Kuhn, J.; Hoehn, M.; Bauer, T.; Hirschle, P.; Schrimpf, W.; Engelke, H.; Wagner, E., Coordinative Binding of Polymers to Metal-Organic Framework Nanoparticles for Control of Interactions at the Biointerface. *ACS nano* **2019**.

31. Wang, S.; McGuirk, C. M.; Ross, M. B.; Wang, S.; Chen, P.; Xing, H.; Liu, Y.; Mirkin, C. A., General and direct method for preparing oligonucleotide-functionalized metal–organic framework Nanoparticles. *Journal of the American Chemical Society* **2017,** *139* (29), 9827-9830.

32. Zhang, Y.; Wang, F.; Liu, C.; Wang, Z.; Kang, L.; Huang, Y.; Dong, K.; Ren, J.; Qu, X., Nanozyme decorated metal–organic frameworks for enhanced photodynamic therapy. *ACS nano* **2018,** *12* (1), 651-661.

33. Peters Jr, T., Serum albumin. In *Advances in protein chemistry*, Elsevier: 1985; Vol. 37, pp 161-245.

# Acknowledgement

지금 이 순간까지 저를 인도해 주시고 대학원 생활을 큰 어려움 없이 무사히 마칠 수 있도록 도와 주신 하나님의 은혜에 감사드립니다.

제일 먼저 저를 받아 주시고 박사기간동안 친절하게 지도해주신 유자형 교수님께 감사드립니다. 부족한 저의 졸업논문을 심사해주신 권태혁 교수님, 김채규 교수님, 박명환 교수님, 그리고 정영도 교수님께 감사드립니다. 함께 실험하며 힘들 수 있던 시간들을 짜증 대신 웃으며 보낼 수 있게 해준 연구실 동료들에게도 감사드리며 앞으로도 Ryu group 에서 즐겁게 실험하기를 바랍니다. 낯선 곳으로 와서 육체적, 정신적으로 힘들 때 따뜻한 마음으로 몸과 마음의 휴식처가 되어준 울산교회 성도님들과 영범이 가정에게 감사인사 드립니다. 저를 낳고 지금까지 키워 주시며 많은 것을 헌신하신 부모님에게 죄송스럽고 감사합니다. 기송이형에게 감사드리며 형수님과 선호와 함께 행복한 가정이 되기를 기도합니다. 그리고 어려울 때마다 함께 고민해주고 박사라는 선택지를 제시해준 평생 친구 요한이에게 감사한 마음을 전하며 요한이의 가정에 행복한일이 가득하기를 바랍니다. 항상 내 옆에서 기다리며 격려해준 저의 사랑스러운 아내 혜선이에게 감사의 마음을 전합니다. 또한 저희 가정이 항상 행복하기를 바라며 사랑스럽고 귀여운 연호가 앞으로도 하나님 안에서 무럭무럭 자라나기를 바랍니다.

마지막으로 저를 도와주고 아껴 주셨던 모든 분들에게 감사를 드립니다.